2014-09-12

Impact of Initial Water Saturation on SAGD Performance

Khaleeq, Aisha

UNIVERSITY OF CALGARY

Impact of Initial Water Saturation on SAGD Performance

by

Aisha Khaleeq

A THESIS

SUBMITTED TO THE FACULTY OF GRADUATE STUDIES

IN PARTIAL FULFILMENT OF THE REQUIREMENTS FOR THE

DEGREE OF MASTER OF ENGINEERING

GRADUATE PROGRAM IN CHEMICAL AND PETROLEUM ENGINEERING

CALGARY, ALBERTA

SEPTEMBER, 2014

Abstract

The Steam Assisted Gravity Drainage (SAGD) is the in situ technology of choice in the Athabasca deposit which is the single largest oil sands resource in Alberta. All operating companies are facing challenges in their SAGD operations. One of the most challenging issues in oil sands thermal in situ operations are reservoirs with challenging features such as thin reservoirs, reservoirs with top water/gas and bottom water thief zones, and reservoirs with higher initial water saturation (Law et al. 2003a, 2003b, 2003c, Gates et al. 2007). At this point, there are no published studies on the impact of high initial water saturation on the performance of SAGD in the McMurray Formation. To address this, the research documented in this thesis investigates the performance of SAGD in water-rich oil sands reservoirs by using thermal reservoir simulation. The research also explored the improvement of operating strategy in water rich oil sands reservoirs by using gas co-injection with steam. The results show that the higher the initial water saturation of the reservoir, the better the steam conformance along the SAGD well pair, the faster the steam chamber growth, and the higher is the injectivity into the reservoir. However, if the initial water saturation is sufficiently high, the oil production rate drops due to lower content of oil in the reservoir. Two operating strategies were tested to determine if the steam-to-oil ratio of SAGD in a relatively high initial water saturation McMurray Formation oil sands reservoir could be improved. In first strategy, gas is co-injected with steam and in the second strategy, a gas slug is injected into the reservoir prior to SAGD operation. The simulations results reveal that NCG co-injection does not improve the performance of the recovery process.

Acknowledgements

First of all, I am thankful to my Lord, my Allah who always blessed me with His special blessings. By grace of my God, I find a knowledgeable, committed professor Professor Ian Gates and I am able to finish my research. I would like to express my deepest appreciate to my supervisor Professor Ian D. Gates, who has provided the opportunity for such an interesting and exciting research topic. Professor Ian Gates has shown the attitude and the substance of a genius: he continually and credibly conveyed a spirit of adventure in regard to my research, and an excitement in regard to teaching. Without his supervision and constant help this dissertation would not have been possible. I would like to thank him for encouraging my research and for allowing me to grow as a research scientist. I also want to thank my committee members, Professors Brij Maini, Hossein Hejazi and Ron Wong who spare time from their busy schedule for serving as my committee members.

A special thanks to my mother whose prayer helped me in achieving my goal, and I would like to thank my husband Khaleeq Awan and my daughter Noor Awan who were my big support in the moment when I need them. Without my husband support, it was not possible for me to complete my thesis and my degree.

Dedication

I dedicate my dissertation work to my family and my loving mother. I give special thanks to my husband Khaleeq Awan and my daughter Noor Awan for being there for me throughout the entire master program. A special feeling of a gratitude to my supervisor, Dr. Ian Gates whose words of encouragement always helped me develop my research skills. I also dedicate this thesis to one of our family friend, Adeel Nisar who has supported me throughout the process.

Table of Contents

List of Tables

List of Figures

Chapter One: **Introduction**

1.1 Heavy Oil and Oil Sands – Locations and Volumes

There are three large oil sands deposits in Alberta, illustrated in Figure 1.1. The largest deposit is the Athabasca, with surface area covering over 45,000 square kilometers, located primarily in the northeast of the province. The center of commercial activity of the Athabasca deposit is the city of Fort McMurray. The Athabasca deposit, mainly contained in the McMurray Formation, ranges from surface mineable resource to in situ reservoirs with depths of up to several hundred meters. Roughly 80% of the Athabasca resource is too deep (>70 m) to mine and has to be produced to surface by using in situ recovery processes. The Wabiskaw deposit, located in the northwest-central Alberta, is often bundled with the Athabasca deposit. The second largest oil sands deposit is the Cold Lake deposit which has a surface area equal to approximately 22,000 square kilometers. It is located south of the Athabasca deposit and its main commercial center is the City of Cold Lake. In the Cold Lake deposit, the bitumen column is mainly hosted in the Grand Rapids and Clearwater Formations with depths ranging from 300 to 600 meters below surface. The third and smallest oil sands deposit is the Peace River deposit which has a surface area of about 8,000 square kilometers. The Peace River deposit ranges from 300 to 770 meters below the surface. The original oil in place in the oil sands deposits is estimated to equal to about 1.8 trillion barrels (AER, 2013). Thus, the value of Western Canada's petroleum resources is immense.

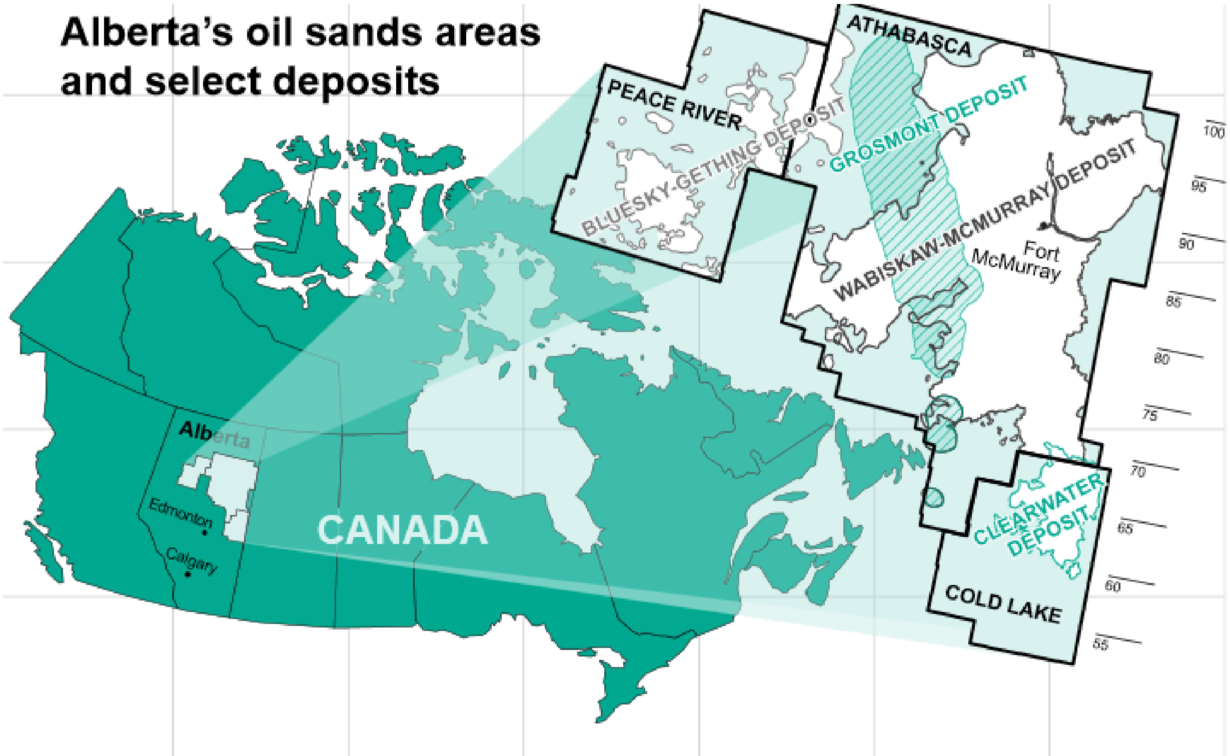

Figure 1.1: Location of the three major crude bitumen deposit in northern Alberta: Athabasca, Cold Lake, and Peace River (ST98-2013 Alberta Energy Regulator).

Canada has the third-largest oil reserves (to clarify, reserves are a measure of oil volume producible with existing technology at current market conditions) in the world, after that of Saudi Arabia and Venezuela. Of Canada's 173 billion barrels of oil reserves, 170 billion barrels are located in the province of Alberta out of which 168 billion barrels are recoverable as bitumen. If only 30% of these deposits are extracted, it is sufficient to meet the needs of North America for over 100 years at current consumption levels. Currently, 50% of Canada`s oil production comes from heavy oil and oil sands reservoirs (20°API) and it will likely slowly rise in the future to meet growing energy demand not only in Canada but also in the United States and overseas.

Bitumen resources are found mainly in high porosity (28-32%) quartz arenites to arkosic sands within the Athabasca, Cold Lake, and Peace River deposits. Fractured carbonates rocks, mainly the Grosmont Formation, have average porosity between 10 and 14% and also host vast amounts of heavy oil (roughly 15% of the oil volume contained in oil sands deposits). There is a large amount of relatively less viscous heavy oil in a series of thinner blanket sands and channel sands extending throughout central to northeastern Alberta in the overlying zones above the Cold Lake oil sands deposit near Bonneville which also extend well into Saskatchewan (up to 120 km east of the border in some areas). This area is referred to as the “heavy oil belt” and this deposit has received substantial development attention because of its lower viscosity heavy oil, typically between 1,000 and 50,000 cP. In many of these operations, the oil is mobilized in situ via solution gas drive. These recovery operations are either cold production or cold production with sand, often referred to as CHOPS (Cold Heavy Oil Production with Sand).

The viscosity of the bitumen held in the Athabasca deposit tends to be between 500,000 and 5 million cP at original reservoir temperature (Mehrotra and Svrcek, 1986). At elevated temperature, the viscosity of the oil drops to less than 10 cP and thus becomes sufficiently mobile to be produced from the reservoir. As a result, the technologies used to produce bitumen are mainly thermal recovery processes where high pressure, high temperature steam is injected into the reservoir.

According to Alberta Energy Regulator (AER, 2013), the heavy oil and bitumen production rate exceeded 800,000 barrels per day (bpd) in 2013 by using cold production and in situ thermal recovery methods. An example projection, including both in situ and mining operations, is displayed in Figure 1.2. The projections reveal that heavy oil and bitumen production in Alberta will potentially rise to about 3 million bpd by 2024.

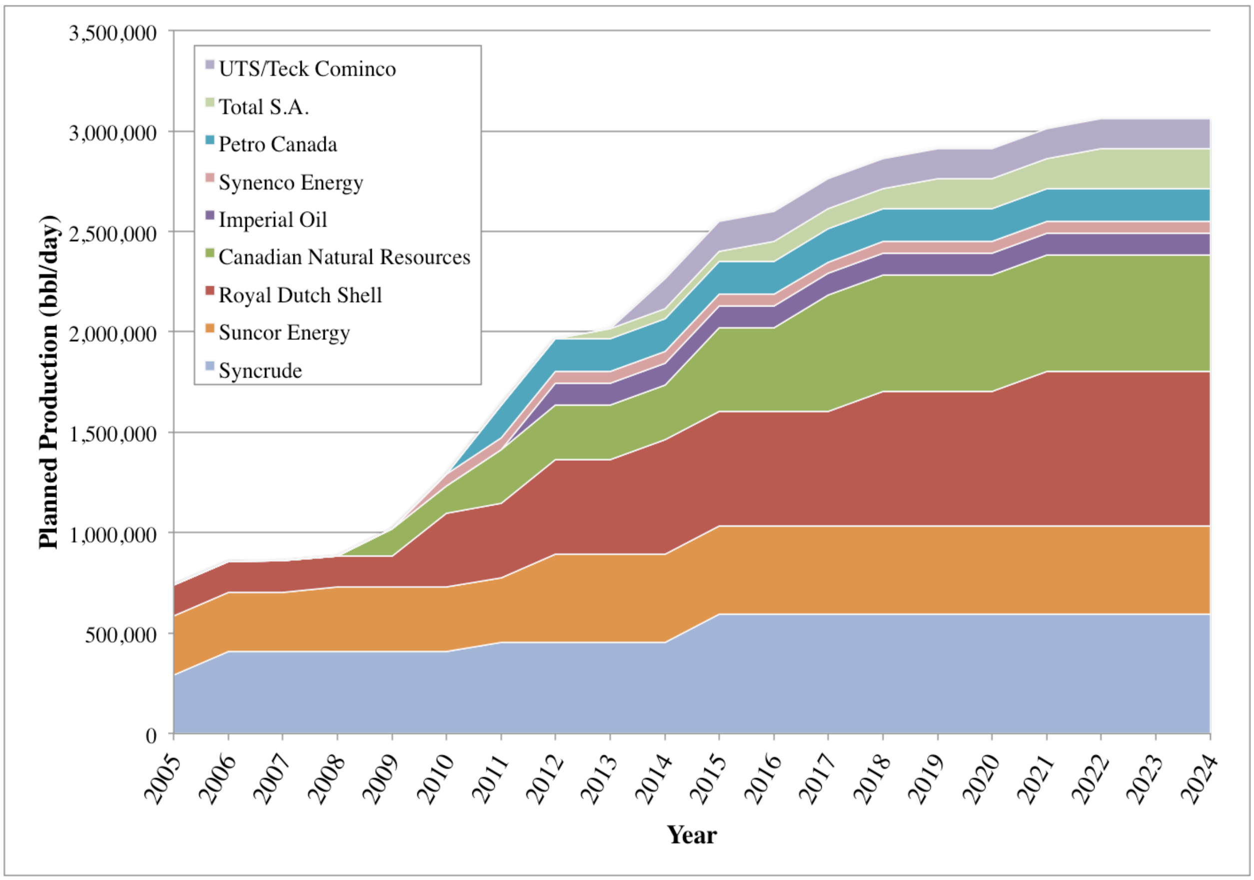

Figure 1.2: Planned production of crude oil by different operating companies for future (AER, 2013).

1.2 Brief Description of the Geology of Oil Sands Reservoirs

Bitumen resources in Western Canada are trapped in both carbonate and clastic (sand) reservoirs (Attanasi and Meyer, 2007). The carbonates formations consist of calcite and dolomite which were created through precipitation of these minerals from organic sources such as coral and other marine organisms. The largest carbonate reservoir containing bitumen in the world is the Grosmont Formation located in central Alberta, shown in Figure 1.1. The volume of oil contained in the Grosmont Formation is equal to about 440 million barrels which accounts for 71% of bitumen volume in place in Alberta carbonate deposits (Alberta Energy and Utility Board, 2006). The key challenges of producing bitumen from the Grosmont Formation is that associated with the complexity of the reservoir due to the presence of fractures, vugs, breccia, matrix, and karsted zones and the viscosity of the oil which tends to be slightly higher than that of the Athabasca deposit. The viscosity of the bitumen in the Grosmont Formation is of order of 1 to 2 million cP (PTAC, 2007).

Bitumen reserves in oil sands deposits are contained in laterally discontinuous, upward fining channel sand bodies, especially in the northern part of the Athabasca deposit. In this deposit, these are mostly associated with point bar depositional environments (Strobl et al. 1997a, 1997b, Su et al. 2013, 2014). Significant reserves occur in laterally extensive marine bar sands at the top of the McMurray Formation in the western part of the Athabasca deposit. The Athabasca oil sands deposit is mainly heterogeneous with respect to reservoir physical characteristics such as geometry and structure, porosity, permeability, mineralogy and distribution, and chemistry of bitumen. For in situ operations, the average depth of the bitumen-bearing deposits are equal to 200 m for the Athabasca deposit, 400 m for the Cold Lake deposit, and 500 m for the Peace River deposit (Nasr and Ayodele, 2005).

An East-West simplified geological cross-section of the Athabasca oil sands deposit is displayed in Figure 1.3. The Athabasca oil sands deposit is the largest Cretaceous oil sands deposit in Alberta with most of the bitumen deposits found in the McMurray Formation, a layer of shale, sandstone, and oil-impregnated sands formed during the Cretaceous period by river and ocean processes. The McMurray Formation is up to 150 m thick and lies over a layer of shale and limestone (the Devonian Waterways Formation) which provides an understrata seal and beneath the Clearwater Formation, a layer of marine shale and sandstone which provides in most locations an overburden seal. The Clearwater Formation is itself overlain by the Grand Rapids Formation, which in turn is dominated by sandstone (Conly et al. 2002, Hein et al. 2000). The McMurray Formation almost vanishes where the Devonian layer rises in a ridge which cuts through the McMurray Formation. North of Fort McMurray, the McMurray Formation is within 75 m of the surface. It is exposed at the surface where the Athabasca River and its tributaries have incised into the landscape. The McMurray Formation is first exposed as outcrop in the Athabasca riverbed at Boiler Rapids, 50 km upstream of Fort McMurray and again near the MacKay River (Conly et al. 2002). Oil sands exposed at the surface of the land are a natural source of hydrocarbons that enter the aquatic and land ecosystems of the area.

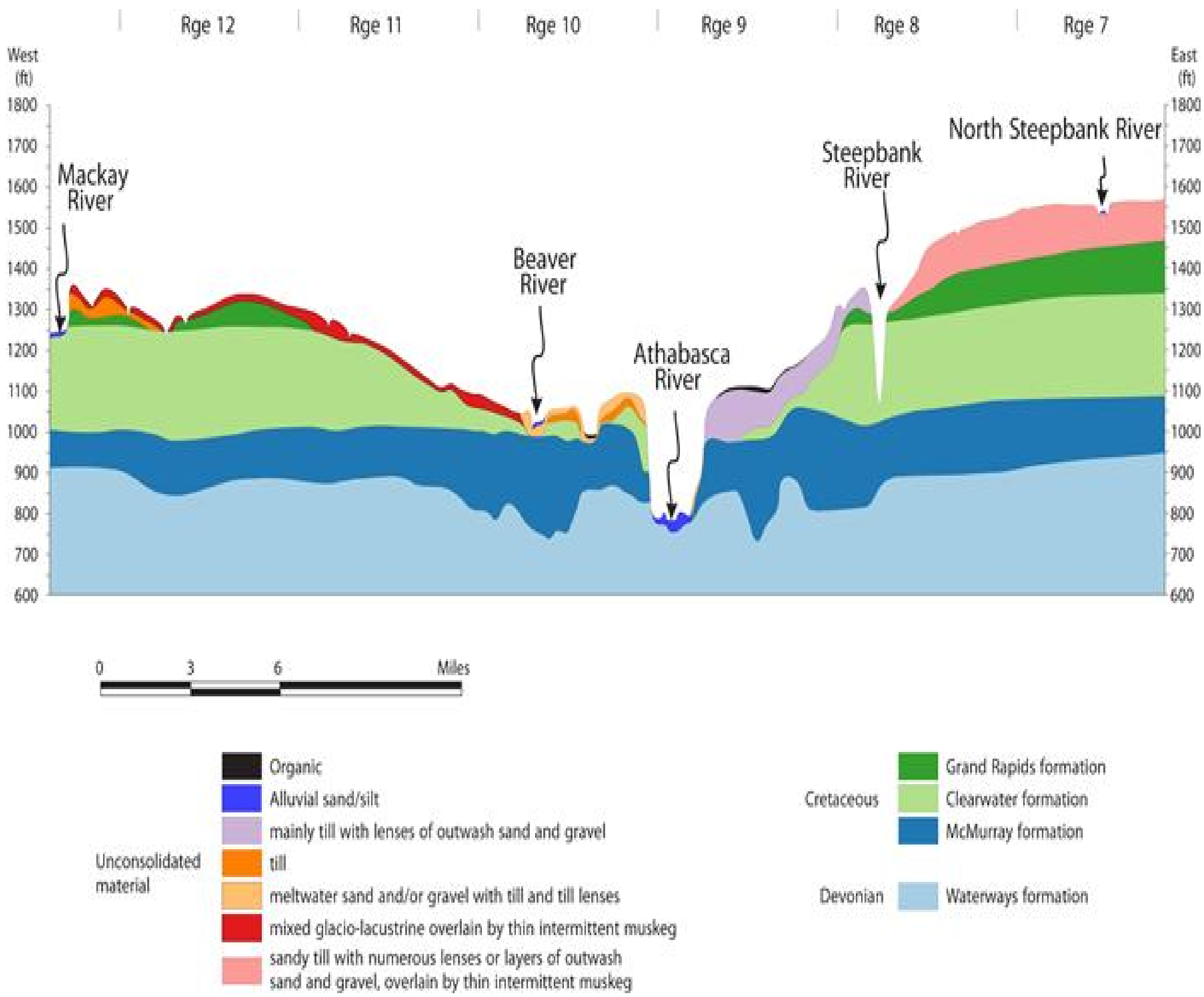

Figure 1.3: East-West geological cross-section of the Athabasca oil sands region (Conly et al. 2002).

The McMurray Formation can be geologically heterogeneous especially in areas that are mainly point bar deposits. In these systems, due to meandering channels, there are stacked channels with shale drapes within the point bar (Strobl et al. 1997a, 1997b, Hein et al. 2000, Su et al.

2013, 2014). The key issues faced by operators is that the heterogeneity of the recovery process can render the performance of the recovery process poorer than would be anticipated in a homogeneous oil sands reservoir. The shale layers within the formation can interfere with steam flow into the reservoir and oil drainage from the reservoir thus lowering the economics of the operation.

1.3 Bitumen General Properties

Bitumen, from unconventional oil sand reservoirs, typically exhibits high viscosities and relatively high densities. Table 1.1 lists general properties of heavy oil and bitumen. Bitumen is colloidal in nature and has no specific melting, boiling, or freezing point (Butler, 1997). It is also insoluble in water. Bitumen are highly impermeable to water flow and are generally hydrophobic and chemically inert and oxidize slowly.

Table 1.1: Definition of the types of heavy oil based on the density, ρ, API gravity, and viscosity, η (EP 2205998 A2).

Definition	ρ/kg·m^{-3}	API	η/mPa·s	Comments
Medium heavy oil	903 to 946	25 to 18	100 to 10	Fluid mobile at reservoir conditions
Extra heavy oil	933 to 1021	20 to 7	10 000 to 100	Fluid not mobile at reservoir conditions
Tar sands and bitumen	985 to 1021	12 to 7	> 10 000	Not a fluid at reservoir conditions
Oil shale				Fluid not mobile at reservoir conditions

Athabasca bitumen has API gravity that ranges from 8 to 15°API. This implies that in some reservoirs, the density of the bitumen is higher than that of water. Bitumen density and viscosity is temperature dependent and bitumen has less mobility at the low temperature encountered at original conditions in McMurray Formation reservoirs. Figure 1.4 displays a typical example of the dependence of bitumen viscosity on temperature. The data reveals that the viscosity of the bitumen at original reservoir conditions, typically less than 10°C, is typically in the millions of cP. After the temperature is raised to over about 200°C, the viscosity for most bitumens drops to less than 10 cP.

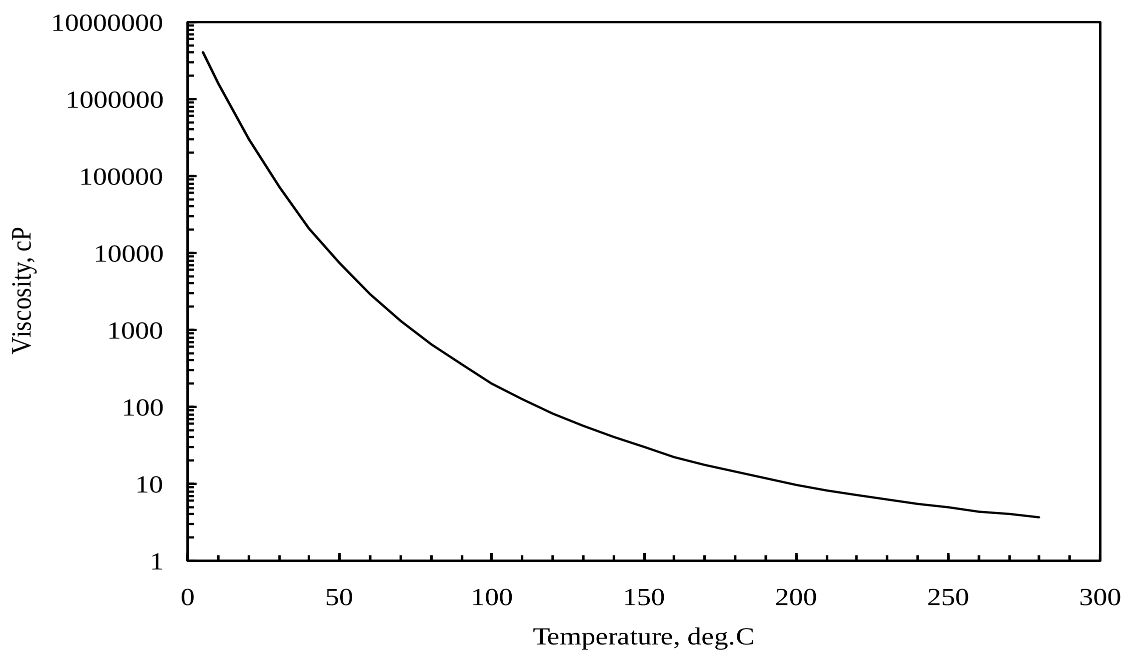

Figure 1.4: Oil viscosity versus temperature (Mehrotra and Svrcek, 1986).

1.4 In Situ Recovery Processes for Oil Sands Reservoirs

There are two general requirements that must be satisfied for a technically successful in situ oil sands recovery process performance. First, the bitumen must be mobilized; in other words, the viscosity of the oil must be lowered so that it can be moved to a production well under reasonable forces such as gravity drainage, solution gas drive, or steam flooding pressure gradients. Second, a drive mechanism must be present that will move the mobilized oil to a production wellbore.

At present, there are two major commercial steam-based recovery processes used in oil sands reservoirs. The first one is Cyclic Steam Stimulation (CSS) and the second one is Steam-Assisted Gravity Drainage (SAGD).

In CSS, a single well is used (Gates, 2013). In the first stage of the process, steam is injected at high pressure into the formation at pressures high enough to dilate or fracture the formation. This enables rapid distribution of the steam within the reservoir. After the target volume of steam is injected, the well is shut in to allow the heat to dissipate from the dilated hot zone; this is referred to as the soak period. After the soak period, the well is put on production and reservoir fluids, including the steam condensate and mobilized oil, flow from the reservoir. The production interval is stopped when the oil rates are no longer economic. At this point, steam injection starts again and the steam-soak-production cycles are repeated until the well is no longer productive. In late cycle CSS, due to the many connections between the individual wells, the process transitions into a cyclic steam flooding operation.

In SAGD, shown in cross-section in Figure 1.5, originally proposed by Roger Butler (1997) in the late 1970's and tested at AOSTRA's Underground Test Facility (UTF) with success, the process consists of two horizontal wells: an injection well and a production well. SAGD is the focus of the research documented in this thesis.

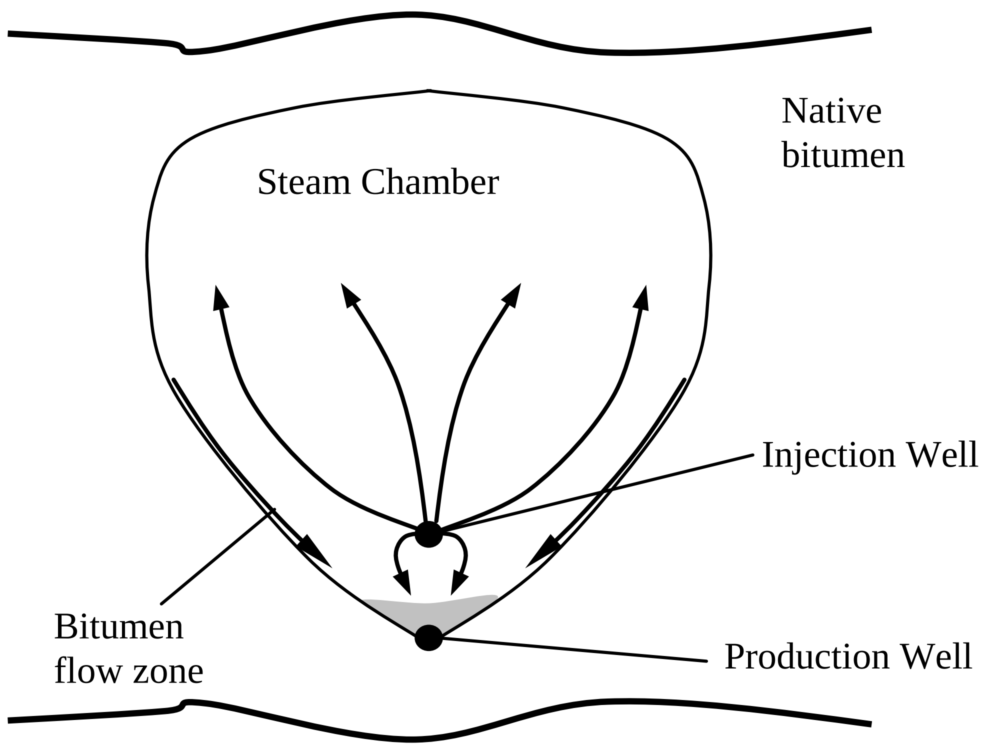

Figure 1.5: Cross-section of Steam-Assisted Gravity Drainage (SAGD) process illustrating steam injection and fluid production. The wells are horizontal wells that go into the page.

In SAGD, steam injected into the formation through the top well enters a depleted-oil chamber. At the edge of the chamber, the steam condenses and releases its latent heat to the oil sands there. The oil sand is heated, thus heating the bitumen which consequently lowers its viscosity. The mobilized oil and steam condensate drain down the edges of the chamber, under the action of gravity, to its base where the production well is located. At start up, in SAGD, a 3 to 6 month preheating period, often referred to as the steam circulation period, is required to establish thermal communication between and around the two wells. This is done by continuously injecting steam into both wells at the initial reservoir pressure which warms the oil sand near the wells providing sufficient mobility of the oil to initiate SAGD. In SAGD, liquids are deliberately accumulated above and around the production well to provide a seal to prevent live steam production through the lower well (Edmunds, 1998; Gates and Leskiw, 2010). With continuous steam injection and bitumen removal from the reservoir, the steam chamber grows upwards and extends laterally within the oil-bearing zone as the process evolves.

In 2012, 49% of in situ oil sands production was recovered by SAGD (Alberta Energy Regulator 2013). In typical practice, the pressure of steam chamber is maintained at a constant value although some operations have stepped down the steam injection pressure with time to reduce heat losses to the overburden (Gates and Chakrabarty, 2006; ConocoPhillips 2013). SAGD is the in-situ technology of choice for Athabasca oil sands because these reservoirs tend to be relatively shallow (with large competent cap rock and thus CSS steam fracturing cannot be done) and have low solution gas content (so cannot use solution gas drive as is the case in CSS). Advantages of SAGD include potentially high recovery factor, reasonable energy efficiency, and the ability to operate close to initial reservoir pressure (thus minimizing the opportunities for steam or oil flow to surface through the overburden).

In commercial production, the key objective of SAGD operations is to inject the least amount of steam per unit of oil produced. This ratio, referred to as the steam-to-oil ratio (SOR where the steam is expressed as cold water equivalent), is one of the main measures of the technical and economic success of the process. In field operations, the best SORs are typically around 2 m^3/m^3 whereas the poorest are greater than 7 m^3/m^3. A low SOR implies that the steam is being efficiently for oil production in that the steam injected is contacting large amounts of oil-rich oil sand leading to bitumen mobilization and its production from the reservoir. To obtain low SORs, one key requirement of SAGD is full well utilization, in other words, uniform steam conformance along the entire SAGD well pair. More effective steam conformance implies that the potential amount of oil mobilized is higher. If the temperature of the bitumen is not raised to over about 160°C, it is not sufficiently mobilized to flow in large volumes to the production well. Thus, this means that steam delivery throughout the reservoir is an important aspect of the process.

Figure 1.6 show an interpretation of 4D seismic data indicating the distribution of steam in a SAGD operation consisting of three well pairs (inter well pair spacing equal to about 100 m) in the McMurray Formation, respectively. The image shows that the heated zones are not uniformly distributed along the well pairs and within the reservoir. The top and middle well pairs exhibit better steam conformance than that of the lower well pair. There are cold spots, which can be interpreted as relatively non-productive zones, along the middle and lower well pairs. Despite the spacing of only about 100 m between the well pairs, the steam conformances are radically different suggesting the impacts of geological heterogeneity and operational differences between the well pairs (Wei 2011).

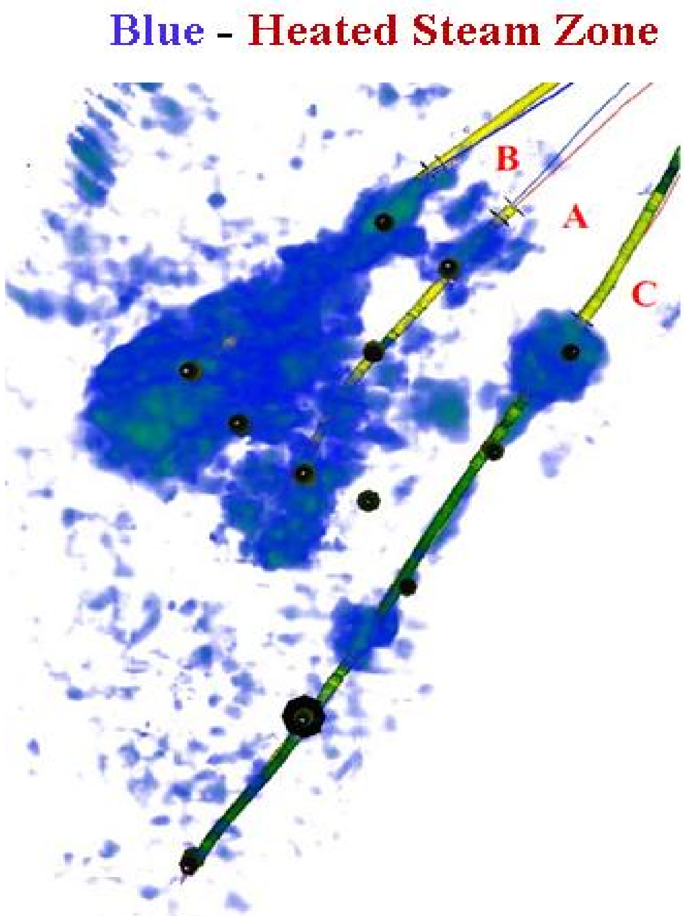

Figure 1.6: Interpretation of 4D seismic data to obtain steam chamber conformance zones along Surmont SAGD pilot well pairs (ConocoPhillips, 2009).

There are numerous factors which control SAGD production rates from the reservoir including geological heterogeneity, well pair length, and operating conditions of the injection and production wells. Butler (1997) derived a simple formula for the oil drainage rate from a SAGD wellpair:

$$Q_o = \sqrt{\frac{2\phi \Delta S_o k k_{ro} \rho_o g \alpha h_f}{m \mu_o}} \ . \qquad 1.1$$

where Q_o is the bitumen drainage rate, ΔS_o is the change in the oil saturation that occurs in the reservoir during drainage, k is the absolute permeability of the oil sands formation, k_{ro} is the relative permeability of the oil phase, g is the acceleration of gravity, h_f is the height of the oil-bearing oil sands, m is a coefficient that determines the relationship between the oil viscosity and temperature, ϕ is the porosity of the formation, ρ is the density of the draining bitumen, α is the thermal diffusivity of the oil sands, and μ is the dynamic viscosity of the draining bitumen; m is given by:

$$\frac{1}{\nu_o} = \frac{1}{\nu_{os}} \left[\frac{T - T_r}{T_s - T_r} \right]^m \ . \qquad 1.2$$

where ν_o and ν_{os} are the kinematic viscosities of the bitumen at temperature T and at the steam temperature T_s; T_r is the original reservoir temperature. Equation 1.1 reveals that the higher the oil content in the reservoir, $\phi\Delta S_o$, and the higher the effective permeability of the oil phase in the reservoir, kk_{ro}, the greater the heat transfer (via thermal conduction as reflected by α), the greater the height of the reservoir, and the lower the viscosity, the greater is the bitumen drainage rate.

The relative permeability of the oil phase depends on the oil saturation: the higher the oil saturation, the higher the oil relative permeability. This implies that the higher the water saturation (at constant gas saturation), the lower is the oil phase relative permeability and the oil drainage rate. Thus, high water saturations in oil sands reservoir have two direct impacts on the oil drainage rate. First, the effective permeability of the oil phase and second, the amount of original oil in the reservoir.

1.5 Typical SAGD Production Performance

In typical practice, a SAGD project evolves through four main stages: start up (pre-heating period), ramp up, steady state, and turn down. In the ramp up stage of SAGD, the SOR is high due to the steam invested in the process during the pre-heating period. As oil production rates ramp up as the chamber grows into the reservoir, the SOR decreases. In this stage, allof the heat delivered to the reservoir is transferred to oil sand (none is lost to the overburden). During ramp up, it usually takes between 18 and 24 months to reach the steady-state stage. In the steady-state stage, the steam chamber has reached the top of the oil sands interval and heat is being lost to the overburden. This implies that the SOR starts to decline since some of the injected steam now supplies heat to non-productive rock. The steam chamber expands in the lateral direction within the reservoir. When steam chambers start to merge between SAGD well pairs, the turn down stage starts. This can happen, depending on the oil depletion rate of the well pairs and spacing between the well pairs, between 6 and 10 years after the steady-state stage starts. In the turn down stage, other follow up processes can be used to lower the SOR such as blow down (continuously produce fluids with no steam injection) and wind down (continuously produce fluids with gas injection).

Most commercial projects in the Athabasca oil sands deposit have a target SOR equal to about 3.0 m^3/m^3. However, only a few operators have been able to achieve this level within first few years. In most applications, the potential recovery factor is usually stated to be greater than 60% however, only a few well pairs are mature enough to have achieved this value. All commercial projects see down time and sources of down time come from maintenance of water treatment and steam generation units in the central processing facility.

Most SAGD projects produce in the range from 175 to 2,700 bbl/d (28 to 430 m^3/d) with SORs that range from about 2 to above 7 m^3/m^3. This implies that there are some good SAGD well pairs as well as poor SAGD well pairs. In Alberta, an average SAGD well pair produces 825 bbl/d (131 m^3/d) after on average 18 months with an SOR equal to about 3.0 m^3/m^3. For the average SAGD well pair, the bitumen production rate plateau during the steady-state stage is maintained until about 50% of the recoverable bitumen is produced which typically takes between three and five years to achieve. On average, production then starts to decline at a rate of 5 to 18% per year.

From data of current field operations, the top three SAGD operations are Cenovus' Foster Creek, Suncor Energy's Firebag, and Suncor Energy's Mackay River if measured by the greatest production rates and SORs (AER, 2013). The production volumes from 2002 to 2010 are listed in Table 1.2; over this period of time, the top three SAGD projects represents over 60% of SAGD overall production rates.

Table 1.2: SAGD production rates, in barrels per day, for the top three SAGD projects in Alberta (AED, 2013).

	Year	2002	2003	2004	2005	2006	2007	2008	2009	2010
Foster Creek	Rate, bpd	14,563	22,238	29,453	29,598	37,582	49,287	52,702	75,454	102,235
	cSOR, m^3/m^3	3.4	2.7	2.6	2.6	2.6	2.5	2.5	2.6	2.5
Firebag	Rate, bpd	-	32	11,031	19,194	33,680	36,936	37,680	49,075	53,609
	cSOR, m^3/m^3	-	-	-	4	3.3	3.1	3	3	3
Mackay River	Rate, bpd	6,672	10,716	16,596	21,297	21,419	20,631	25,414	29,348	31,496
	cSOR, m^3/m^3	-	3.2	2.7	2.5	2.5	2.5	2.5	2.5	2.5
Top 3 SAGD Total		21,235	32,986	57,080	70,089	92,681	106,854	115,795	153,878	187,340
All other SAGD Total		9,359	11,583	15,547	16,351	15,717	21,358	64,453	90,629	135,304
Total SAGD		30,594	44,569	72,627	86,440	108,398	128,212	180,248	244,507	322,644
Top 3 as Percent of Total		69%	74%	79%	81%	86%	83%	64%	63%	58%

There has been unprecedented growth of the oil sand industry over the past decade and future investment will be of order of an additional $100 billion dollars by 2025 with projected growth of the production rate to over 3 million barrels per day within about 10 years from now. The challenge faced by oil sands operators is that many of the target reservoirs are not ideal with strong geological heterogeneity, top gas/water and/or bottom water zones, and thinner reservoirs or water-rich reservoirs. Although SAGD commercial projects have been in development for 25+ years, companies are still in the process of learning how to apply SAGD more effectively under different reservoir and operating conditions and at this point, it remains unclear how to operate SAGD in challenging reservoirs. In the research documented here, SAGD production of oil sands reservoirs with relatively high water saturation is examined.

1.6 Research Questions

This thesis documents an investigation on the performance of SAGD in water-rich oil sands reservoirs by using thermal reservoir simulation. The key research questions examined in the research described here are as follows:

1. How does increased water saturation affect the performance of SAGD?
2. Can gas co-injection with steam improve the performance of SAGD in water-rich reservoirs?
3. What is the best design for a gas co-injection process with steam to minimize the SOR of a SAGD operation in a water-rich reservoir?

1.7 Organization of Thesis

The thesis is divided into five Chapters. Chapter 2 is a literature review which focuses on SAGD operations and field practices and previous studies of SAGD in challenging oil sands reservoirs. Chapter 3 describes a detailed numerical simulation study to evaluate the impact of initial water saturation on SAGD performance. Chapter 4 further explores the improvement of operating strategy in water rich oil sands reservoirs by using gas co-injection with steam. The conclusions and recommendations arising from the research results are listed in Chapter 5.

Chapter Two: **Literature Review**

2.1 Introduction

In ideal reservoirs, Steam Assisted Gravity drainage (SAGD) is an efficient thermal in-situ process to recover heavy oil and bitumen from oil sands reservoirs. Many large commercial projects in Alberta are using SAGD technology (AER, 2013). The gravity drainage idea was originally conceived by Dr. Roger Butler, a research engineer in Imperial Oil (Esso), in the late 1970s. In the first field test performed in the late 1970s and early 1980s, Esso drilled horizontal production wells and overlying vertical steam injectors into the Clearwater Formation in the Cold Lake oil sand deposit. The results of the Cold Lake pilot suggested that there was potential for economic production from an oil sands reservoir under gravity drainage.

The first commercial SAGD operation was the Foster Creek operation in Alberta Canada, built in 1996. By 2010, Foster Creek had became the largest commercial SAGD project in Alberta to reach royalty payout status. The drilling of up to 1,000 m long horizontal well pairs with their extended reach is inexpensive compared to drilling of many vertical wells to achieve the same contact area. Thus, the relatively low cost of horizontal well pairs and up to 60% recovery factor makes SAGD commercially attractive for oil companies.

In this Chapter, the literature is reviewed on SAGD physics and practice and studies of SAGD performance in challenging reservoir. Given that most companies are not targeting water-rich oil sands reservoirs, the number of published studies on systems with relatively high water saturation throughout the oil column is sparse.

2.2 SAGD – Stages and Basic Physics

The first stage of SAGD is the pre-heating stage where steam is injected at reservoir pressure and the initial mobility of the bitumen in the reservoir surrounding the steam injection and fluid production well pair is raised to the point that a depletion chamber can be established in the reservoir. At original conditions, the viscosity of the bitumen in oil sands is typically greater than 1 million cP. When its temperature is raised to steam temperature (usually greater than 200°C), its viscosity drops to less than 10 cP. In some cases, steam circulation is done at elevated pressure to accelerate heating. Typically steam circulation time is between 3 to 6 months. Start-up period may be accelerated using several different methods, namely cold water dilation, steam dilation, solvent soaking, and electrical heating.

After the interwell region is heated (typically to above 80°C), SAGD mode (the second stage) starts where steam is injected into the top well and fluid production starts in the bottom well which displaces the mobilized oil from the reservoir leading to the creation of a small steam chamber surrounding the well pair. At the edge of the steam chamber, the steam condenses and releases latent heat to the oil sands beyond heating the oil within the oil sand. This result in a liquid water (steam condensate) phase which flows under gravity with the mobilized bitumen to the base of the steam chamber where the production well is located.

In the second stage of SAGD process, the oil rate ramps up due to the expansion of the steam chamber – the larger the chamber, the greater the heat transfer area, and the higher is the oil drainage rate. In typical practice, the ramp up stage, steam is injected into the reservoir at constant pressure. During the ramp-up period the communication zone between the wells is expanded along the full length of the well pair and steam chamber not only grows vertically up to the top of the bitumen zone but it becomes fully established along the well pair. After the steam chamber reaches the top of the oil column, it spreads across the reservoir and a fraction of the energy injected as steam is lost to the overburden. Sometimes injected heat is lost into thief zones but SAGD has an advantage over cyclic steam stimulation because the injection pressure is much lower than fracture pressure to avoid steam breakthrough into thief zones or through the overburden to the surface.

The SAGD process is energy-intensive. With the presence of the overburden, shale layers, and thief zones, only a fraction of the injected energy in the steam is delivered to bitumen which lowers the thermal efficiency of the process. Beyond geological heterogeneity, one of the main reasons for less than ideal thermal efficiency is the presence of water zones or zones with relatively high water saturation (lean oil zones). In systems with relatively large water saturations, a large fraction of the injected energy is transferred to the formation water within the reservoir thus reducing the amount transferred to the oil. This, coupled with the relatively smaller oil content of the reservoir rock, means that the energetics of water-rich systems is poorer than that of oil-rich reservoirs.

Another reason for less than ideal energy efficiency is due to the operation strategy itself. For example, as described above, after steam reaches the overburden, a fraction of the injected heat is lost to the cap rock which despite its energy investment, returns no oil for production. Water-saturated shale barriers imbedded in pay zone also consume the energy of steam without producing oil. Furthermore, if the shale barriers are laterally extensive and/or located close enough to the injection wells, these barriers retard or even stop vertical propagation of the steam chamber and drainage of oil (Su et al. 2013). In field operations, in the absence of sub cool steam-trap control, it is also observed that injected steam can be produced by the production well without delivering heat energy to the oil sands formation. (Ito and Suzuki, 1999; Edmunds, 1998; Gates and Leskiw, 2010).

It is critical that the energy of the steam is directed to the oil sands within the formation. Figure 2.1 shows an example of steam conformance interpreted from seismic data for one of Cenovus SAGD field project. Similar to the image of ConocoPhillips SAGD pilot displayed in Figure 1.6, the image reveals that the steam conformance along SAGD well pairs can be poor (cold spots and non-uniform steam conformance). These results exhibit poor utilization of several of the horizontal well pairs. An analysis by Zhang et al. (2005) of 4D and cross well seismic and production data and the results of the studies reported by Su et al. (2013, 2014) indicate that steam conformance and oil recovery are strongly influenced by reservoir geology.

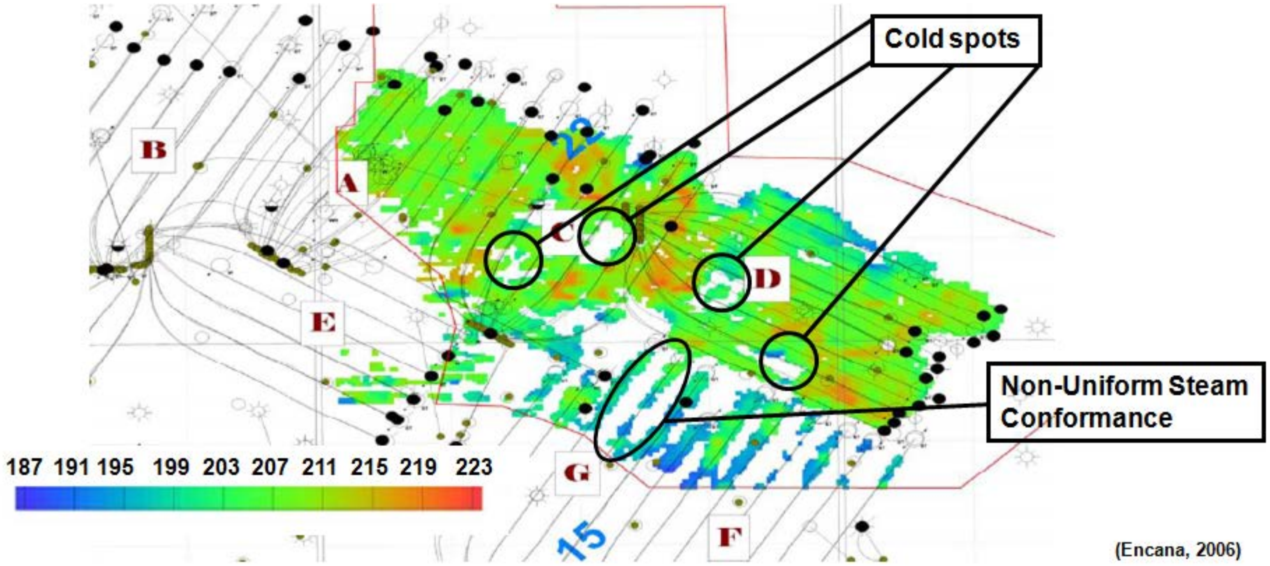

Figure 2.1: SAGD steam conformance from 4D seismic data. Data shows that there are cold spots and non-uniform conformance along well pairs (from EnCana, 2006).

2.3 Studies on the Improvement of SAGD Performance

For improvement of SAGD performance, often as measured by the steam-to-oil ratio (SOR), the oil production rate, and cumulative oil recovered (recovery factor), many reservoir studies have been done using thermal reservoir simulation (Gates and Chakrabarty, 2005; Gotawala and Gates, 2008; Gates, 2008; Stalder, 2010; Su et al. 2013, 2014), laboratory studies and field studies Nasr et al (1997) conducted laboratory experiments with sand packed models and observed better results when they injected a small amount of steam in the producer wells in addition to injector wells. Zhao et al. (2005) conducted physical model experimental tests and simulation to study a gas injection SAGD wind-down process using a stainless steel test cell which represents a 2D slice of a SAGD well pair perpendicular to the wells. The insulated cell was placed inside a pressure vessel and was filled with Ottawa sand which had permeability equal to 115 Darcy and porosity equal to 33%. The lab experiment showed that 12.5% of OOIP could be recovered by a non-condensable gas injection process following the SAGD operation. Oskouei et al. (2010) conducted laboratory SAGD experiments to evaluate the effect of mobile water saturation on SAGD. The results demonstrated that the higher the mobile water saturation, the lower the oil volume produced and the higher is the steam-to-oil ratio.

None have examined the case where SAGD is conducted in a water-rich McMurray Formation oil sands reservoir. In most McMurray Formation oil sands reservoirs that are targets for production, the initial water saturation exceeds 0.85. Most studies in the literature have the general goal of improving one or both of the SOR and recovery factor. This has been done by changing well placement, well configuration, co-injection of solvents or non-condensable gas or both, tubing string adjustments, in-well control devices, or automated control systems to direct steam within the reservoir. Many of the reservoir simulation studies have focused on single SAGD well pair models although pad scale studies are now becoming more common (Su et al. 2014).

Reservoir simulation models are helpful to understand process dynamics and to provide guidance for field development planning as well as sensitivity analysis of multiple parameters on process performance. Oil sands recovery processes are very expensive to test in the field and thus most new technologies are tested in small-scale laboratory physical model experiments and then scaled up to field scale by using reservoir simulation. In the research documented here, a commercial thermal reservoir simulator is used to understand the impact of high initial water saturation on process performance.

Over the past few decades, numerous studies have been done to understand SAGD dynamics and to test operating conditions and injectants (solvent and gas) in analytical, numerical reservoir simulation, laboratory experiments, and field scale pilots.

Butler and Yang (1992) conducted SAGD experiments on two different types of reservoirs, one reservoir with different permeabilities in horizontal layers and another reservoir with thin shale layers. They used two dimensional scaled reservoir model in order to compare the experimental runs with horizontal barriers of different lengths. They concluded that a short horizontal barrier does not affect the SAGD performance but a long barrier decreases the production.

Butler and Chow (1996) used a commercial thermal reservoir simulator (CMG STARS^{TM}) to investigate the feasibility of the SAGD process. The simulator results matched reasonably with the measured data for cumulative oil production, recovery percentage, and temperature profiles in the model at different times.

Butler and Ong (1990) also investigated the impact of wellbore pressure drop and well size on SAGD performance, and they focused on mixed viscosity relationships and hydraulic capacity of the production well. Their research concluded that SAGD performance would be hindered if the

the well has a small diameter which would cause hydraulic losses in the well and twist the liquid interface corresponding to the well pair.

As described by Butler (1997), for process of SAGP, a very high concentration of non-condensable gas accumulates in the steam chamber, particularly near the top, resulting in a lower temperature at the top and it provides a kind of thermal cushion to reduce heat loss to overburden and to achieve higher production. Despite limited field evidence that SAGP may results in lower steam-to-oil ratios (Cenovus, 2012), it remains unclear whether SAGP will support equal or enhanced oil rates when compared to SAGD.

Maini and Heidari (2008) studied the effect of drainage height and permeability on SAGD performance and they concluded that under unsteady state conditions, the production rate vary with respect of different drainage height and permeability. Improvement of SAGD performance has also been studied by introducing a new well configuration.

Since the research documented here is focused on SAGD, process improvements with solvents as well as in-well control devices will not be reviewed here.

In 1995, Kisman and Yeung conducted a reservoir simulation study using properties from the Burnt Lake oil sand area which proved that lower operating pressure decreases oil production but improves the SOR. In 1997, Chan et al. showed through a series of two-dimensional (2D) simulations that smaller injector and producer well spacing gives higher recovery efficiency.

Edmunds and Chhina (2001) conducted series of reservoir simulations and by using economic analyses concluded in favor of low pressure SAGD instead of high pressure SAGD due to the improvement of the cumulative SOR (cSOR is the ratio of cumulative steam injected and cumulative oil produced). Although low pressure operation is more energy efficient, Das (2005) conducted a reservoir simulation study that demonstrated an improvement of SAGD performance with a low pressure operation and that it is more amenable to the application of artificial lift and has benefits of lower H2S generation and reduced silica production in the produced water.

Gates and Chakrabarty (2005) showed through stochastic optimization and thermal reservoir simulation that lower cSOR was obtained when the steam injection pressure was reduced through the operation after the steam chamber contacted the overburden. Since the steam is at saturation conditions, when the steam pressure is lowered, so too is its temperature and thus heat losses to the overburden are reduced when the team injection pressure is reduced. Gates et al. (2007) examined the performance of SAGD in reservoirs with a top gas zone. They showed, by analyzing the flowing steam quality gradient, that altering the steam injection pressure can be used to control heat losses to the top zone.

Many researchers used numerical simulation on a wide scale to investigate the physical process and operation of SAGD. Poliker et al. (2000) used two dimensional simulation studies and proposed a Fast-SAGD process which utilizes additional single horizontal wells (offset wells) alongside the SAGD well pairs and these offset wells operated in a cyclic steam stimulation

(CSS) mode after the steam chamber at the SAGD well pairs has fully developed which helps the steam chamber expand laterally. Bharatha et al (2005) used simulation in order to study the effect of dissolved gas on SAGD process. They concluded that operating pressure is most important factor in reducing the effect of dissolved gas saturation effect. Das (2005) conducted a simulation study and concluded that low pressure operation are more energy efficient and they are more amenable to the application of artificial lift. Shin and Polikar (2006) concluded with help of two-dimensional simulation that Fast-SAGD has a lower cumulative steam-oil ratio and higher oil recovery as much as 34% greater than conventional SAGD. Stalder (2007)'s simulation comparison of SAGD and XSAGD (series of horizontal injection wells placed perpendicular to producer) showed accelerated recovery and higher thermal efficiency in XSAGD.

A research was conducted by Nasr and Korpany (2000) to study the impact of top water and gas caps on SAGD performance. They used CMG STARS^{TM} simulator to predict the field scale performance and it was concluded that gas cap was less effective heat sink as compared to the top water zone based on the differences in thermal conductivity for water saturated and gas saturated sands. Thermal conductivity for water saturated sand is about four times more than for gas saturated sand.

Another interesting research was conducted by Alturki et al. (2011) to examine the feasibility of using SAGD in oil sands reservoir with no caprock and top water zone, They used a reservoir model consists of a shallow Athabasca Oil Sands reservoir with a 94 meter active top water zone.

They studied seven different cases and concluded that larger the top water zone, the worse would be economics of the process and the bitumen recovery would be lower. They also concluded that the key in maintaining and growing the steam chamber is a balance between injection pressure pressure of top water zone. The higher the pressure difference between the top water zone and the steam chamber would result in higher cSOR and lower production rate and recovery.

2.4 Impact of Formation Water on SAGD Performance

Oskouei et al. (2010) laboratory experiments to determine the effect of mobile water saturation on SAGD are among the only results that are available on the effect of water saturation on SAGD performance. As yet, no one has conducted detailed studies of SAGD performance in water-rich McMurray Formation oil sands reservoirs.

In perhaps the only work that examined the effect of intraformational water zones within the oil column, Fairbridge et al. (2012) studied the effect of water zone extent, connectivity, saturation and operating conditions on SAGD performance and water movement within the reservoir during SAGD operation. The two water configurations evaluated by Fairbridge et al. (2012) are displayed in Figure 2.2. They found that that the spatial distribution of water zones within the oil column determined the extent of the effect on well performance. Their results showed that water zones had the potential to seed steam chamber growth since the steam flowed into the water zones faster than that of the oil since the water mobility is much higher than that of the oil. Their results also suggest that the connectivity and extent of intraformational water zones within oil sands reservoirs must be accurately characterized to evaluate their impact on SAGD performance.

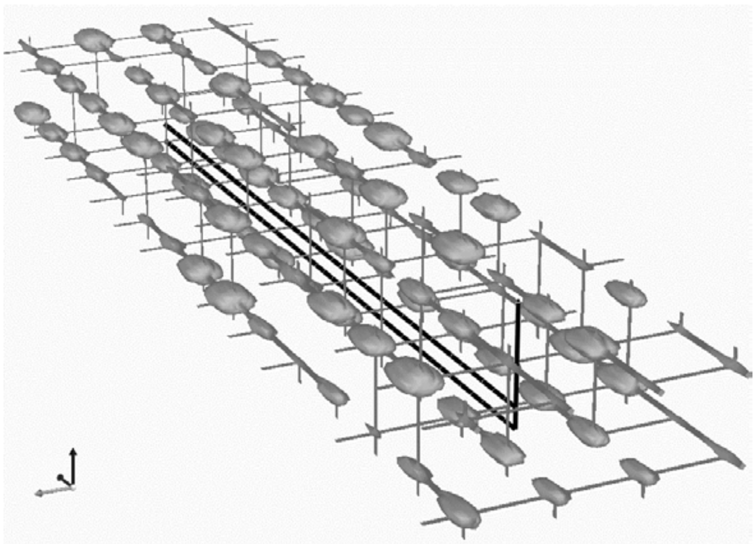

(a)

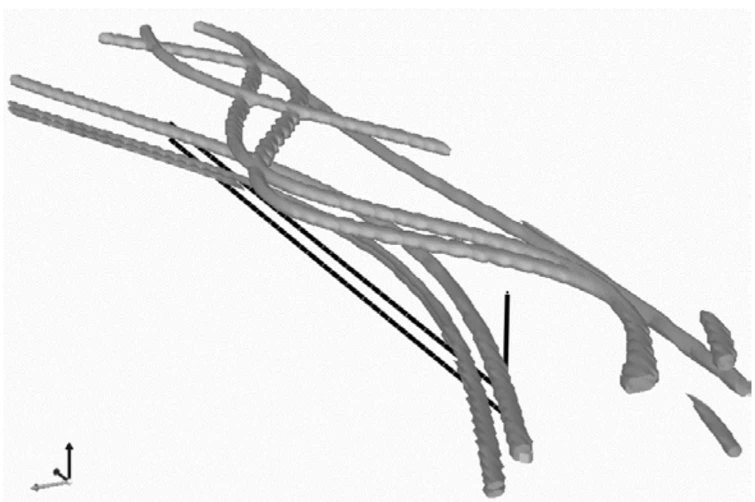

(b)

Figure 2.2: Fairbridge et al.'s (2012) (a) nodal model and (b) channel model of high water saturation zones (indicated by the grey zones within the model). The SAGD injection and production wells are also shown.

2.5 What is missing in the literature today?

Studies on the impact of top gas/water zones and bottom water zones on SAGD performance can be found in the literature (Nasr and Korpany 2000, Gates et al. 2007, Alturki et al. 2011). The effect of initial high water saturation on the SAGD process is essentially unexplored with no publications in the literature on this subject. Thus, given the availability of oil sands reservoir with up to 40% water saturation and higher, there is a need to investigate the impact on SAGD operation and potential simple means to improve process performance to make high water saturation reservoirs economical for commercial projects. This motivated the research documented here in this thesis.

Chapter Three: **Impact of Initial High Water Saturation on SAGD Performance**

3.1 Introduction

The preferred choice for Steam-Assisted Gravity Drainage (SAGD) operations are thick, high permeability, oil-rich reservoirs with no top gas/water or bottom water with a sufficient cap rock to contain the process within the oil reservoir. This is driven chiefly by the economics of the process where thick and oil-rich reservoir imply large amounts of oil (the storage) and high permeability implies injectivity (of steam) and productivity of mobilized oil.

Although most operators target the thickest and most oil-rich and permeable oil formations first for production, there is a large amount of bitumen resource that is impaired due to thin reservoirs, top and bottom thief zones, and high initial water saturation.

The focus of the research conducted for this thesis is on oil sands reservoirs that have relatively high initial water saturation. In this chapter, we examine the impact of initial water saturation on the performance of SAGD well pairs in a heterogeneous reservoir (based on McMurray oil sands Formation). In most cases, in an oil-rich reservoir, the original water saturation in McMurray oil sands reservoirs tends to be between 0.03 and 0.15 (corresponding to an original oil saturation ranging from 0.85 to 0.97).

Reservoirs with high initial water saturations suffer since the oil content of the reservoir is lower and due to relative permeability effects, the oil effective permeability is lower than that encountered in oil-rich reservoirs. If cold production were done, only water would be produced from the reservoir (since the viscosity of the bitumen is typically over 1 million cP).

3.2 Reservoir Simulation Model

For the research documented here, a three-dimensional thermal reservoir simulation model was created from log and core data for the Leismer oil sands area, McMurray Formation, now operated by Statoil and supplied to the Gates Research Group by the prior owner of the oil sands area. The geological model is heterogeneous with porosity, horizontal and vertical permeabilities, and phase saturations varying spatially within the domain.

The grid in the cross-well direction is displayed in Figure 3.1. The grid block dimensions in the vertical direction are listed in the caption of Figure 3.1. The total thickness of the reservoir is equal to 22 m. The reason that the grid block dimensions varied was due to the underlying geology of the reservoir as determined from the logs. The dimensions of the grid blocks in the cross-well direction are equal to 1 m.

Two SAGD well pairs are located in the model – one is positioned at the left boundary whereas the other is located at the right boundary. The top wells are the injection wells and the bottom wells are the production wells. The left and right boundaries are symmetry boundaries so as to model the behavior of the two well pairs among a pad of wells. Both SAGD well pairs are positioned vertically at the same depths – the production wells are located 2 m above the base of the reservoir. The injection wells are positioned 5 m above the production wells.

Figure 3.2 shows the grid arrangement in the down-well direction. In the down-well direction, the grid block dimensions were set equal to 3.33 m. The total length of the reservoir simulation model is equal to 900 m whereas the length of the well pairs is equal to 700 m. Beyond the ends of the well pairs are 100 m long zones. In total, the grid blocks number 101 in the cross-well direction, 270 in the down-well direction, and 28 in the vertical direction. This gives a total number of grid blocks equal to 763,560.

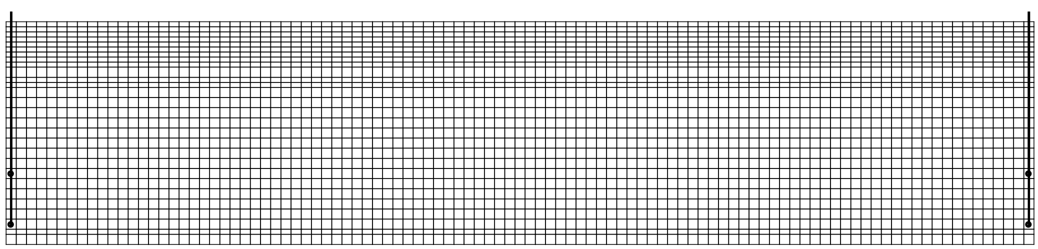

Figure 3.1: Arrangement of grid blocks in the cross-well direction. In the vertical direction, from the bottom, the grid block dimensions are 1 m, 0.5 m, 14 x 1 m, 2 x 0.5 m, 1 m, 9 x 0.5 m. In the down-well direction, the grid blocks are 3.33 m long. In the cross-well direction, the grid blocks have dimension equal to 1 m.

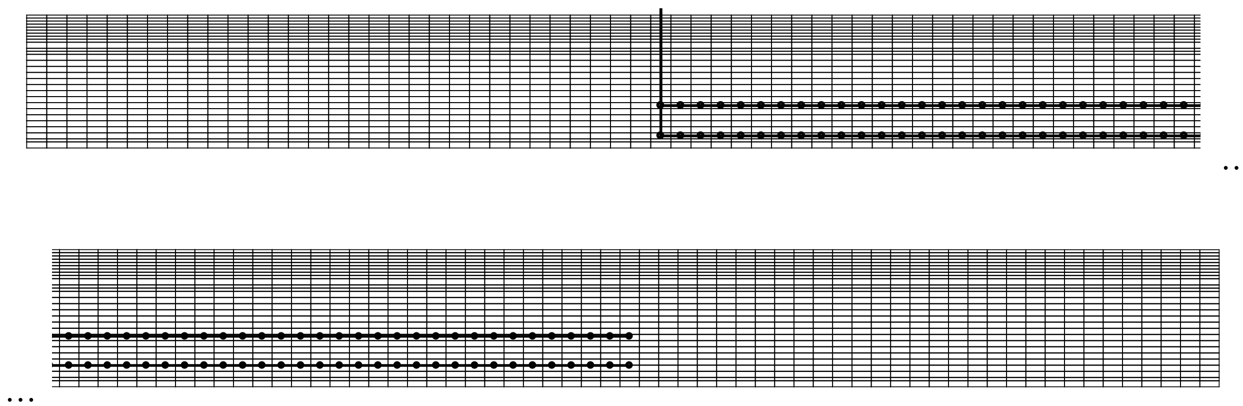

Figure 3.2: Arrangement of grid blocks in the down-well direction – the top image displays the heel end whereas the bottom image shows the toe end of one of the SAGD well pairs. In the down-well direction, the grid blocks are 3.33 m long. The total length of the reservoir domain is equal to 900 m. The length of the well pairs is equal to 700 m.

Figure 3.3 displays views of the porosity distributions (in the 3D view, the reservoir model is partially transparent so the left SAGD well pair is visible. The images show that there are layers with zero and relatively low porosity (dark blue ones are equal to zero whereas light blue ones are equal to about 0.09) and others with relatively high porosity (up to 0.3822). The average porosity is equal to 0.3076 which is typical of that of McMurray Formation oil sands reservoirs.

Figure 3.4 shows views of the horizontal permeability distribution. The horizontal permeability ranges from zero (corresponding to the zero porosity intervals) up to about 8.5 D. The average value of the horizontal permeability is equal to about 3 D which is typical of an Athabasca oil sands reservoir. The vertical to horizontal permeability ratio is set equal to 0.25. This means that the vertical permeability distribution is the same as the horizontal permeability one except the values in the scale are multiplied by 0.25.

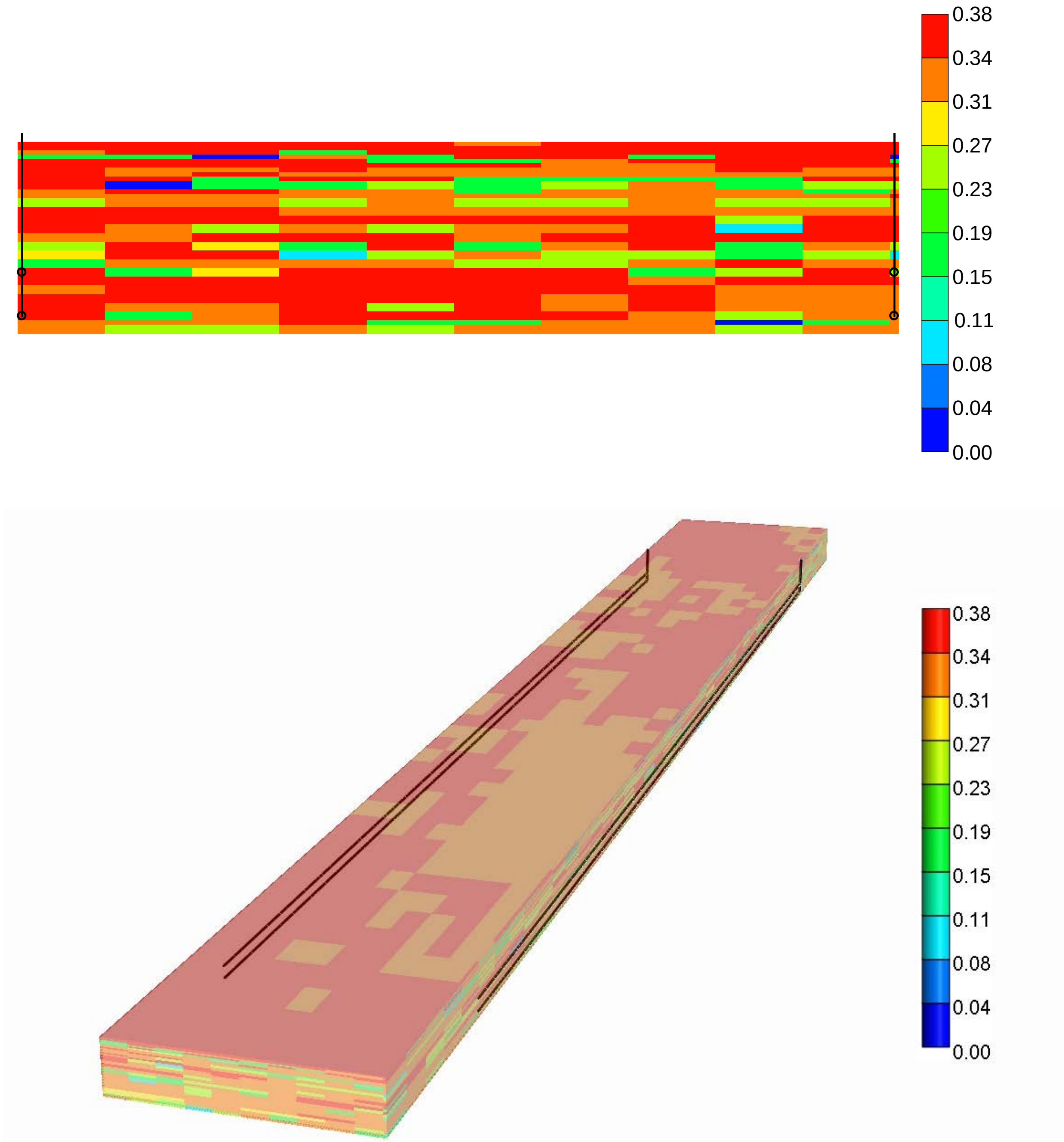

Figure 3.3: Porosity distributions in the cross-well plane at the mid-point of the well pairs and three-dimensional view of the porosity distribution.

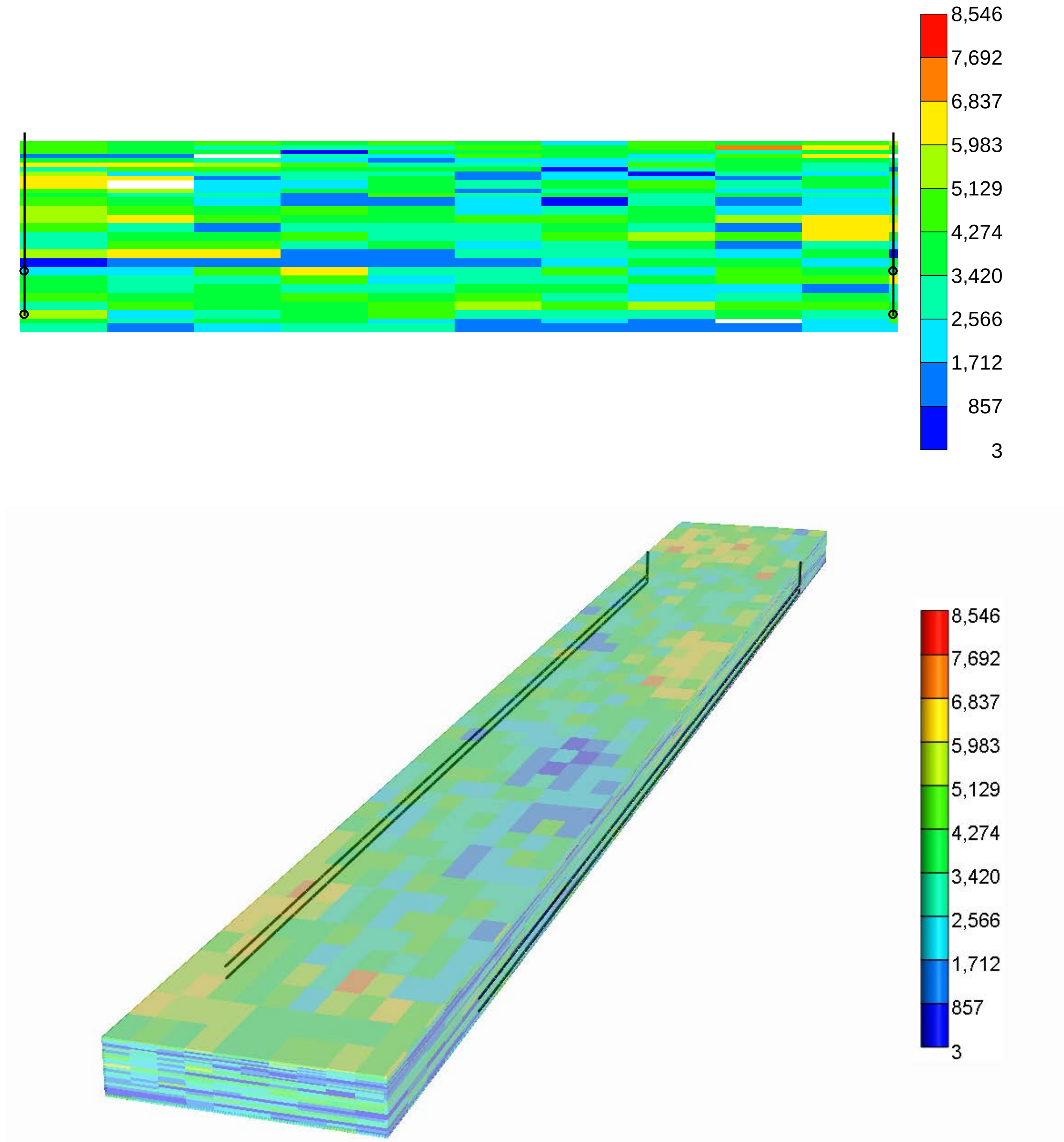

Figure 3.4: Horizontal permeability distributions, in D, in the cross-well plane at the mid-point of the well pairs and three-dimensional view of the horizontal permeability distribution.

The horizontal permeability distribution shows the presence of relatively tight streaks within the reservoir. These, physically, correspond to shale layers. From examination of the permeability in the cross-well view, the tight streaks dip, to some extent, in the left to right direction corresponding to shale layers originating from a point bar deposit.

Figure 3.5 displays views of the initial oil saturation for the base case reservoir. With the exception of the zero porosity grid blocks, the minimum oil saturation of the base case reservoir model is equal to 0.5646. The maximum oil saturation in the model is equal to 0.9493. The average value of the oil saturation is equal to 0.8235. The initial oil saturation distributions reveals that there a slightly richer oil zone roughly two-thirds up the reservoir height with thickness, on average, equal to about 7 m. The oil saturation tends to be slightly lower towards the lower half of the domain and at the extreme top of the reservoir model.

Since the initial gas saturation in the model is equal to zero, the initial water saturation of the base case reservoir is the complement of the oil saturation, displayed for completeness in Figure 3.6. The minimum water saturation in non-zero porosity grid blocks is equal to 0.0507 whereas the maximum value is equal to 0.4354. The average water saturation in the base case is equal to 0.1765. In the reservoir model, there is no top gas/water or bottom water zone.

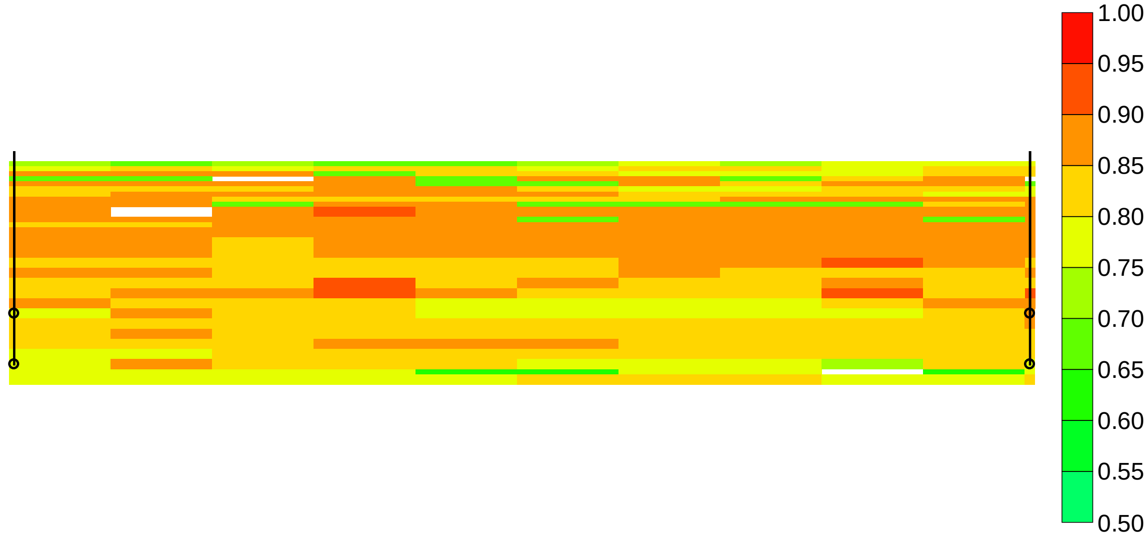

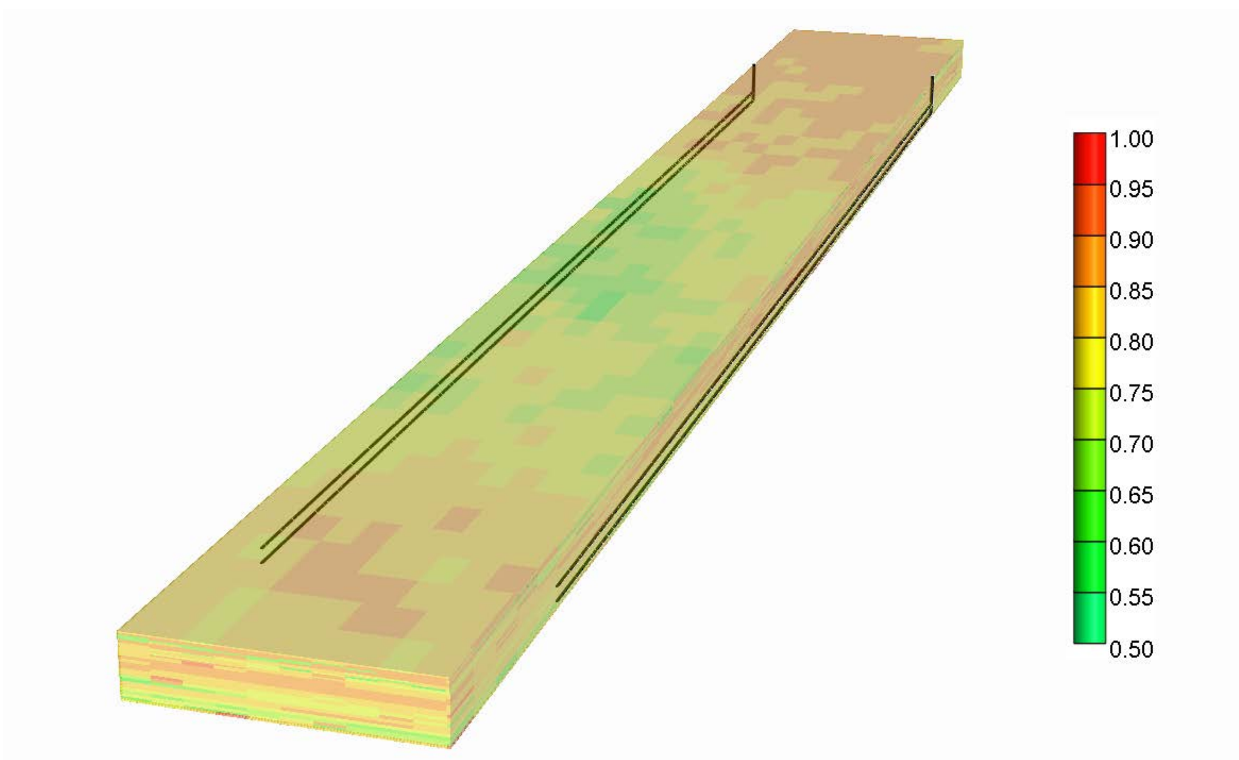

Figure 3.5: Base case initial oil saturation distributions in the cross-well plane at the mid-point of the well pairs and three-dimensional view of the oil saturation distribution. Note that the color scale starts at 0.5.

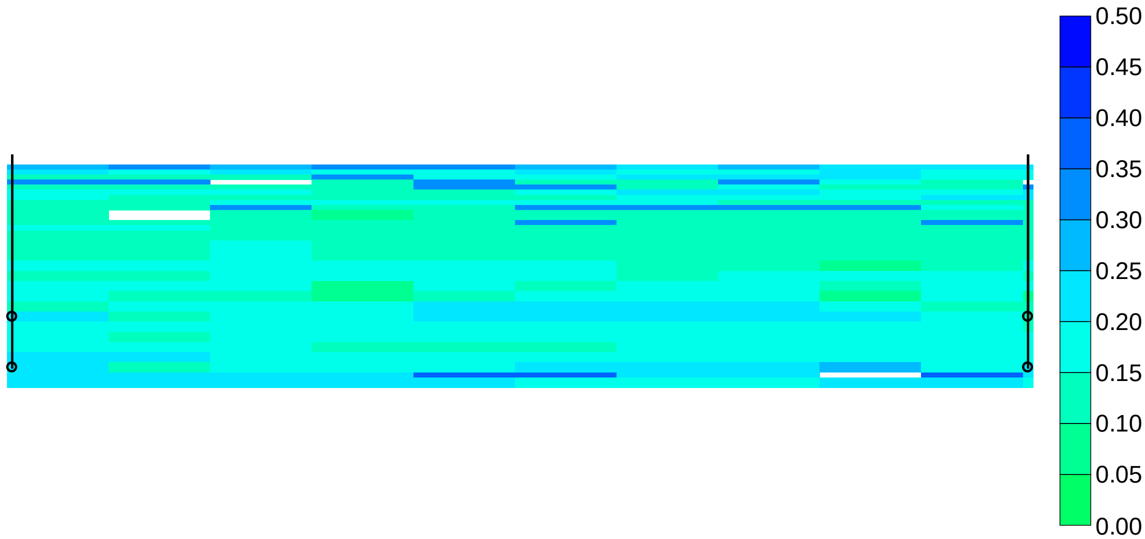

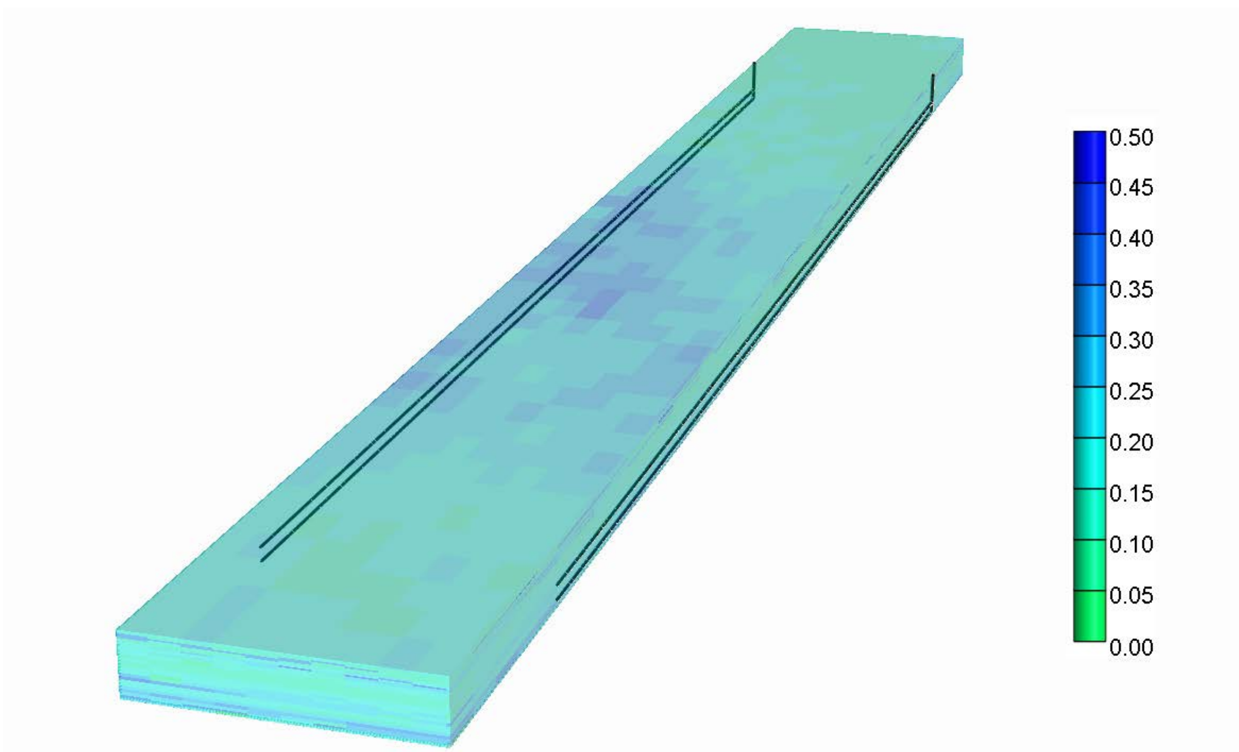

Figure 3.6: Base case initial water saturation distributions in the cross-well plane at the mid-point of the well pairs and three-dimensional view of the oil saturation distribution. Note that the color scale ends at 0.5.

To summarize, the average properties of the base case reservoir, as well as other properties of the reservoir model are listed in Table 3.1. All of the properties are typical of that of a McMurray Formation oil sands reservoir. The depth of the oil sands reservoir is equal to 375 m. The initial pressure of the oil sands formation is equal to about 2,700 kPa.

The relative permeability curves are also listed in Table 3.2. The relative permeability curves were taken from history-matched curves for the UTF Phase B SAGD pilot (Good et al. 1997). The UTF Phase B SAGD pilot was conducted in the McMurray Formation. The curves suggest that the reservoir rock is water wet. In the model, the capillary pressure is assumed to be much smaller than that of viscous, gravity and pressure forces since the bitumen is viscous and at higher temperatures where the oil becomes mobilized, the interfacial tension becomes small.

Table 3.1: Average properties of the reservoir model.

Property	**Value**
Depth to reservoir top, m	375
Net pay, m	22
Pressure at 397 m, kPa	2,670
Temperature, °C	15
Porosity, fraction	0.3076
Initial oil saturation, $S_{oi,}$ fraction	0.8235
Horizontal permeability, k_h, D	3
Vertical permeability, k_v, D	0.75
Effective rock compressibility, 1/kPa	$14e^{-6}$
Rock heat capacity, kJ/m^3 °C	2,350
Rock thermal conductivity, kJ/m day °C	660
Oil thermal conductivity, kJ/m day °C	12.5
Water thermal conductivity, kJ/m day °C	53.5

Table 3.2: Relative permeability curves.

Oil-water relative permeability curves	Sw	Krw	Krow
	0.15	0	0.992
	0.2	0	0.979
	0.25	0.0004	0.95
	0.3	0.0012	0.72
	0.35	0.0029	0.6
	0.4	0.0057	0.47
	0.45	0.0098	0.35
	0.5	0.0156	0.24
	0.55	0.0233	0.165
	0.6	0.0331	0.11
	0.65	0.0456	0.07
	0.7	0.0606	0.04
	0.75	0.0787	0.015
	0.8	0.1	0
	0.85	0.1251	0
	0.9	0.1537	0
	0.95	0.1866	0
	1	0.2237	0
Gas-oil relative permeability curves	So	Sl1	Krg
	0.005	0.155	1
	0.0575	0.2075	0.95
	0.11	0.26	0.84
	0.1625	0.3125	0.72
	0.215	0.365	0.6
	0.2675	0.4175	0.47
	0.32	0.47	0.35
	0.3725	0.5225	0.24
	0.425	0.575	0.165
	0.4775	0.6275	0.093
	0.53	0.68	0.075
	0.5825	0.7325	0.045
	0.635	0.785	0.027
	0.6875	0.8375	0.02
	0.74	0.89	0.01
	0.7925	0.9425	0.005
	0.845	0.995	0
	0.8975	1	0

At the edges of the steam chamber, the heated oil sand there thermally expands. This leads to dilation of the oil sands at the edge of the chamber. This effect has been modelled by using the Beattie-Boberg-McNab (1991) dilation-recompaction model where the porosity of the oil sands depends on the pore pressure in the formation. Figure 3.7 shows a graphical depiction of this model. The model was developed to deal with steam fracturing of heavy oil and oil sands reservoir by Imperial Oil in high pressure and high temperature steam injection processes such as Cyclic Steam Stimulation (CSS).

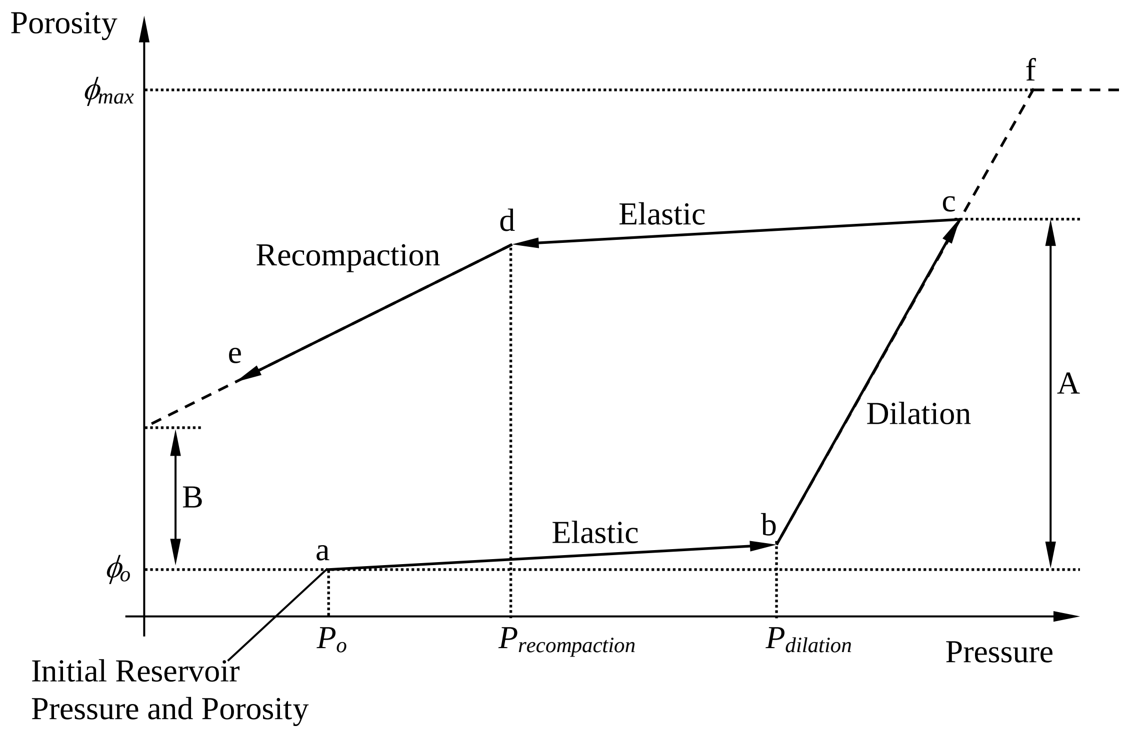

Figure 3.7: Beattie et al. (1991) dilation-recompaction model.

In the reservoir model developed here, the dilation pressure, $P_{dilation}$, corresponds to the fracture pressure of the reservoir which for this reservoir is of order of 8 MPa. In the cases studied here, the injection pressure never reaches this value and thus, the reservoir is not fractured. During steam injection, the pressure and porosity path remains on the a-b line drawn in Figure 3.7. The rock compressibility is for this line is listed in Table 3.1. After the porosity rises, the permeability is given by (Gates, 2013):

$$\frac{k}{k_0} = e^{k_{mul}\frac{\phi-\phi_0}{1-\phi_0}} \qquad 3.1$$

where k_0 is the original permeability, k_{mul} is a multiplier, and ϕ_0 is the original porosity. In the model used here, the value of the multiplier, in all directions is equal to 5. This value is typical of values used to represent dilation at the edges of steam chambers.

For the overburden and understrata, they are assumed to be perfect seals with zero permeability. Heat losses into the overburden and understrata are modelled by using the Vinsome and Westerveld (1980) heat loss model. The heat capacity and thermal conductivity of the overburden and understrata rock is the same as that in the reservoir as listed in Table 3.1.

3.3 Fluid Components

For water and steam properties, the internal databases from the thermal reservoir simulator, CMG STARS^{TM}, (CMG, 2013), was used. The solution gas was represented by methane. For the bitumen, a two component oil was used based on viscosities of the oil at the top and bottom of the reservoir. The viscosities of the top and bottom oils, as well as the liquid equivalent viscosity of the solution gas, versus temperature are listed in Table 3.3 (the reservoir simulator requires for the viscosity mixing rule that the viscosity of the solution gas is a liquid-equivalent viscosity that when the solution gas is mixed with the oil given the correct live oil viscosity).

The viscosities were obtained from experimental measurements which were then fitted to the Walther viscosity-temperature correlation:

$$\ln \ln (\mu + 0.7) = A \ln (T + 273.15) + B \qquad 3.2$$

Table 3.3: Viscosities of top and bottom oil components and liquid-equivalent viscosity of the solution gas components.

Temperature, °C	Top Oil Viscosity, cP	Bottom Oil Viscosity, cP	Solution Gas Liquid Equivalent Viscosity, cP (Gates and Chakrabarty, 2006)
5	4523614	14627862	1.15E+02
12	1246217	4420687	9.81E+01
20	336922.9	1291722	6.84E+01
30	81167.38	331656	5.41E+01
40	23833.29	100864.6	4.34E+01
50	8256.561	35419.21	3.52E+01
60	3286.742	14062.17	2.89E+01
70	1471.423	6203.039	2.40E+01
80	727.8683	2996.271	2.01E+01
90	392.1015	1565.645	1.70E+01
100	227.2724	875.9733	1.46E+01
110	140.3285	520.2501	1.26E+01
120	91.5278	325.5854	1.09E+01
130	62.6183	213.3676	9.56E+00
140	44.6674	145.6378	8.43E+00
150	33.0524	103.0622	7.49E+00
160	25.2599	75.3141	6.70E+00
170	19.8623	56.6375	6.03E+00
180	16.0164	43.6994	5.46E+00
190	13.2065	34.5021	4.97E+00
200	11.107	27.8104	4.55E+00
210	9.5067	22.8386	4.18E+00
220	8.2649	19.0741	3.86E+00
230	7.2855	16.1745	3.58E+00
240	6.5019	13.9058	3.34E+00
250	5.8666	12.1056	3.12E+00
260	5.3454	10.6583	2.93E+00
270	4.9132	9.4811	2.76E+00
280	4.5512	8.5129	2.61E+00

The viscosity variation of many oil sands reservoirs has been observed and at initial conditions, the ratio of the viscosity of the top oil to that of the bottom oil is typically between 1:2 to 1:10 (Gates et al. 2008). A graded viscosity distribution is used in the model, displayed in Figure 3.8. In the fluid model used here, the top oil, at initial reservoir conditions, has a viscosity equal to about 450,000 cP. The viscosity of the oil at the bottom of the reservoir has a viscosity equal to about 1.5 million cP.

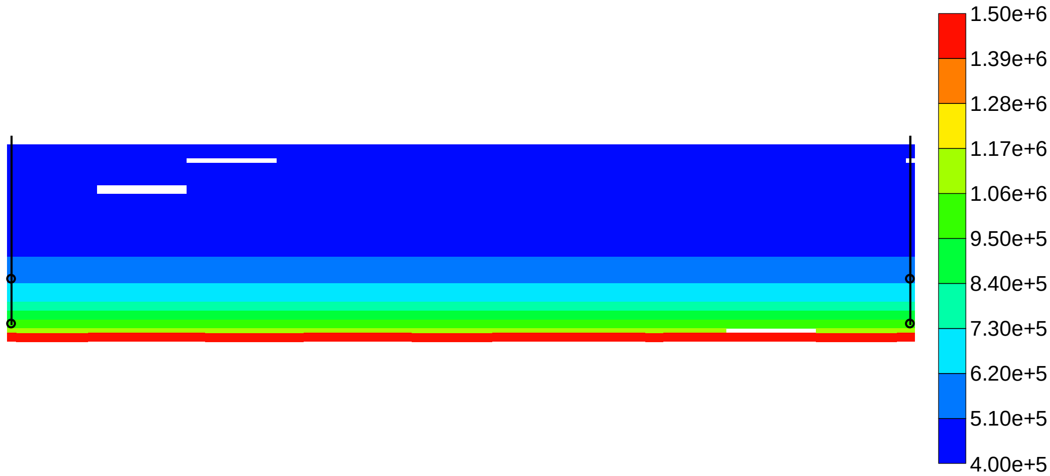

Figure 3.8: Initial oil phase viscosity distribution in the cross-well plane mid way through the SAGD well pairs. The white grid blocks correspond to zero porosity grid blocks.

To obtain the graded viscosity profile in the reservoir model, the mole fractions of the top and bottom oil components, and solution gas, are listed in Table 3.4. The solution gas mole fraction corresponds to a solution-gas ratio equal to about 3 m^3/m^3. The live oil phase viscosity is given by the logarithmic mixing rule:

$$\ln \mu_{oilphase} = x_{TOIL} \ln \mu_{TOIL} + x_{BOIL} \ln \mu_{BOIL} + x_{C1} \ln \mu_{C1}$$

where *TOIL*, *BOIL*, and *C1* refers to the top oil, bottom oil, and solution gas, respectively.

Table 3.4: Viscosities of top and bottom oil components and liquid-equivalent viscosity of the solution gas components.

Grid block center depth, m	Top oil mole fraction	Bottom oil mole fraction	Solution gas mole fraction
375.5	0.9246	0.0154	0.06
376.5	0.9246	0.0154	0.06
377	0.9246	0.0154	0.06
378	0.9246	0.0154	0.06
379	0.9246	0.0154	0.06
380	0.9246	0.0154	0.06
381	0.9246	0.0154	0.06
382	0.9246	0.0154	0.06
383	0.9246	0.0154	0.06
384	0.9246	0.0154	0.06
385	0.9246	0.0154	0.06
386	0.921	0.019	0.06
387	0.9145	0.0255	0.06
388	0.9047	0.0353	0.06
389	0.8912	0.0488	0.06
390	0.8736	0.0664	0.06
391	0.8514	0.0886	0.06
391.5	0.8241	0.1159	0.06
392	0.7912	0.1488	0.06
393	0.752	0.188	0.06
393.5	0.7056	0.2344	0.06
394	0.6512	0.2888	0.06
394.5	0.5875	0.3525	0.06
395	0.5126	0.4274	0.06
395.5	0.4242	0.5158	0.06
396	0.3183	0.6217	0.06
396.5	0.187	0.753	0.06
397	0	0.94	0.06

The molecular weights and critical properties for the top and bottom oils are 406.7 g/mol, 1,478 kPa and 618.85°C and 1092.8 g/mol, 792 kPa and 903.85°C, respectively. The solubility of the solution gas in the oil phase is dictated by K-values which are given by the correlation:

$$\text{K-value} = (K_{v1} / P) \exp[K_{v4} / (T + K_{v5})]$$

where K_{v1} = 5.45x10^5 kPa, K_{v4} = -879.84°C, and K_{v5} = -265.99°C (CMG, 2013). The top and bottom oil densities are equal to 983.2 and 1,158 kg/m^3.

3.4 Well Constraints

Prior to SAGD production mode, the injection and production wells are operated as steam circulation wells. This is modelled by inserting temporary line heaters (operated at 200°C) in the locations of the injection and production wells. In the field, when steam circulation is done, thermally expanded oil expands into the wells and is produced to the surface. Here, to relieve the pressure due to thermal expansion, the production wells and temporary production wells positioned in the locations of the injection wells are operated with a minimum bottom hole pressure equal to the initial reservoir pressure at the depths of the wells. In the model, steam circulation is operated for three months.

After the pre-heating stage, the line heaters are removed and the temporary production wells in the locations of the injection wells are removed. Thereafter, SAGD operation mode starts with steam injected into the oil formation through the top wells and fluids produced from the bottom wells. For the models evaluated here, for the injection wells, the steam injection pressure is set equal to 4,000 kPa (corresponds to saturated steam injection temperature equal to 250.36°C). The steam quality at the sand face is taken to be equal to 0.95.

For the production wells, the maximum steam rate is constrained to 1 m^3(cold water equivalent, CWE) per day. This production well constraint mimics steam trap control by limiting the amount of live steam production from each well pair. All steam volume reported here are cold water equivalent.

3.5 Cases

For the study reported here, three cases were studied including the base case. The second and third cases were the same as the base case except that the water saturation was raised to an average value of 0.35 and 0.44, respectively. To compare the models on the same scale, the water saturation distributions for the mid cross-well plane are displayed in Figure 3.9. Despite the change of the initial water saturation, for all models, the oil and water relative permeability curves remained unchanged.

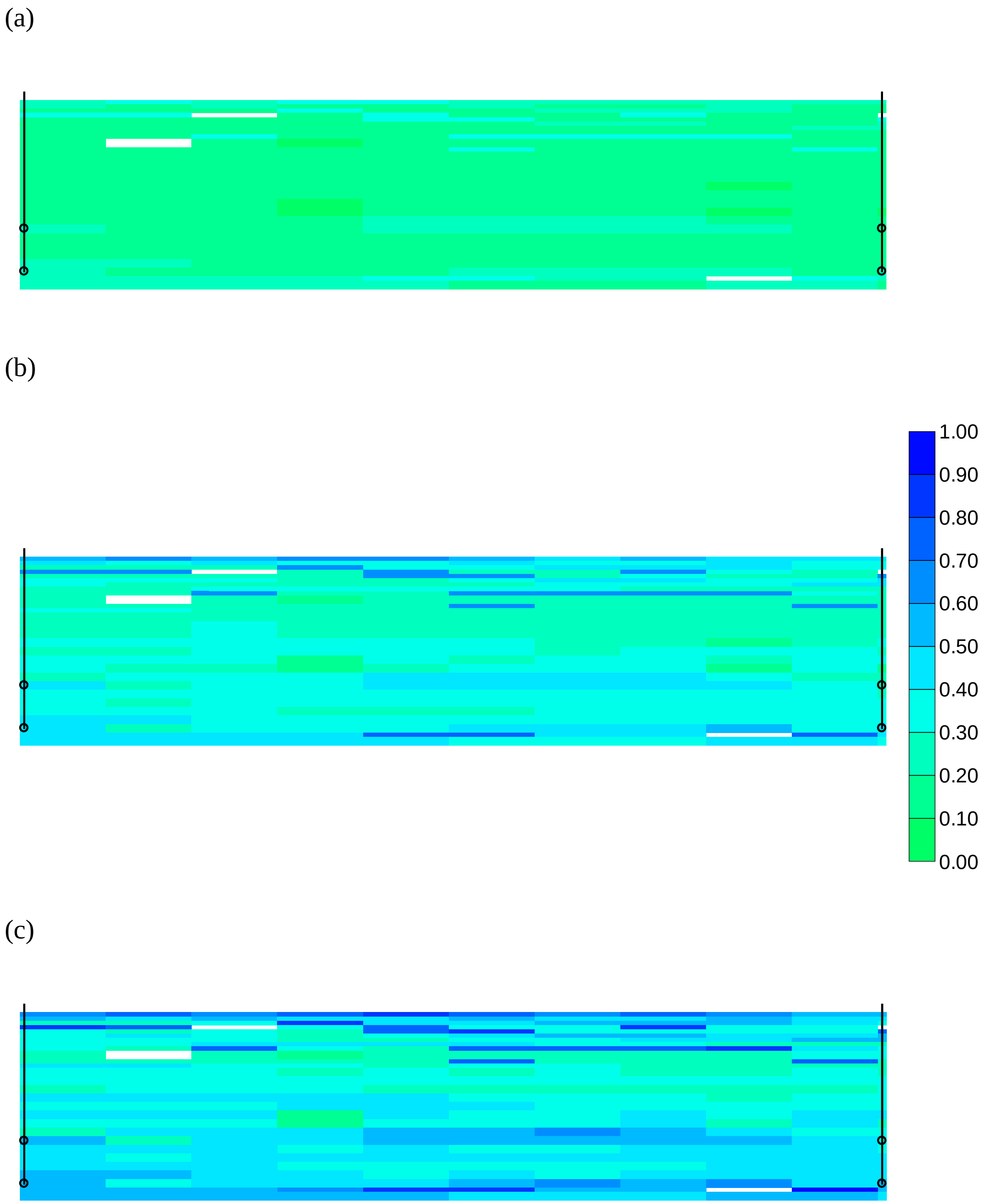

Figure 3.9: Initial water saturation distributions in the cross-well plane midway through the SAGD well pairs for the (a) 0.1765, (b) 0.35, and (c) 0.44 cases. The white grid blocks correspond to zero porosity grid blocks.

All cases were run by using the CMG STARS^{TM} thermal reservoir simulator (CMG, 2013). This reservoir simulator is a leading thermal reservoir simulator for SAGD simulation and has been used extensively in research and industrial environments to evaluate SAGD operations. STARS^{TM} is essentially a finite volume thermal reservoir simulator that solves the components mass balances, energy transfer, phase behaviour, and multiphase flow (Darcy's law) in porous media. A full description of the STARS^{TM} simulator and governing equations, discretization, and time stepping is listed in the CMG User's Manual (CMG, 2013). Each simulation case was run in parallel using 8 cores on a 16 core workstation (3.47 GHz processors) and took on average about 2.5 weeks to simulate 10 years of SAGD operation.

3.6 Results and Discussion

Figure 3.10 displays the effect of initial water saturation on the total cumulative steam injected and cumulative water produced. The individual cumulative volumes for each well pair are shown in Figure 3.11. The results reveal that the higher the initial water saturation, the higher the steam injected and consequently, the larger the volume of water produced. In the lower water saturation case (S_{wi} = 0.1765), the results are consistent with field operations where the SAGD well pair is sealed and the cumulative produced water volume is slightly below that of the cumulative steam injected. At higher initial water saturations, the results shift and the cumulative injected water is lower than the cumulative water produced. This suggests that formation water is being produced from the reservoir with the steam condensate. This is similar to the field results from ConocoPhillips Surmont SAGD pilot where the produced water is higher than the injected steam due to the presence of a overlying water zone above the oil column. The results shown in Figure 3.11 reveal that the individual well pairs exhibit different steam injection and water production behaviours. This is caused by the heterogeneity of the formation. The results suggest that despite the difference of the initial water saturation, the difference between the cumulative injected steam and produced water volumes between the left and right well pairs does not change significantly.

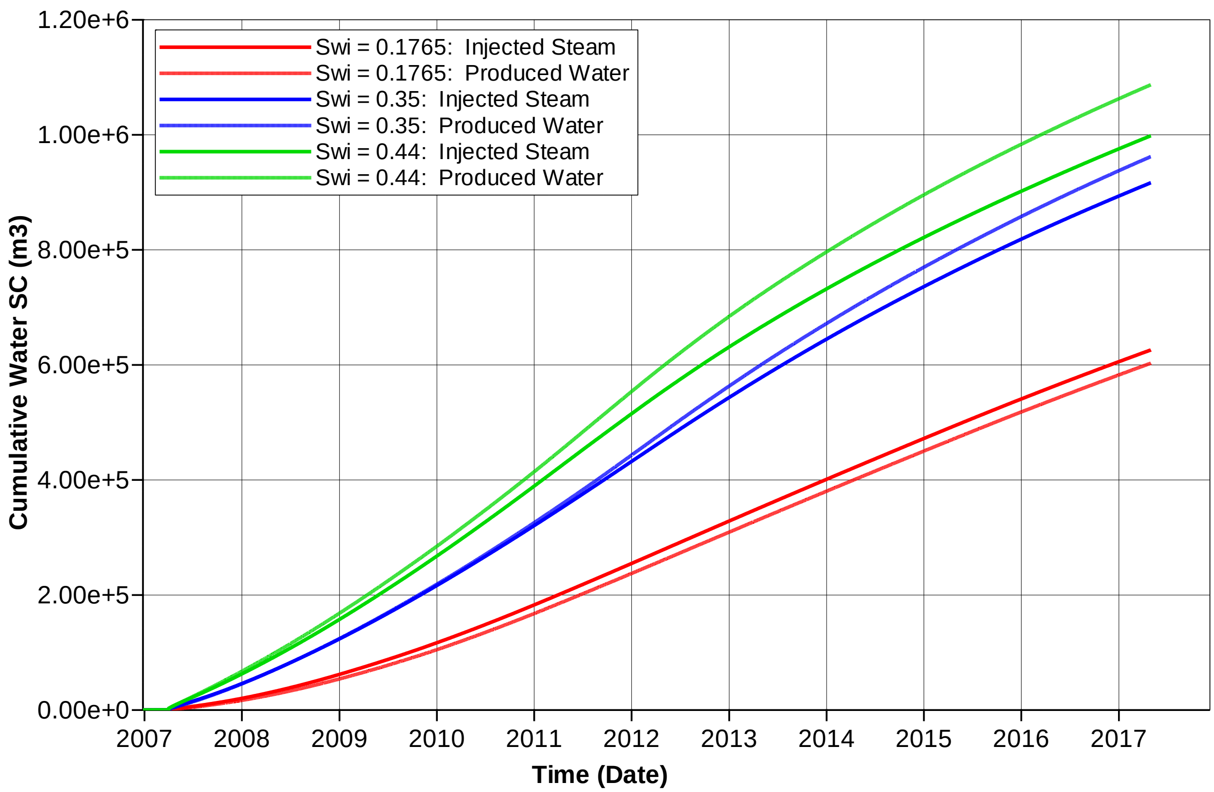

Figure 3.10: Effect of initial water saturation on total cumulative steam injected and cumulative water produced.

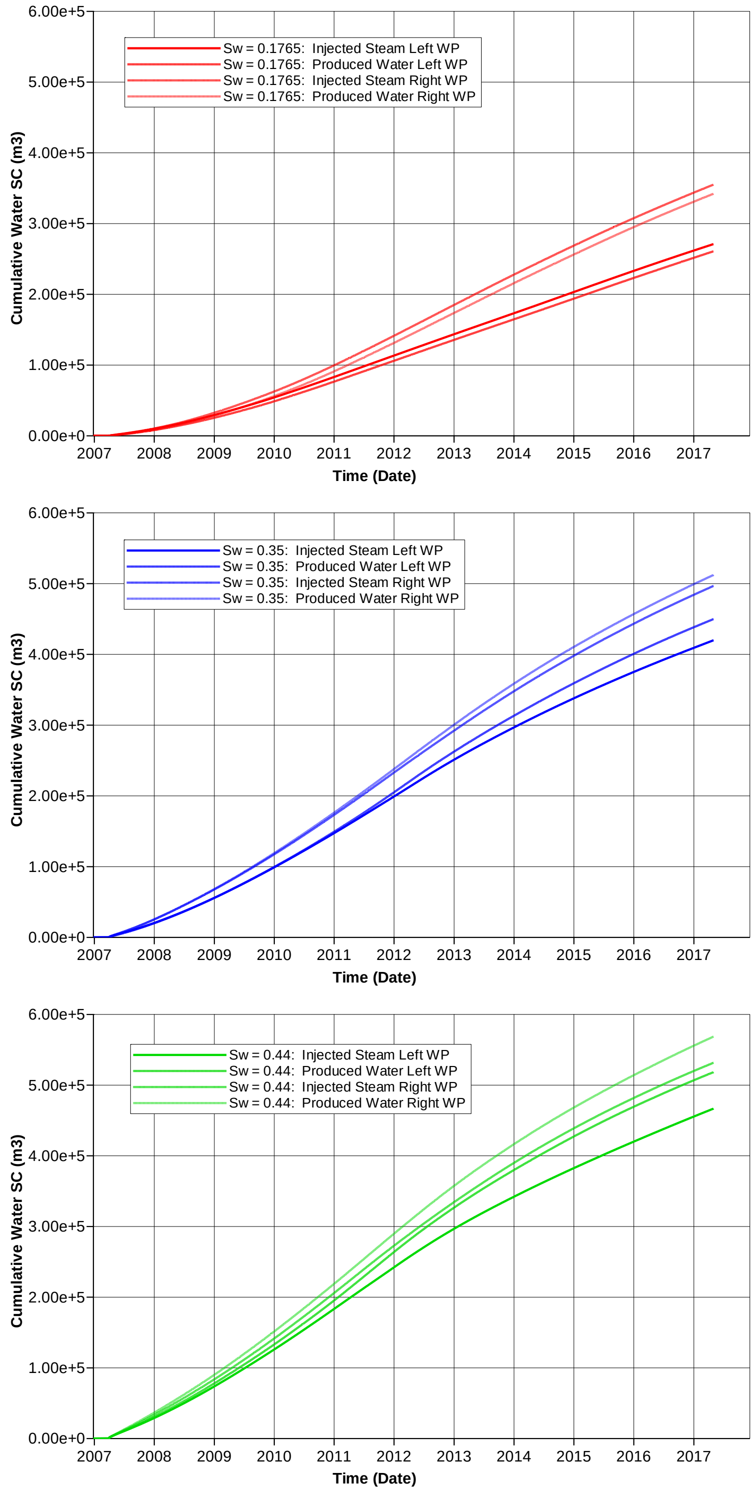

Figure 3.11: Effect of initial water saturation on cumulative steam injected and cumulative water produced for each well pair.

Figure 3.12 presents the total cumulative produced oil volumes from the three cases. The results reveal that surprisingly, the cumulative oil produced from the 0.1765 and 0.35 initial water saturation cases are similar whereas the 0.44 initial water saturation case is lower than the other two cases. It would be expected that the higher the initial water saturation, the lower the cumulative oil produced yet up to initial water saturation equal to 0.35, the cumulative oil produced is similar. Given the results in Figure 3.10, however, it requires substantially more steam in the 0.35 initial water saturation case to achieve this volume of oil. Since the oil content of the reservoir is lower, in the 0.44 initial water saturation case, even with larger steam injection volumes than the other two cases, the cumulative oil volume produced drops.

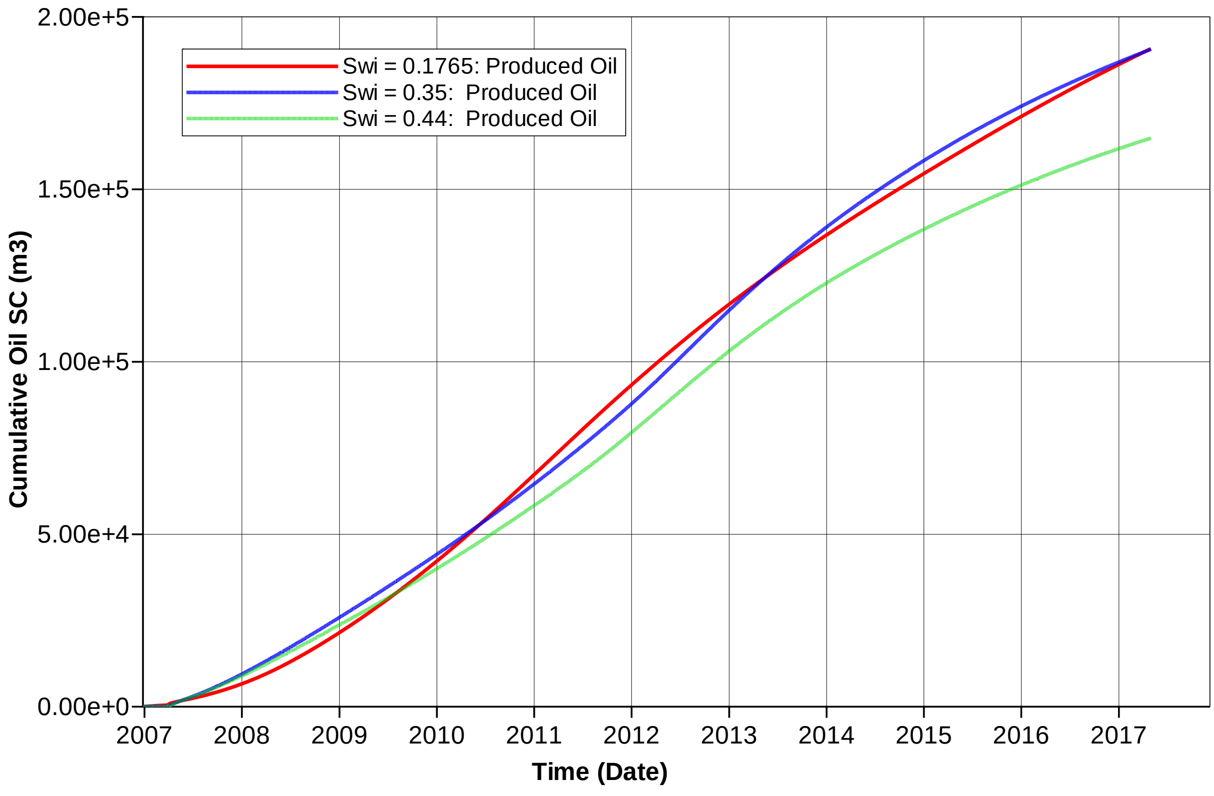

Figure 3.12: Effect of initial water saturation on total cumulative oil produced.

Figure 3.13 displays the effect of the initial water saturation on the cumulative oil produced from each well pair. The results demonstrate the strong effects of heterogeneity on the performance of the well pairs. At the lowest initial water saturation case, the spread between the cumulative produced oil volumes of the two wells is largest whereas as the initial water saturation rises, the difference between the performances of the left and right well pairs diminishes. This suggests that the performance becomes more uniform between the well pairs as the initial water saturation increases. Given that the relative permeability curves are unchanged among the three cases, the higher the initial water saturation, the lower is the mobile oil saturation interval.

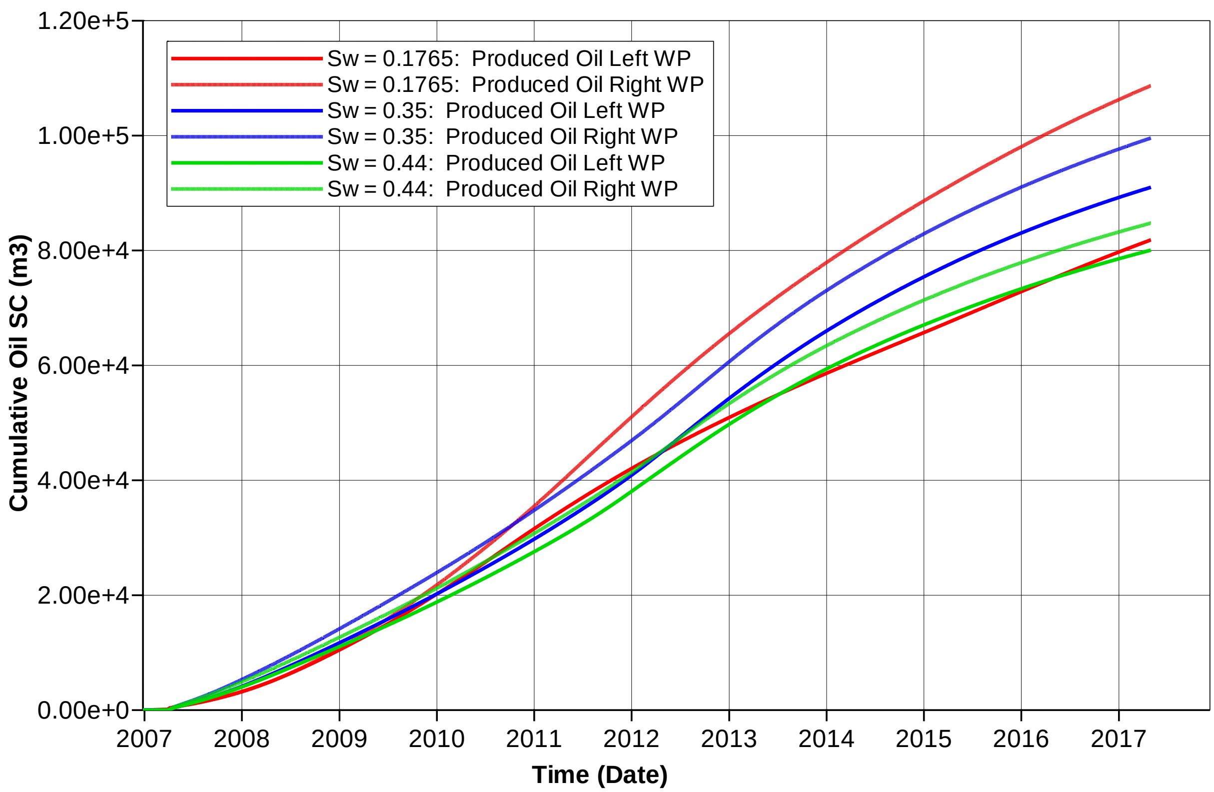

Figure 3.13: Effect of initial water saturation on cumulative oil produced for each well pair.

Figure 3.14 shows profiles of the cumulative steam-to-oil ratio (cSOR, steam expressed as cold water equivalent, CWE) for the left and tight SAGD well pairs versus the initial water saturation. The cSOR, at a given point of time, is equal to the ratio of the cumulative steam injected to the cumulative oil produced from an individual well pair. The results show that the higher the initial water saturation, the higher is the cSOR. For the left well pair, at the lowest initial water saturation, the cSOR profiles achieve an cSOR equal to about 3.0 m^3/m^3 by 2008 but then dip as low as about 2.6 m3/m3 by 2012 and then rise to 3.3 m^3/m^3 after 10 years of operation. These results are typical of McMurray Formation reservoirs with similar porosity, permeability, and initial oil saturation. For the right well pair, the results are slightly higher at throughout the operation but result in about the same cSOR after 10 years of operation. At 0.35 initial water saturation, the cSOR profiles for both of the well pairs are just under 5.0 m^3/m^3. At the highest initial water saturation case, the cSOR profiles tends to achieve about 6.7 m3/m3 in the first few years and then drops to between 5.7 and 6.2 m^3/m^3 for the left and right well pairs, respectively. The results reveal that despite the difference in cumulative steam injected and water and oil produced of the well pairs that arises from reservoir heterogeneity, the cSOR profiles between the well pairs at a given initial oil saturation are similar.

The results suggest that the process is thermally more efficient at lower initial water saturation which is to be expected given that both the oil content in the reservoir and oil relative permeability are higher at lower initial water saturations.

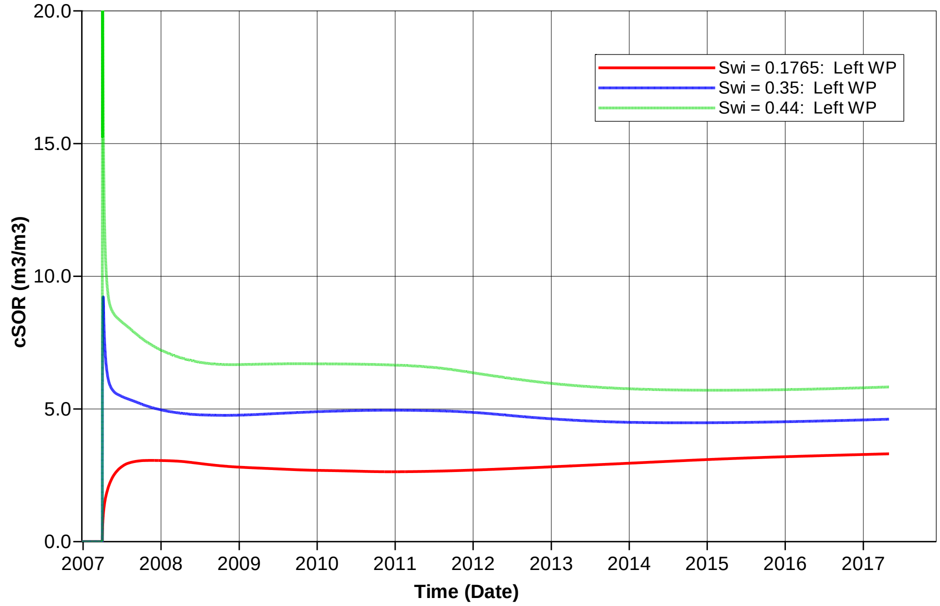

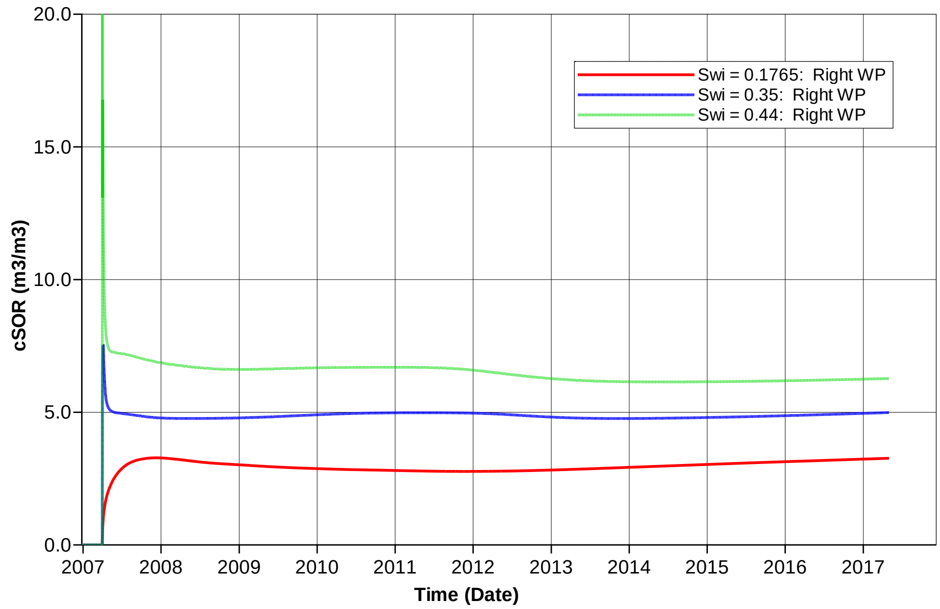

Figure 3.14: Effect of initial water saturation on cumulative steam-to-oil ratio for each well pair.

For completeness, Figures 3.15, 3.16, and 3.17 present the injected steam rates, produced water rates, and produced oil rates, respectively, for the left and right SAGD well pairs. The steam injection rates vary to realize the constant steam injection pressure set as a well constraint. The differences of the results between the left and right well pairs demonstrate that the steam injection and produced water rates vary due to the heterogeneity of the reservoir. Also, the higher the initial water saturation, the higher the steam injection rate required to maintain the pressure in the system. In the higher initial water saturation cases, the mobility of the water phase in the reservoir at original conditions is higher which means that fluid injectivity is higher.

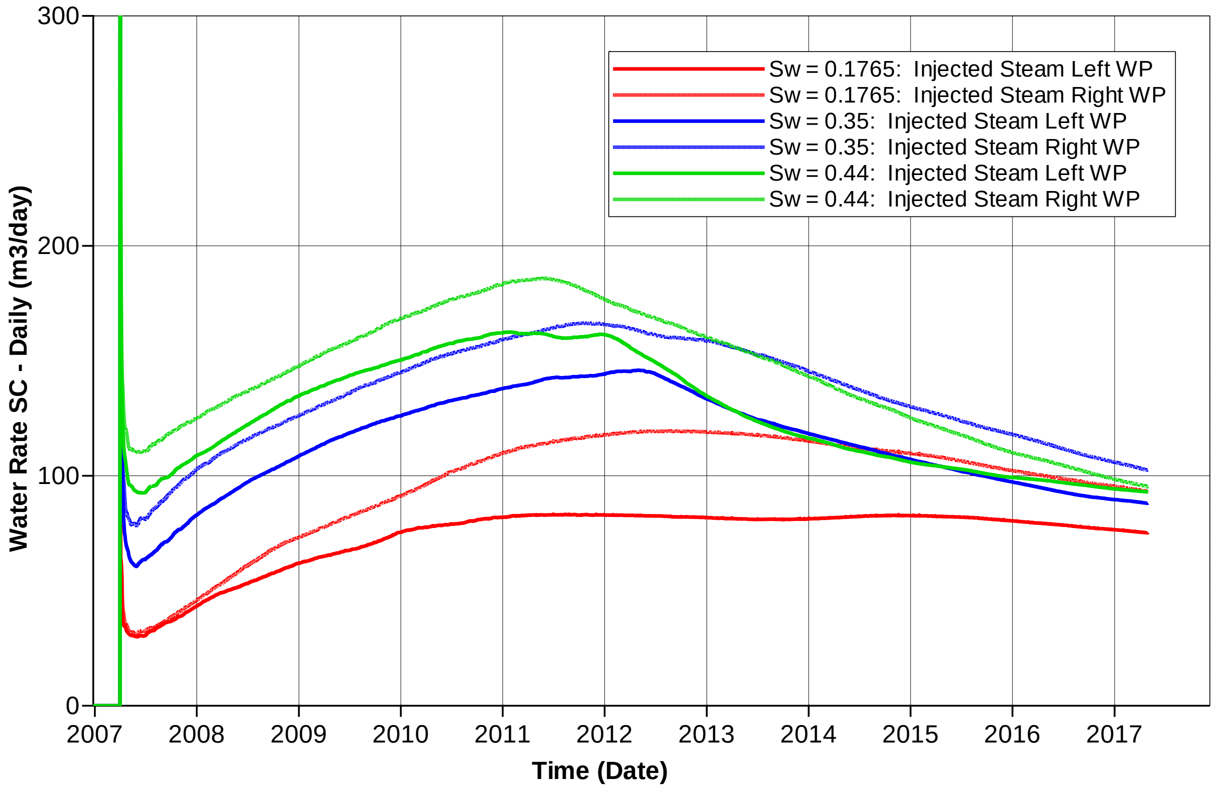

Figure 3.15: Effect of initial water saturation on steam injection rates for each wellpair.

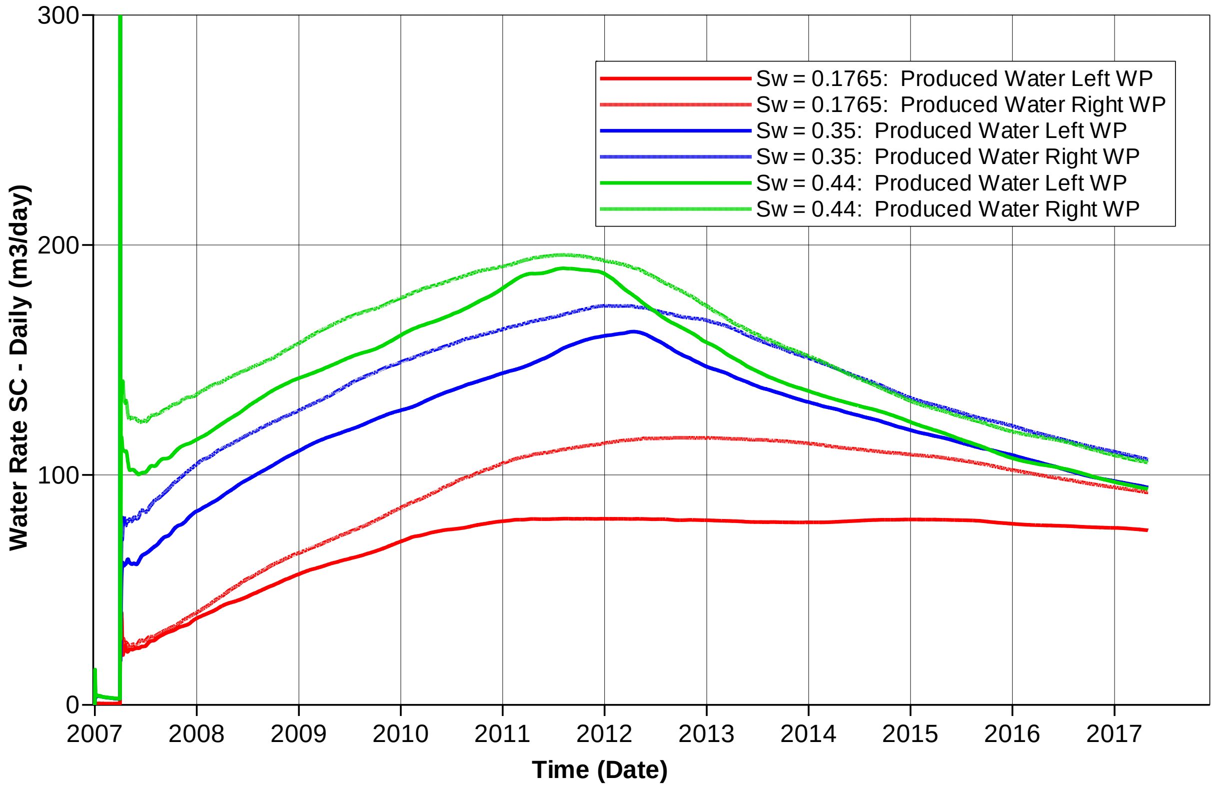

Figure 3.16: Effect of initial water saturation on water production rates for each wellpair.

The produced water rate corresponds directly to the injected steam rate. Despite the similarity of the cumulative oil production profiles shown in Figure 3.12 for the 0.1765 and 0.35 initial water saturation cases, the oil production rate profiles shown in Figure 3.17 reveal that the oil production profiles of the two cases are quite different. One key observation of the oil rate profiles is that the higher the initial water saturation, the more similar are the left and right SAGD well pair oil rate profiles.

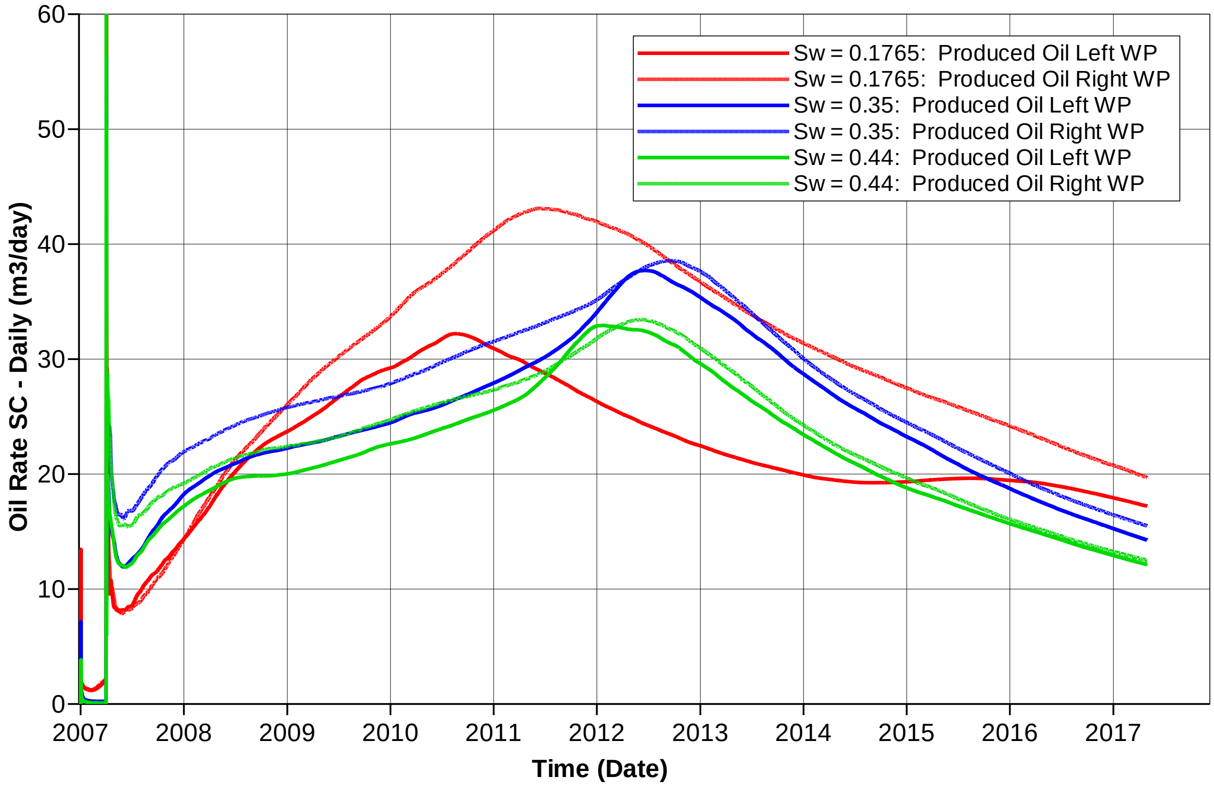

Figure 3.17: Effect of initial water saturation on oil production rates for each wellpair.

Figures 3.18 to 3.21 provide two-dimensional (2D) and three-dimensional (3D) visualizations of the steam chamber and phase saturations as the process evolves for the case where the initial water saturation is equal to 0.1765. The pre-heating (steam circulation) stage is done after 0.26 years at which SAGD mode starts. The temperature distributions at the mid-plane of the well pairs displayed in Figure 3.18 reveals the different growth rates of the steam chamber. An examination of the horizontal permeability distribution with the lower permeability streak just above the injection well depth in Figure 3.4 explains why the left well pair steam chamber extends more in the horizontal direction. This lower permeability streak affects the growth of the left steam chamber throughout its evolution. The steam chambers reach the top of the oil column just after 2 years of operation. After about 7 years of operation, the steam chambers are in thermal communication with each other. From the images for years 2 until 7 years, the thermal conduction length scale (estimated from the length between the red and dark blue colored grid blocks) at the edge of the chambers is estimated to be of order of 5 to 7 m at the nose of the chamber. At the lower edges of the chamber, the thermal conduction region, as the process evolves, the thermal layer grows thicker with time.

Figure 3.19 shows the distribution of oil saturation versus time at the mid plane of the well pairs for the case with initial water saturation equal to 0.1765. The affect of the zero porosity shale layer at the left side of the domain (three-quarters from the bottom of the domain) is pronounced between Years 2 and 4. The chamber evolves around the shale layer with chamber development promoted under the layer. This demonstrates the impact of heterogeneity on steam flow and oil drainage. Toward the top of the depletion chamber, the transition zone between the oil sand and the chamber is of order of 1 to 2 m. For the rest of the chamber, the thickness of the transition zone is between 3 and 7 m. After 10 years of operation, nearly all of the oil in the domain has been depleted.

Figure 3.20 displays distributions of the phases (oil, water, and gas) in the case with initial water saturation equal to 0.1765. The distributions reveal that the transition zone between the depletion chamber and the oil-rich zone is water. The thickness of the transition zone is thin, of order of 1-2 m at the top of the depletion chamber but it grows larger towards the base of the chambers with thicknesses of order of 7+ m. The affect of the relatively tight streak directly above the left injection well (as shown in Figure 3.4) is more apparent at 2 years where there is a water-rich zone between two steam smaller subchambers. The subchambers merge to form a connected steam chamber. The results show that a thin, of order of a gridblock, layer of water directly adjacent to the depletion chamber edge.

Figure 3.21 display 3D views of the recovery process in the case with initial water saturation equal to 0.1765. The oil saturation is shown on the surfaces of the grid blocks (with cutoff of 0.5 so that grid blocks containing less than 0.5 oil saturation are not displayed) and a 230°C temperature isosurface is displayed in red. The results reveal that after 1 year of operation, that reservoir heterogeneity affects the ability of the steam to be injected into the reservoir and as a consequence, the there are ‘hot’ spots along the well. It turns out that the mid plane of the well pairs in the cross-well direction, steam chambers have evolved at that particular location. The 3D view reinforces the importance of examining steam chamber growth in 3D versus single 2D slices. As the process evolves, the steam chambers grow along the well pairs but the steam chamber of the left well pair is largely constrained to half of the well pair. In other words, the steam conformance along the left well pair is relatively poor. The right well pair achieves reasonably good steam conformance along the well pair. After 10 years of operation, the steam chambers have merged but this is localized to an approximately 100 m long interval near the mid plane of the well pairs.

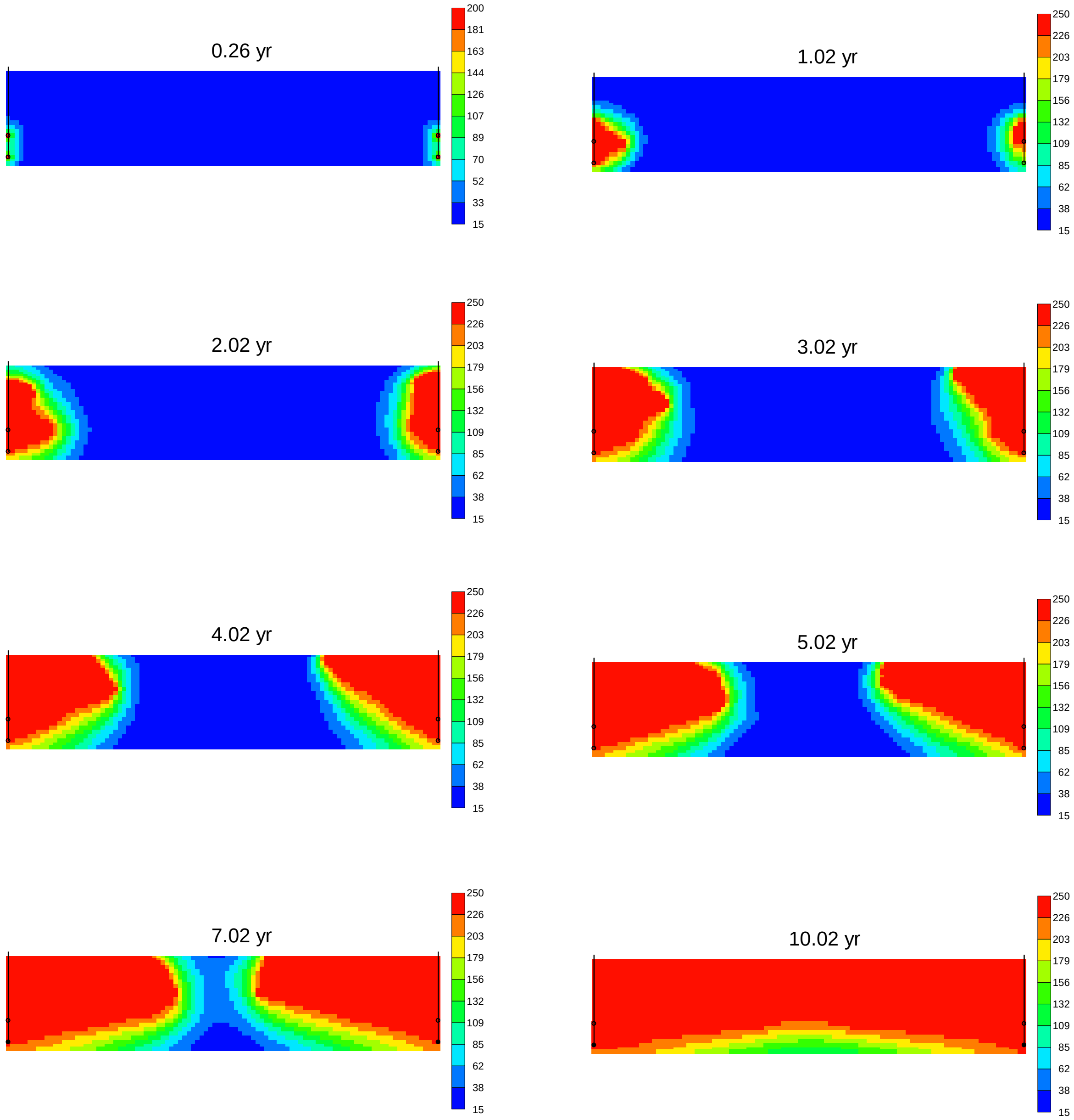

Figure 3.18: Evolution of temperature, in °C, at mid well pair plane for case with initial water saturation equal to 0.1765.

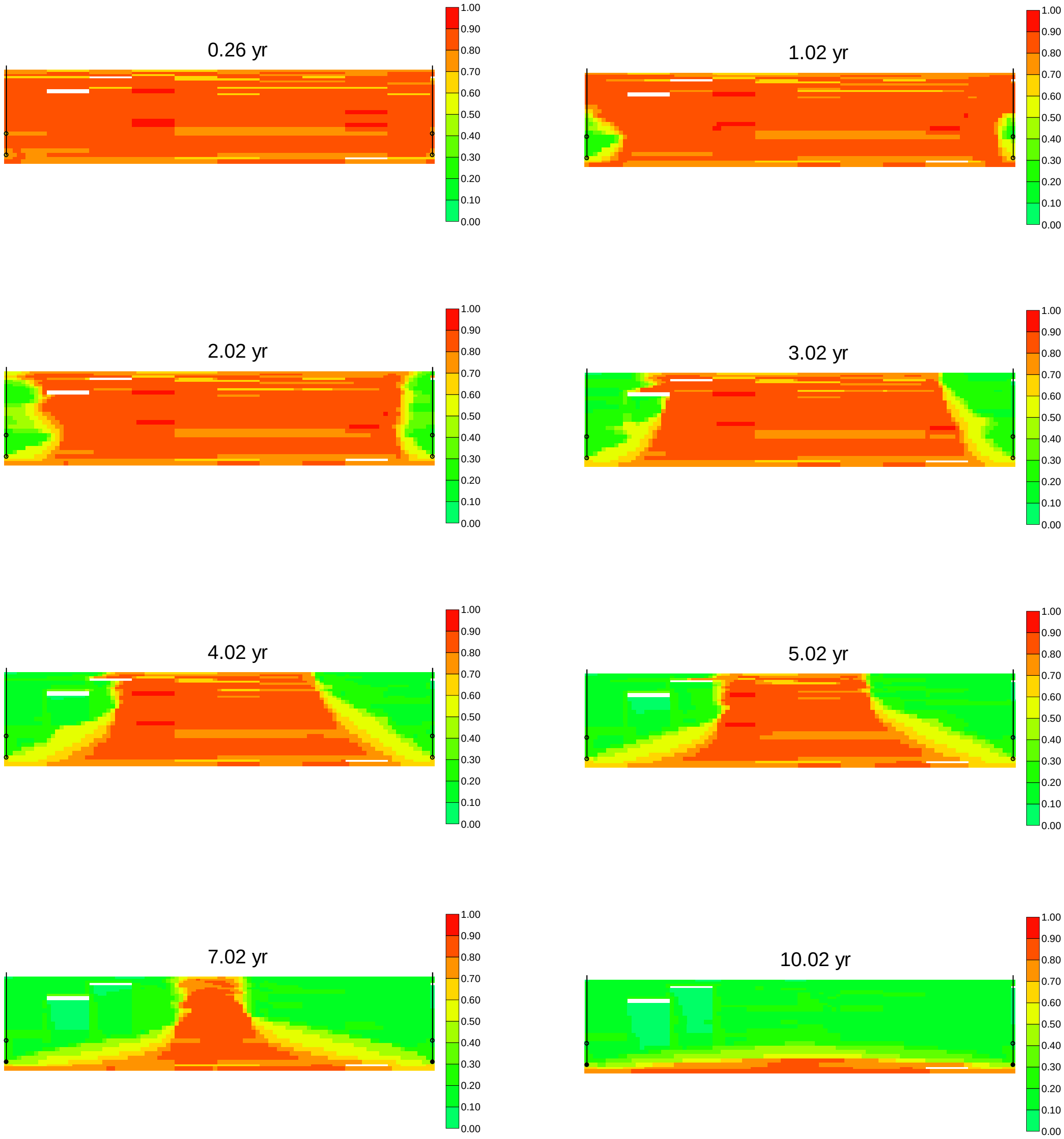

Figure 3.19: Evolution of oil saturation at mid well pair plane for case with initial water saturation equal to 0.1765.

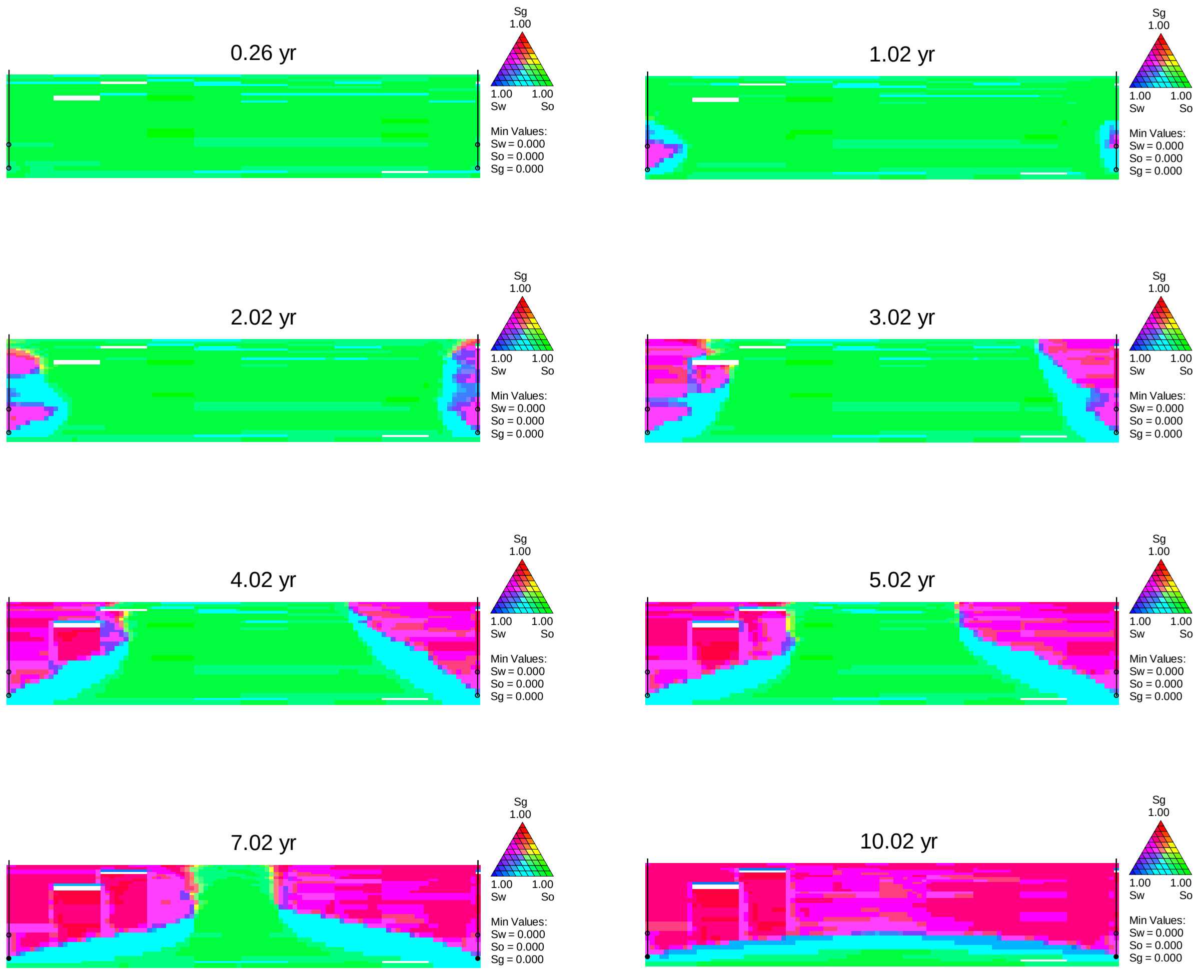

Figure 3.20: Evolution of phase distributions at mid well pair plane for case with initial water saturation equal to 0.1765. Red represents gas phase, blue represents water phase, and green represents oil phase.

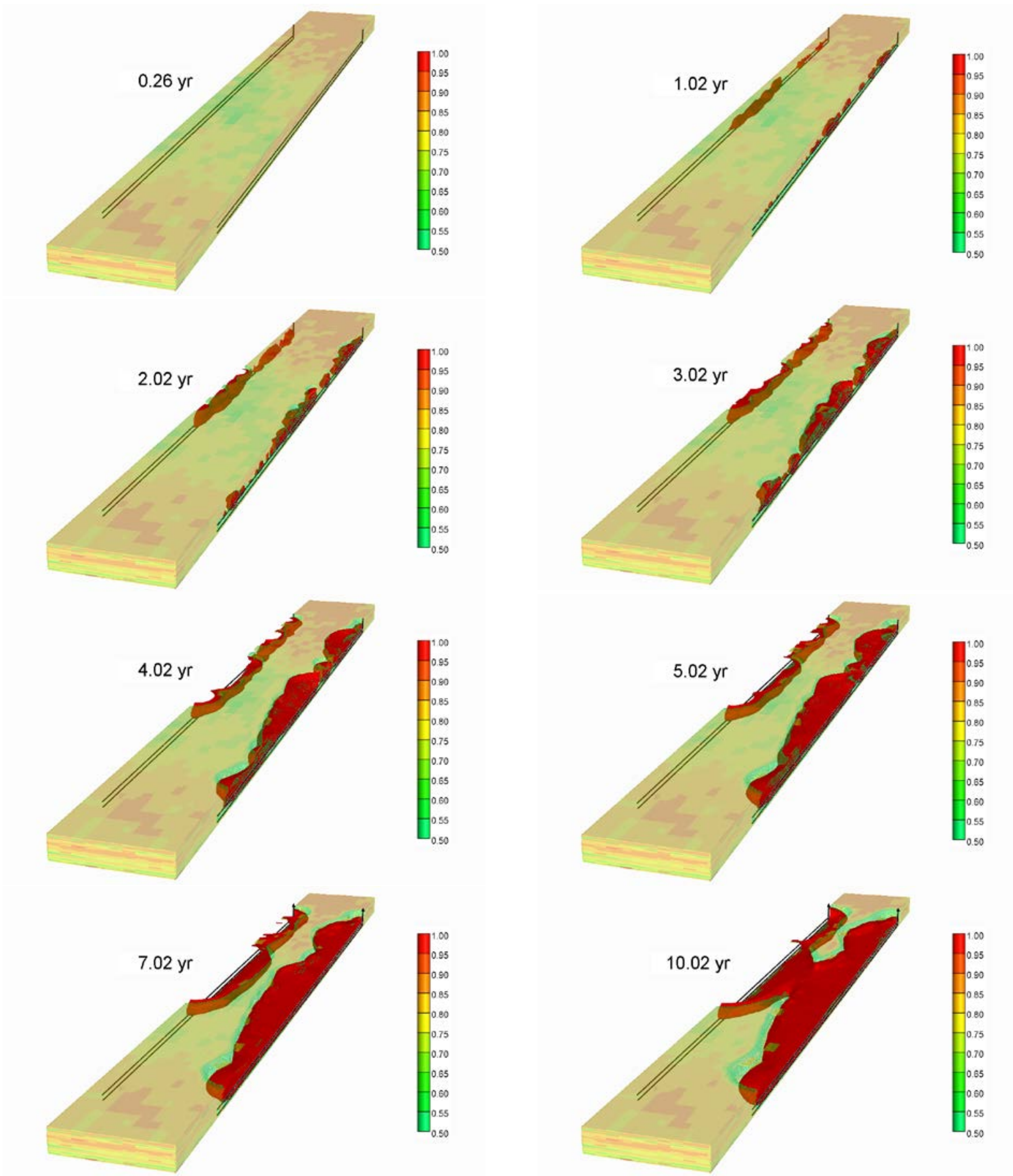

Figure 3.21: Evolution of steam chamber for case with initial water saturation equal to 0.1765. The grid blocks display the oil saturation with display cut off equal to 0.5 (only blocks with saturation greater than 0.5 displayed) and temperature isosurface equal to 230°C.

Figures 3.22 to 3.25 shows views of the distributions of the temperature, oil saturation, phases, and steam chamber development for the case with initial water saturation equal to 0.35. Broadly, the results, with respect to the growth of the steam chamber, are similar to that of the lower initial water saturation case.

A comparison of the results shown in Figure 3.22 versus that of the lower water saturation case displayed in Figure 3.18 shows that the steam chambers are larger in the 0.35 case. The larger the initial water saturation, the higher the injectivity of steam into the formation and the greater the volume required to maintain the injection pressure constraint. Thus, the steam chambers grow faster than that of the lower water saturation case and hydraulic communication of the chambers is reached just before 5 years of operation whereas in the lower initial water saturation case, this does not occur until beyond 7 years of operation.

It has also been proved by Oskouei et al. (2010) that the steam chamber in an miniature experimental oil sands reservoir with higher water saturation (32%) grew faster and in elliptical shape than the circular shaped steam chamber in low water saturation (14.7%). Despite the faster growth of the chamber, the oil volume is not greater than that of the lower initial water saturation case since the oil content of the reservoir is decreased. Another reason for lower oil recovery rate at higher water saturation could be lower volume of reservoir is contacted, hence less heat is retained in the reservoir. Therefore, as expected the thermal efficiency was not better with higher water saturation, so it required more steam injection and as a result, more produced water.

The oil saturation distributions displayed in Figure 3.23 reveal that the depletion chambers are larger in the higher initial water saturation case than that of the lower case. The distributions show that an oil bank forms ahead of the edge of the depletion chamber. The thermal front extends beyond the depletion chamber and heats the oil there which becomes sufficiently mobile to form a bank.

Figure 3.24 shows distributions of the oil, water, and gas phases as the process evolves in the 0.35 initial water saturation case. The 3D views of the steam chamber for the 0.35 initial water saturation case reveals that the steam chambers achieves greater steam conformance along the left well pair than was achieved at the lower initial water saturation case.

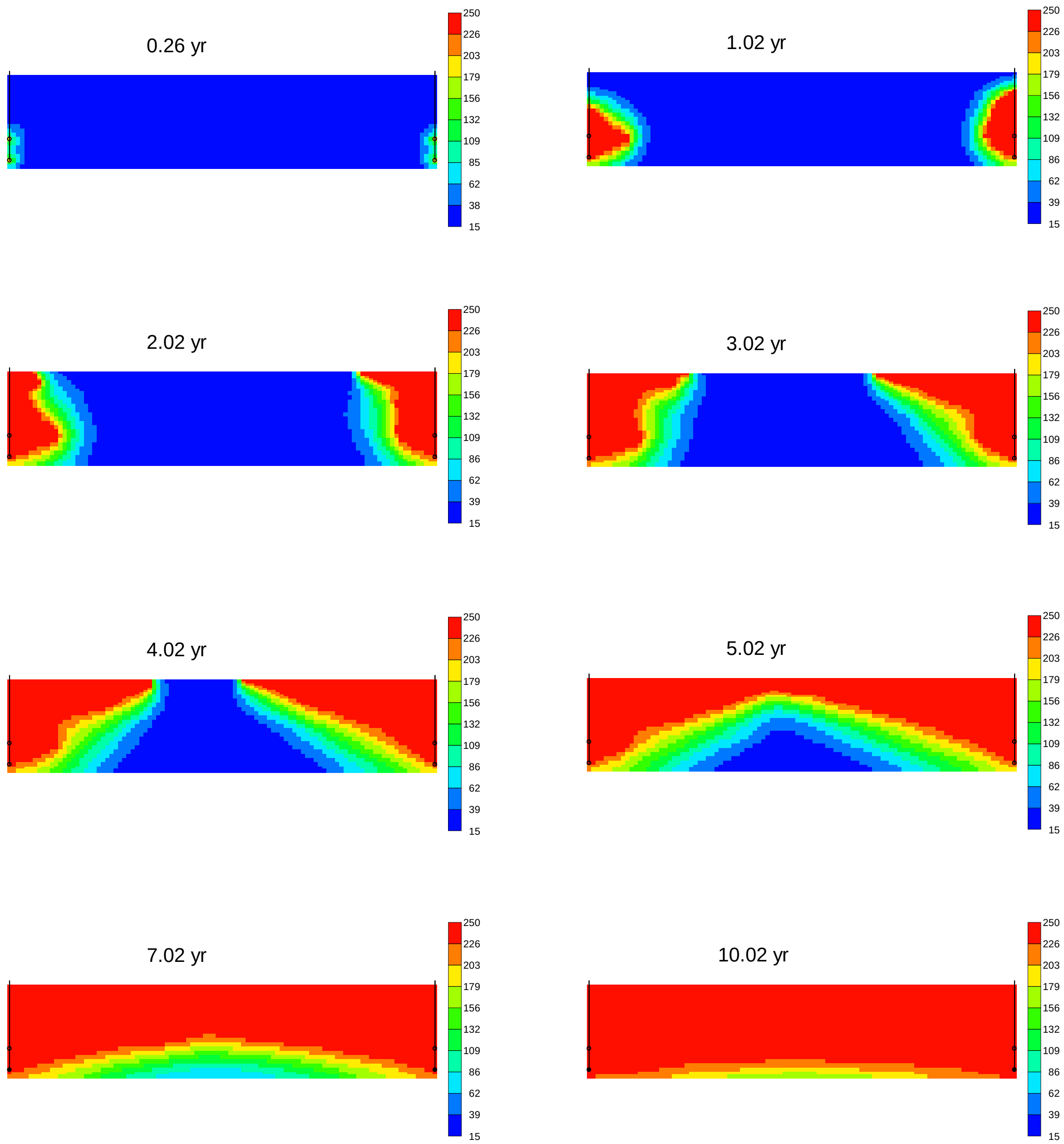

Figure 3.22: Evolution of temperature, in °C, at mid well pair plane for case with initial water saturation equal to 0.35.

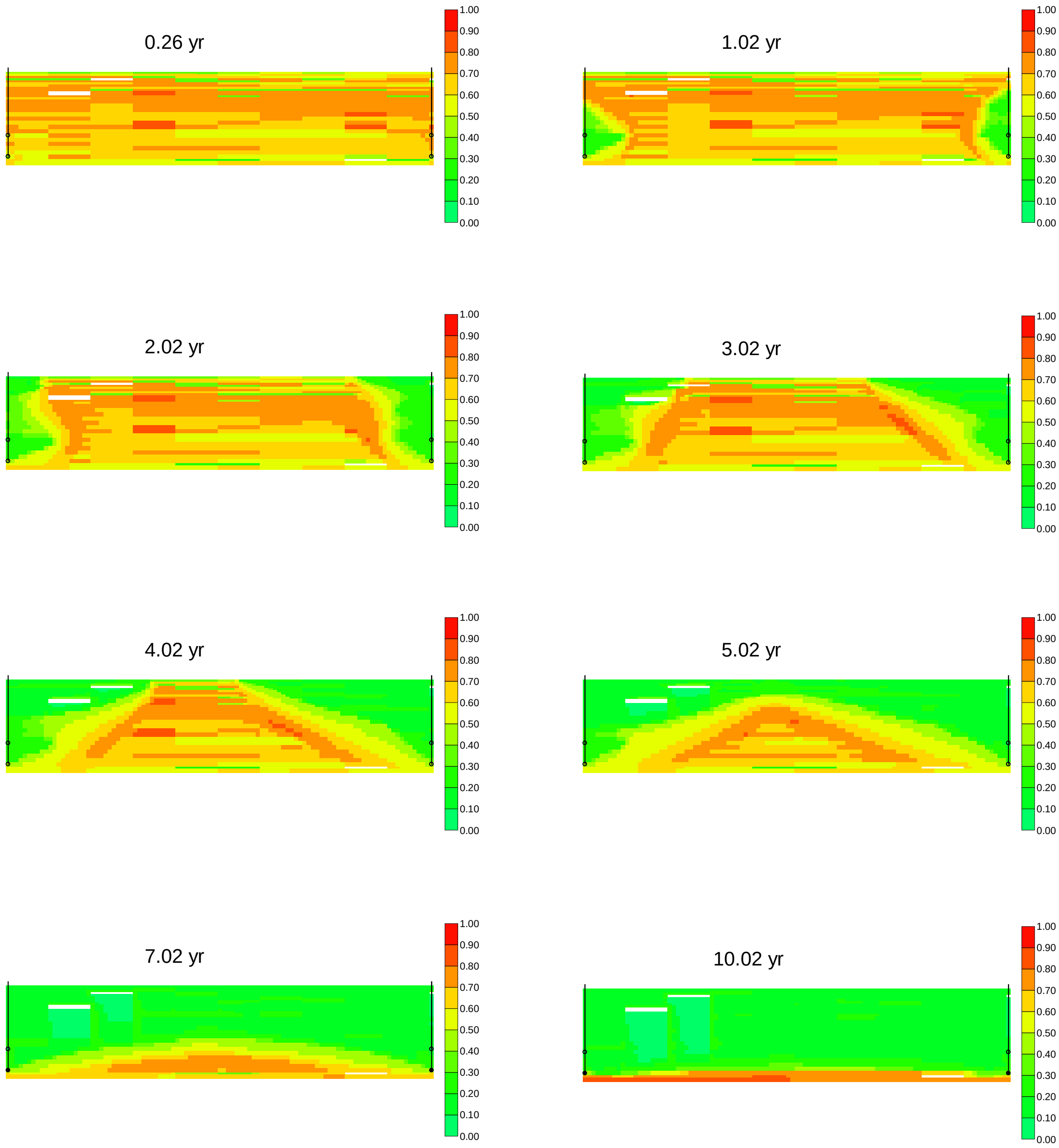

Figure 3.23: Evolution of oil saturation at mid well pair plane for case with initial water saturation equal to 0.35.

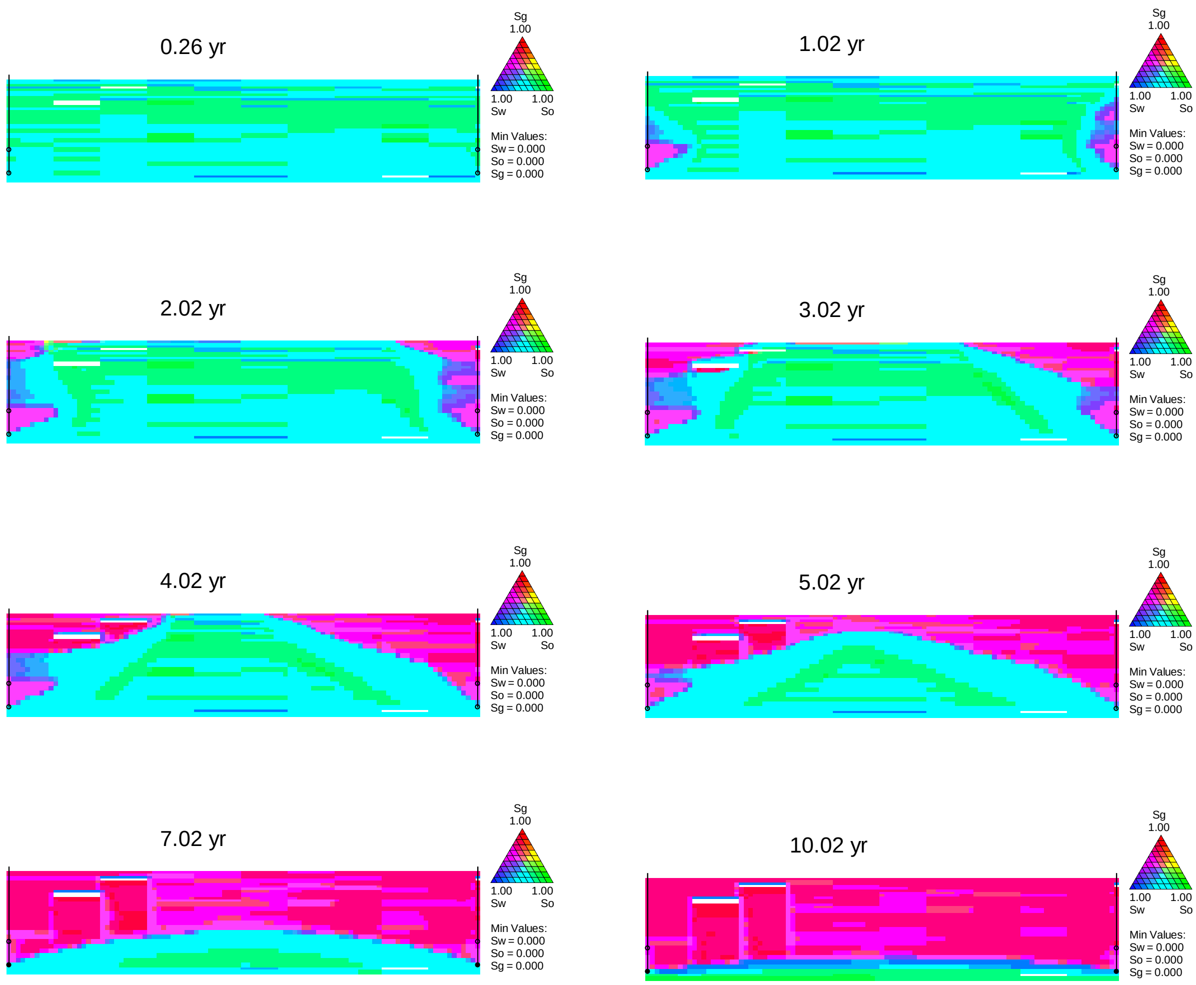

Figure 3.24: Evolution of phase distributions at mid well pair plane for case with initial water saturation equal to 0.35. Red represents gas phase, blue represents water phase, and green represents oil phase.

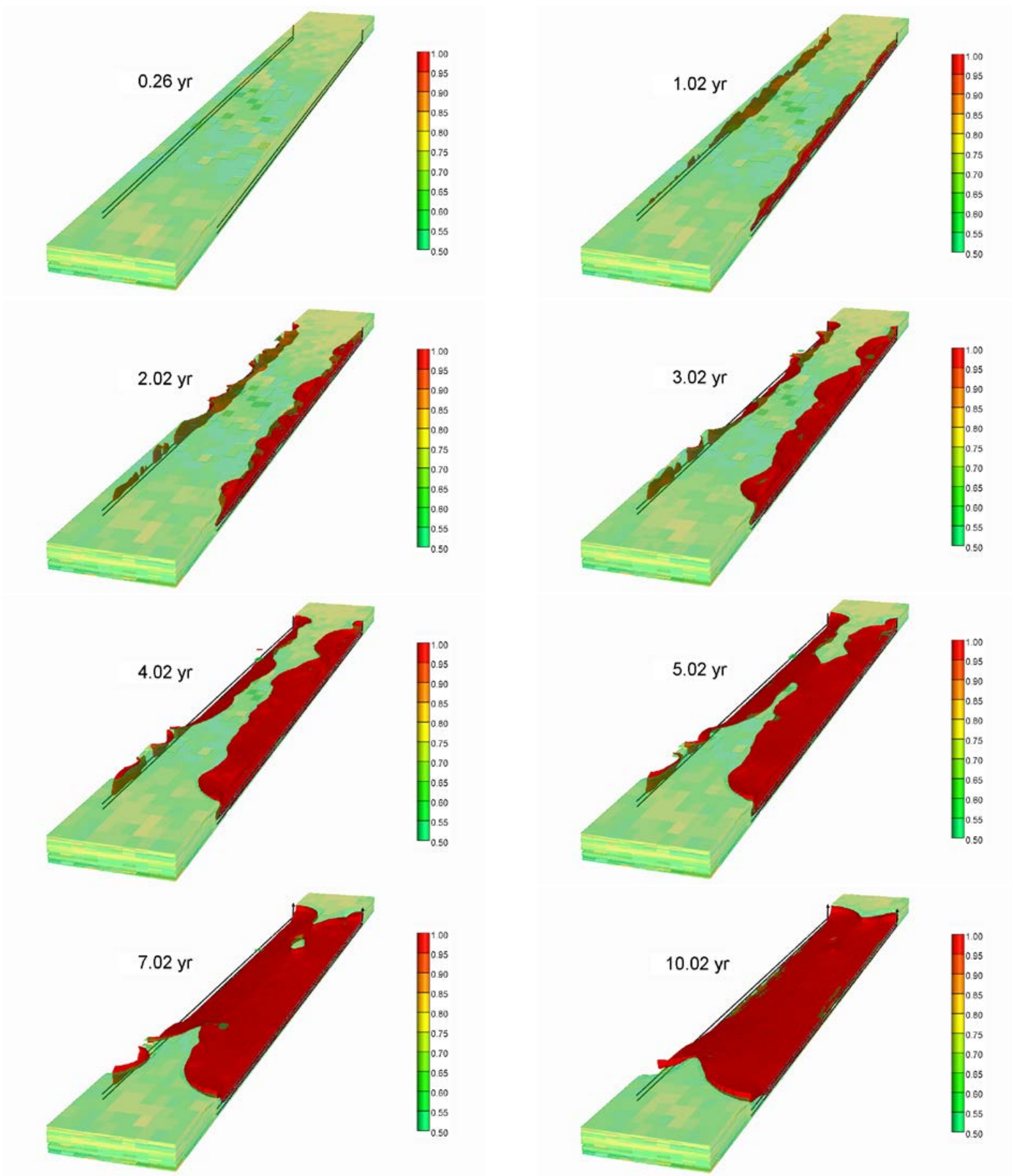

Figure 3.25: Evolution of steam chamber for case with initial water saturation equal to 0.35. The grid blocks display the oil saturation with display cut off equal to 0.5 (only blocks with saturation greater than 0.5 displayed) and temperature isosurface equal to 230°C.

Figures 3.26 to 3.29 displays views of the temperature, oil saturation, oil, water, and gas phases, and steam chamber development for the case where the initial water saturation is equal to 0.44. The results show that the steam chamber is even larger than the lower initial water saturation cases at a given time. The steam chamber merge, at the mid plane of the well pairs, at just after 4 years of operation.

Figure 3.27 shows that, similar to the 0.35 case, an oil bank forms ahead of the depletion chamber. Due to the lower oil saturation in the reservoir in the 0.44 case, the oil bank is not as pronounced as that of the 0.35 case. The evolution of the oil, water, and gas phases shown in Figure 3.28 reveals that some of the high water saturation intervals between the depletion chamber are enriched by mobile oil. For example, compare the zones between the wells at Years 3 and 4. The high water saturation interval found in the distribution at Year 3 is filled with mobilized oil which flows from the bank and it disappears by Year 4. Oil banking and filling of high water saturation zones was also observed by Fairbridge et al. (2012).

The 3D views presented in Figure 3.29 reveal that the greater injectivity of steam into the reservoir helps to generate greater steam conformance along the left well pair than that of the lower initial water saturation cases. Even after 1 year of operation, the conformance of the left well pair is relatively high compared to that of the lower initial water saturation cases. By Year 10, the steam conformance along and between the well pairs is nearly 100%.

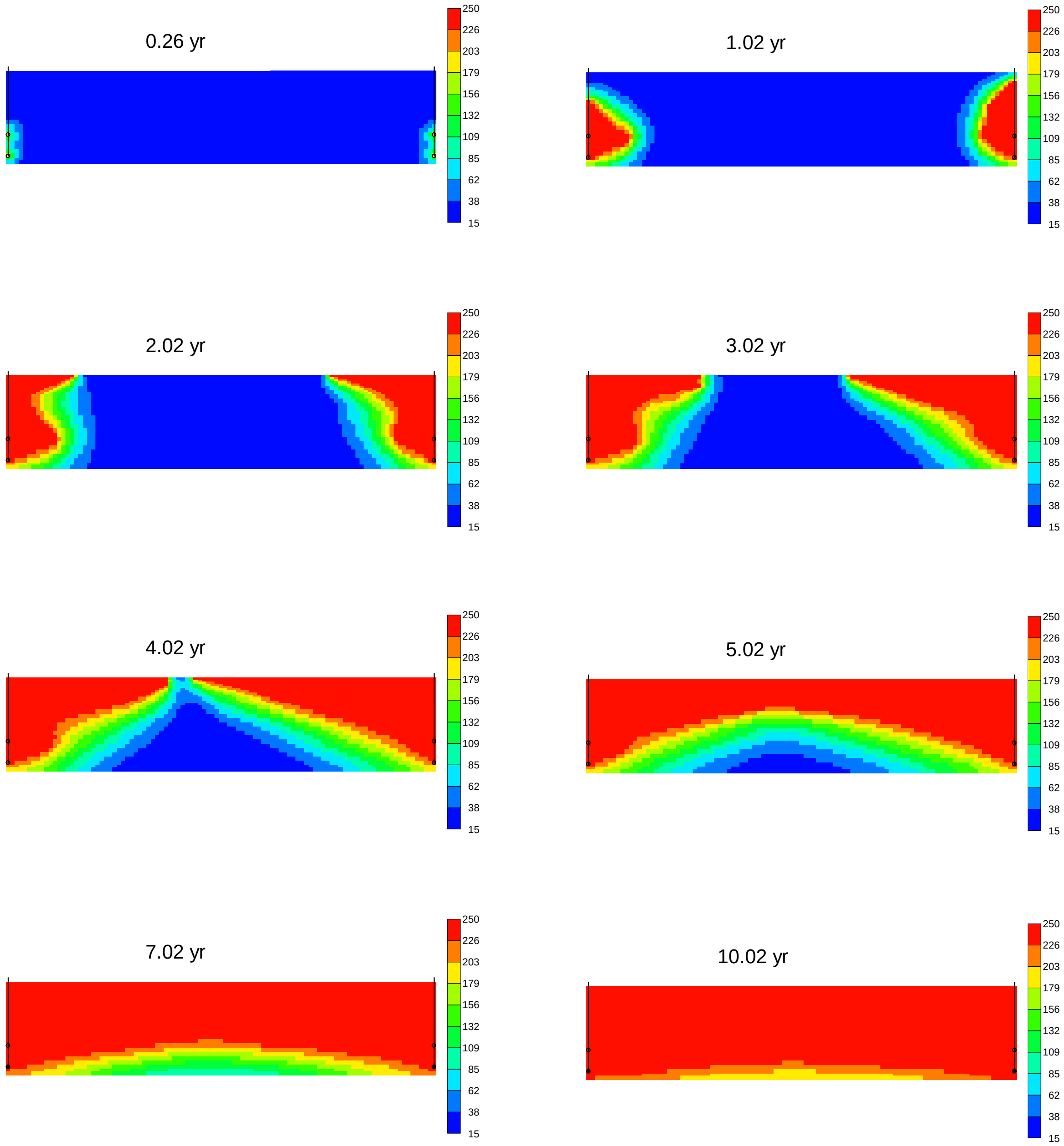

Figure 3.26: Evolution of temperature, in °C, at mid well pair plane for case with initial water saturation equal to 0.44.

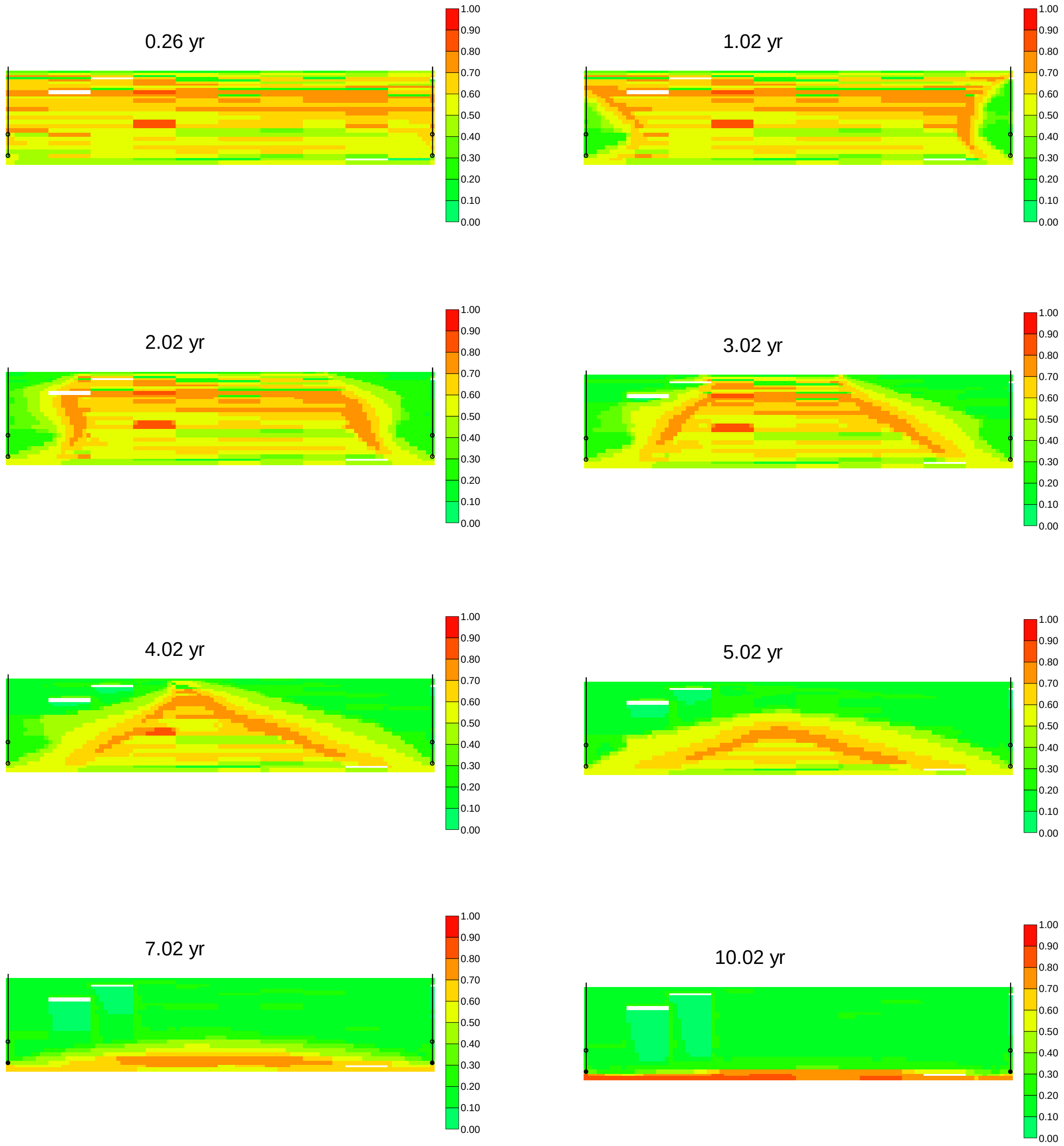

Figure 3.27: Evolution of oil saturation at mid well pair plane for case with initial water saturation equal to 0.44.

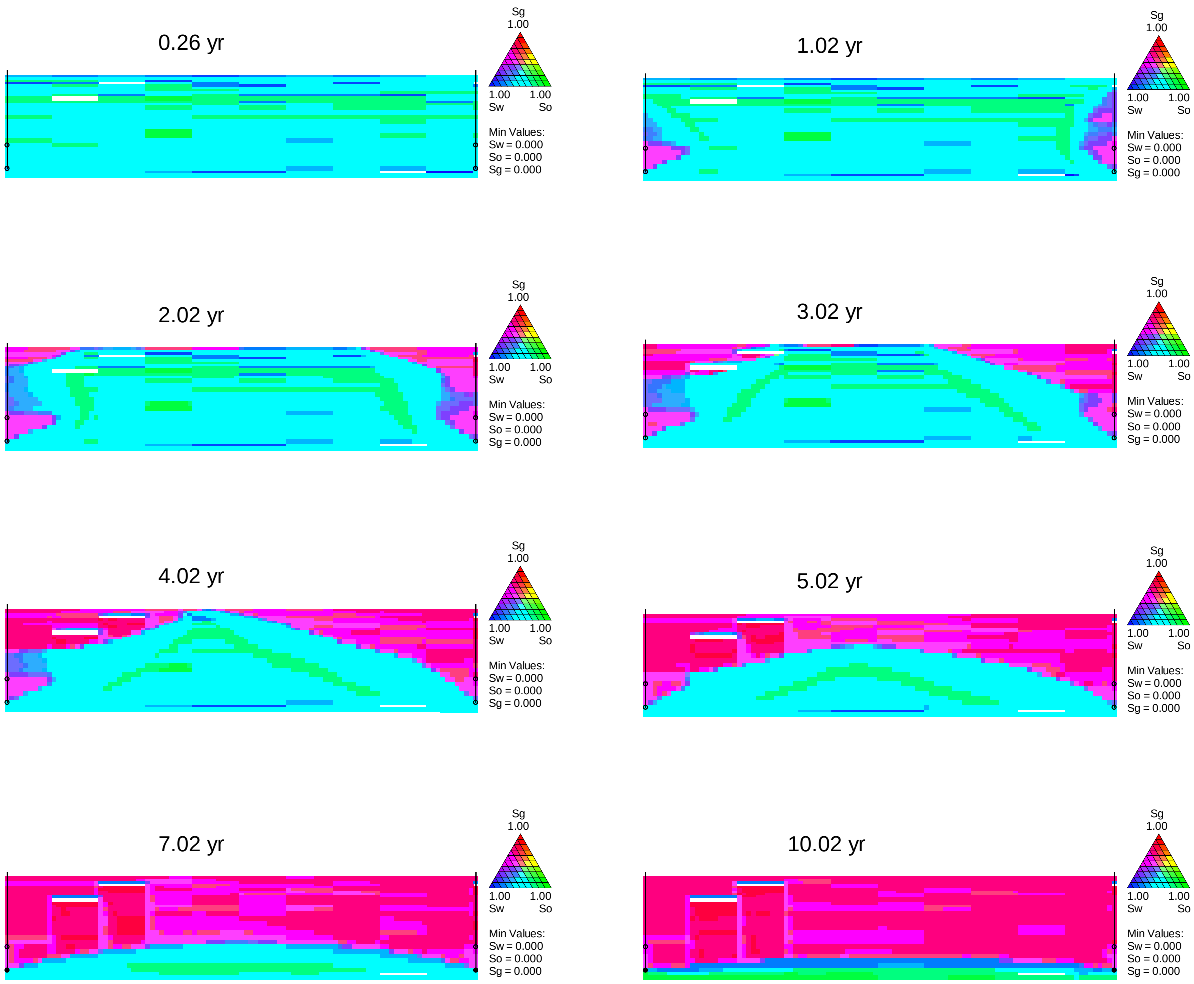

Figure 3.28: Evolution of phase distributions at mid well pair plane for case with initial water saturation equal to 0.44. Red represents gas phase, blue represents water phase, and green represents oil phase.

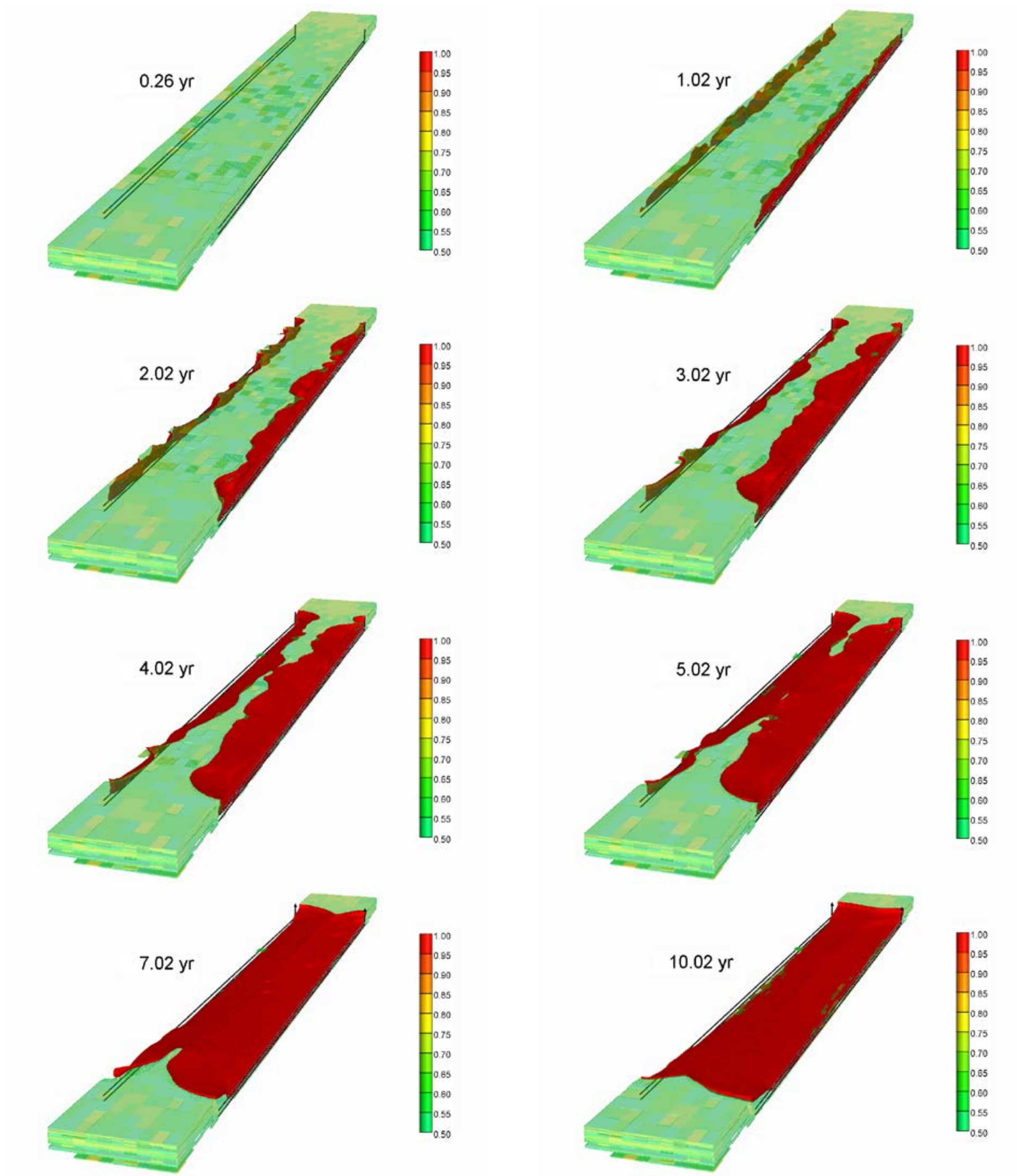

Figure 3.29: Evolution of steam chamber for case with initial water saturation equal to 0.44. The grid blocks display the oil saturation with display cut off equal to 0.5 (only blocks with saturation greater than 0.5 displayed) and temperature isosurface equal to 230°C.

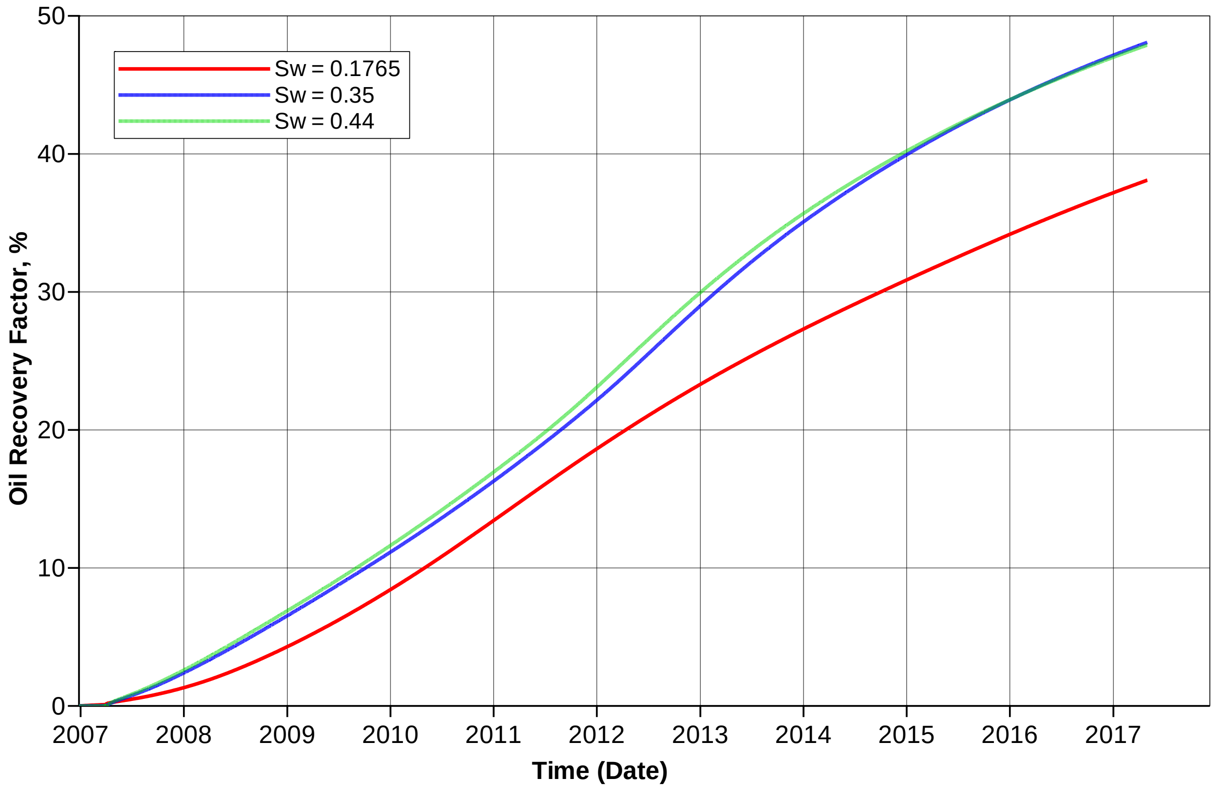

Figure 3.30: Recovery factor versus initial water saturation.

Figure 3.30 is a plot of the recovery factor versus time for the three cases. The recovery factors achieved are typical of that of SAGD operations in the McMurray Formation. The results show that the lower initial water saturation case has the lowest recovery factor whereas the two higher cases have higher and similar recovery factor profiles. The reason the lower initial water saturation case has lower recovery factor is primarily due to its higher initial oil content in the reservoir. From a conservation point of view as would be promoted from the Alberta Energy Regulator, the reservoir should be produced to maximize the recovery of oil. Thus, this suggests that from this point of view, the higher water saturation cases would achieve a more desirable outcome than that of the low initial water saturation case.

The results presented above show that the higher the initial water saturation of the reservoir, at a sufficiently high value, the cumulative oil volume produced reduces. This is consistent with the experimental results of Oskouei et al. (2010). The reduction exhibited by the results of the simulations documented here is due to the lower oil content of the reservoir. Also, the steam volume injected is higher due to the greater injectivity of the formation and as a consequence, the produced water volume is raised. With respect to thermal efficiency, the greater the initial water saturation, the higher is the cumulative steam-to-oil ratio. This is due to the greater injectivity of steam into the reservoir and the lower content of oil within the reservoir.

The results also suggest that greater initial water saturation may aid in achieving improved steam conformance along SAGD well pairs. This is due to the greater injectivity of steam into the formation due to the mobility of the oil along the well pair. This is at constant porosity and permeability (both horizontal and vertical) and thus, this implies that the initial water saturation of the reservoir can play a large role in initiating the steam chamber along the well. This is a significant finding since this implies that perhaps for high oil saturation reservoirs where steam injectivity may be limited, perhaps steam bullheading into the injection and production wells, as tested by Suncor (Suncor, 2013) to create a hot zone between the wells (instead of steam circulation) could have benefit since steam condensate accumulated around the well pair may serve to create a more uniform steam chamber along the well pair when SAGD mode starts. This aspect of start-up is beyond the scope of the research described in this thesis. Also, hot steam condensate moving into the reservoir around the well pairs enhances heat transfer in the near well pair region since it involves both conduction and convection.

3.7 Conclusions

The conclusions are as follows:

1. The higher the initial water saturation of the reservoir, the greater is the steam-to-oil ratio.
2. Higher initial water saturation may lead to higher injectivity of the formation which permits faster access to oil which can result in enhanced oil production rates. However, if the initial water saturation is sufficiently high, the oil production rate drops due to lower content of oil in the reservoir.
3. The higher the initial water saturation of the reservoir, the better is the steam conformance along the SAGD well pair (with all geological and rock-fluid properties unchanged).
4. For higher water saturation, the steam chamber grows in elliptical shape rather than circular shape which means smaller volume of reservoir is contacted, which leads to a low thermal efficiency, hence it requires more steam injection because there is less accumulated energy within the reservoir.
5. The steam chamber grows faster with higher water saturation resulting in early hydraulic communication of the neighboring steam chambers.

6. Despite the difference of initial water saturation, the difference between the cumulative injected steam and produced water volumes between the left and right well pairs does not change significantly.
7. The higher the initial water saturation, the more similar is the oil rate profiles of the left and right SAGD well pairs.

Chapter Four: **Impact of Gas Co-Injection on SAGD in Reservoirs with High Water Saturation**

4.1 Introduction

There has been a lot of research, both modelling and experimental, and field piloting to evaluate methods to improve the steam-to-oil ratio of SAGD operations (Gates and Wang, 2011). In field trials, most of the pilots have focused on solvent, typically butane or diluent, or non-condensable gas (NCG) co-injection with steam. For solvent processes, in most cases, the solvent volume fraction in the steam is less than 5% (Nasr and Isaacs 2001, Leaute and Carey, 2005) although some field tests have used as high as 20% (2012-ImperialOilonSA-SAGDPilot). For non-condensable gas processes, first proposed by Butler as the Steam and Gas Push (SAGP) process (Butler, 2997), natural gas is added to the steam. Typically, the volume fraction of gas added to the steam is also less than 5%. This has been tested by several companies with mixed results.

In the research documented here, the addition of natural gas injection has been evaluated in an attempt to improve the steam-to-oil ratio of a relatively high initial water saturation reservoir. Gas injection into the reservoir can achieve several potential benefits (Ito et al., 2001, Heron et al. 2008, Alturki et al. 2011). First, if it rises to the top of the steam chamber, it provides an insulating layer that lowers heat losses to the overburden which consequently improves the steam-to-oil ratio. Second, it helps to maintain the pressure of the steam chamber at reduced steam injection rate. This reduces the steam injection rate and providing the oil rate is not decreased, the steam-to-oil ratio is improved. However, on the other hand, the steam saturation conditions are at the partial pressure of the steam which can lower the temperature of the steam and the gas can also insulate the edge of the steam chamber which reduces the amount of heat directed to the bitumen there. Thus, it remains unclear whether NCG can help the thermal efficiency of the recovery process.

Here, two operating strategies are tested to determine if the steam-to-oil ratio of SAGD in a relatively high initial water saturation McMurray Formation oil sands reservoir can be improved.

In the first strategy, NCG is co-injected with steam as described by Butler's SAGP process (Butler, 1997). In this case, the idea is that the NCG will be distributed within the reservoir with the steam and provide an insulating layer between the steam chamber and the highly mobile water within the formation.

In the second strategy, a NCG slug is injected into the reservoir prior to SAGD operation. The idea behind this strategy is that the gas can displace the highly mobile water from the well pair and thus when steam injection starts, the steam would displace the gas outwards from the well pair and access the bitumen there. This would shield to some extent the steam chamber from the mobile water within the formation. A version of this is being proposed by Cenovus for a top water oil sands reservoir (Cenovus, 2013). In Cenovus's application, they will inject NCG into a top water zone to displace the water from the zone and then conduct SAGD in the lower oil sands interval.

In both of the strategies evaluated here, there is a danger that the injected NCG will provide an insulating layer between the steam chamber and the oil sands beyond thus harming heat transfer.

4.2 Reservoir Model

The reservoir simulation model described in Chapter 3 was used for the research documented here. The case used was the one with average initial water saturation equal to 0.35. No changes were made to the grid, geology, well locations, or fluid properties. For NCG, methane was used (same properties as that of the solution gas). A diffusion coefficient for methane was not explicitly specified in the model (as was the case for the simulation cases in Chapter 3).

4.3 Operating Strategies

Similar to the cases described in Chapter 3, a pre-heating stage was conducted for a period of 3 months. In total, five NCG-based cases were conducted. The first three were with the first strategy described above (SAGP). The remaining two were with the second strategy described above where a NCG slug is injected into the reservoir prior to SAGD operation. The injection fractions and timing are summarized in Table 4.1. In all cases, the quality of the steam is equal 0.95 and the total injection pressure is equal to 4 MPa. For the production well, a maximum steam rate constraint was imposed to mimic steam trap control (same as in Chapter 3).

Table 4.1: NCG con-injection cases.

Case	Type of Case	Fraction of Gas in Injection Stream	Timing of NCG Injection
Base Case	SAGD (no NCG injection)	-	-
SAGP-0.3	SAGP	0.3% NCG in Vapour Phase Injection	Continuous during SAGD operation
SAGP-0.7	SAGP	0.7% NCG in Vapour Phase Injection	Continuous during SAGD operation
SAGP-2.2	SAGP	2.2% NCG in Vapour Phase Injection	Continuous during SAGD operation
SLUG-3	NCG SLUG prior to SAGD operation	100% NCG in slug, 0% during SAGD operation	3 months before SAGD operation
SLUG-6	NCG SLUG prior to SAGD operation	100% NCG in slug, 0% during SAGD operation	6 months before SAGD operation

4.4 Results and Discussion

4.4.1 SAGP Cases

Figure 4.1 displays the cumulative oil volume produced for the base and SAGP cases (rate profiles for the cases are shown in the Appendix). The results reveal that over the concentrations of injected gas studied, the changes of the oil produced are small. In the case with 2.2 volume percent injected (in the injected vapour phase), the cumulative oil recovered is slightly higher than the other profiles after about 4 years of operation but beyond about 6 years of operation, its oil rate drops and the cumulative oil volume produced for this case is lower than that of the other cases.

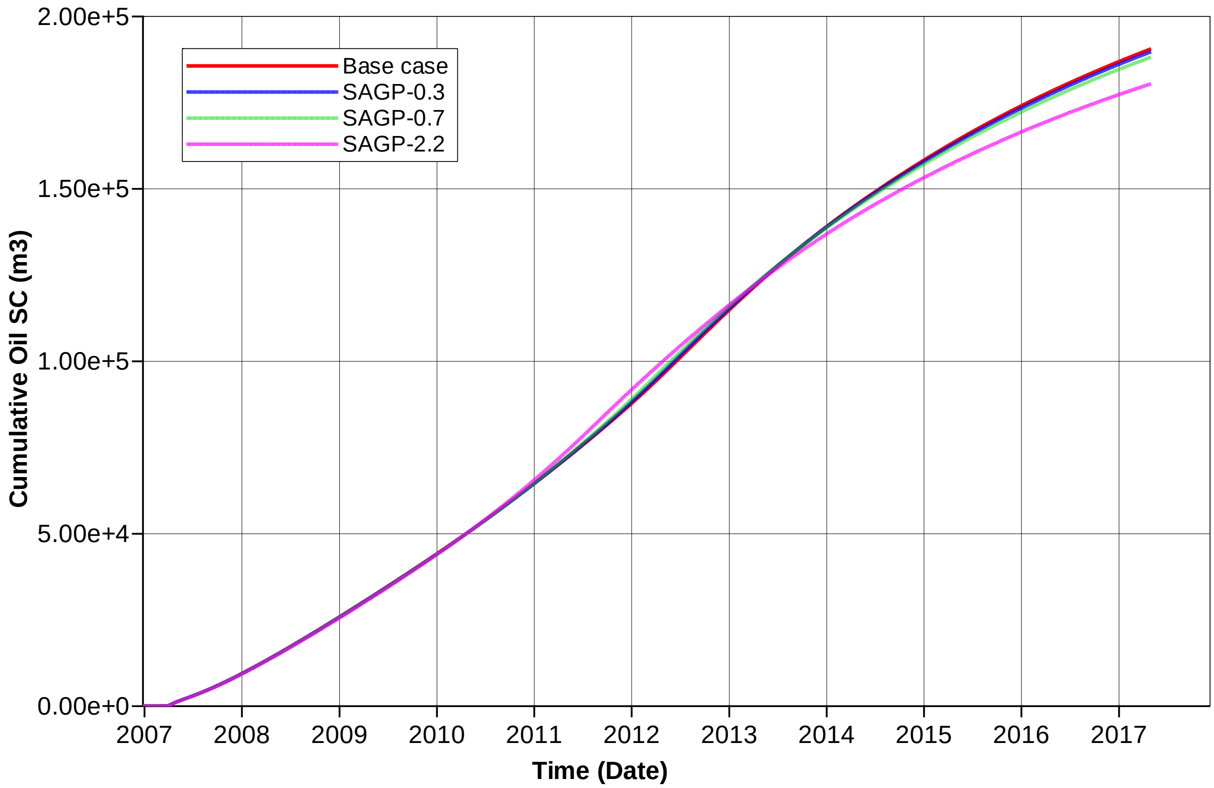

Figure 4.1: Cumulative oil volume produced from SAGP cases.

Figure 4.2 displays the cumulative steam (expressed as cold water equivalent) and cumulative produced water (both formation water and steam condensate) for the base and SAGP cases (the rate profiles for these cases are shown in the Appendix). The results show, consistent with the base case, all of the SAGP cases produce more water than is injected. With the addition of NCG, the steam rate is reduced to maintain the constant injection pressure of 4 MPa. With the reduction of the amount of steam injected, the volume of produced water also drops.

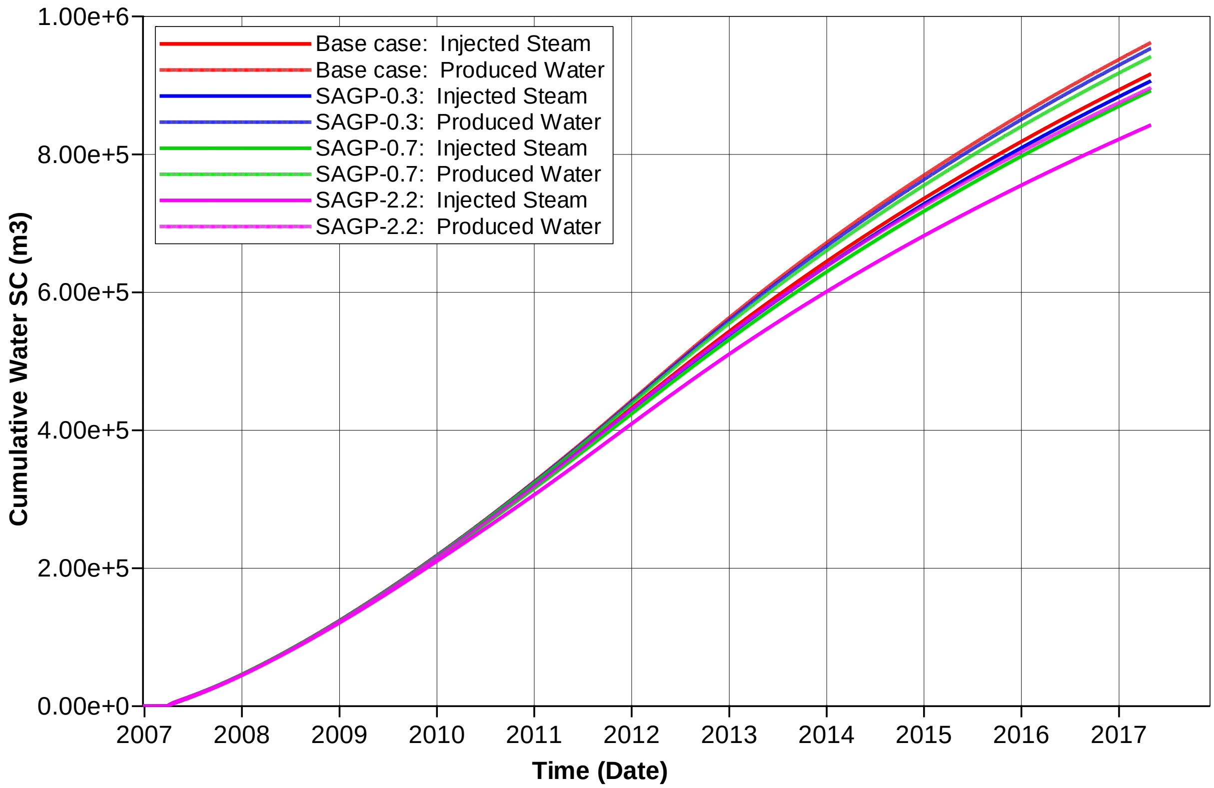

Figure 4.2: Cumulative steam (expressed as cold water equivalent) injected and water produced of the SAGP cases.

Figure 4.3 shows the cumulative steam-to-oil ratios (cSORs) for the left and right well pairs for the base and SAGP cases. The results show that despite a reduction of the steam injected, the cSOR for the cases are slightly decreased with the highest NCG co-injection case showing the largest reduction of the cSOR profile. However, the reduction is not very significant. As shown most clearly by the highest NCG co-injection case, the co-injection of gas helps with reducing the steam volume injected but it appears to also harm the production rate of oil. Most likely, larger amounts of NCG co-injection may reduce the steam requirement further but with lower volume of produced oil, it remains unclear if it will be beneficial with respect to the economics which are most tied to the cSOR and the oil rate.

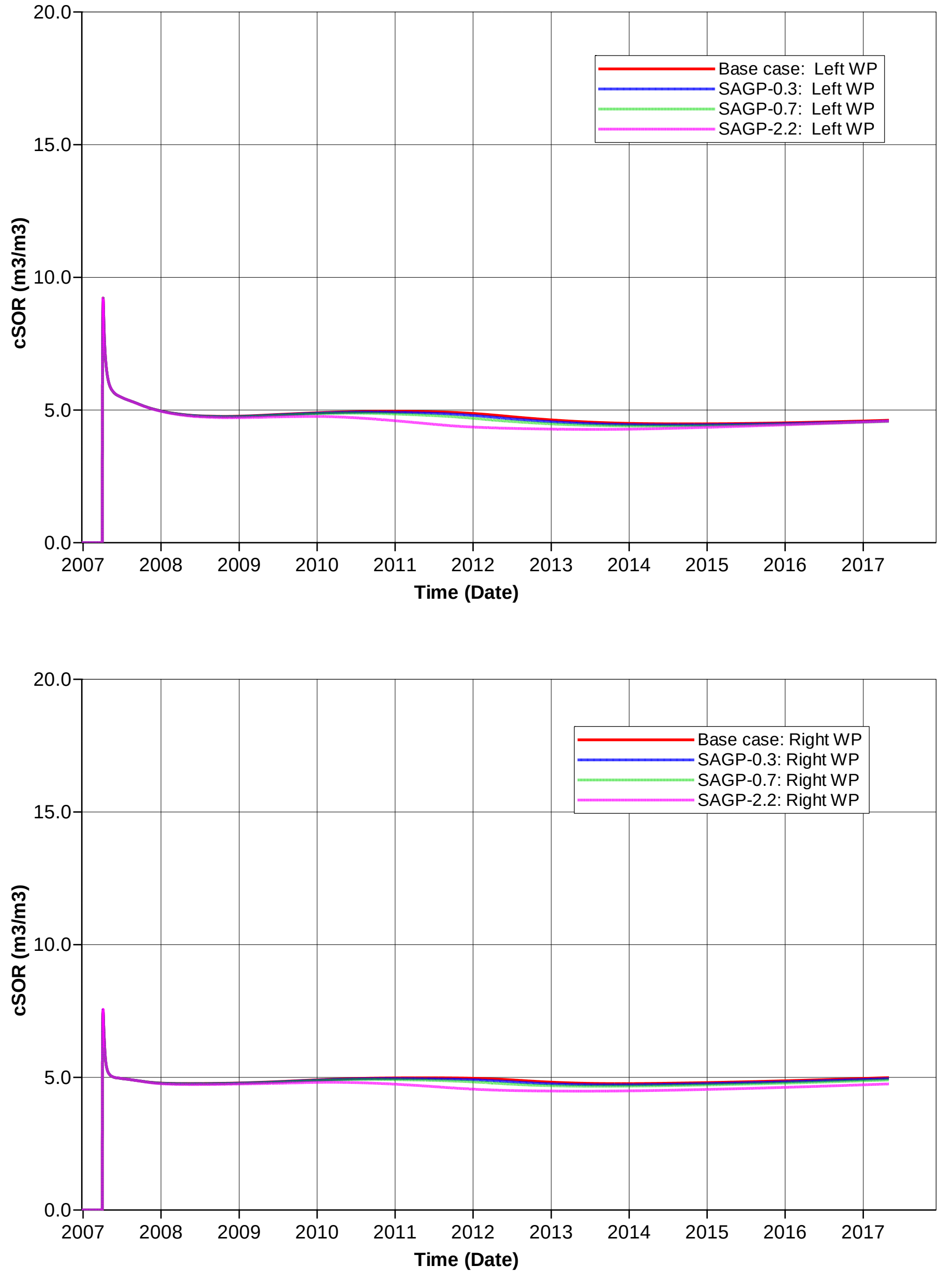

Figure 4.3: cSOR profiles for SAGP cases.

Figure 4.4 displays the gas saturation distribution after 5 years of operation for the base and SAGP-2.2 cases at the mid plane of the well pairs. To make the comparisons more clear, the images in Figure 4.4 display only the left well pair and the first 50 m of the reservoir. A comparison of the two distributions reveals that the gas saturation is larger in the SAGP case than that of the base case. The results suggest that the greatest differences of the gas saturation distributions occurs at the edge of the steam chamber.

Figure 4.5 displays the distribution of the relative permeability of the water phase at the same cross-section as that of the gas saturation distribution in Figure 4.4. A comparison of the results reveal that the relative permeability of the water phase is decreased with the addition of NCG to the injected steam. This is most pronounced at the boxes near the left well pair. In some lcoations, the water relative permeaiblity has been reduced by an order of magnitude. This reduction of the water relative permeability will hinder water flow within the system.

Figure 4.6 displays a comparison of the oil relative permeability distributions after 5 years of operation. A comparison of the two distributions reveals that, similar to that of the water phase, the oil relative peremabilities are slight higher in the base case than that of the SAGP case. This implies that oil drainage is being harmed by the presence of the added gas saturation in the reservoir which results in lower cumulative oil produced from the reservoir. The results reveal that the presence of the additional gas saturation interferes with liquid phase flow.

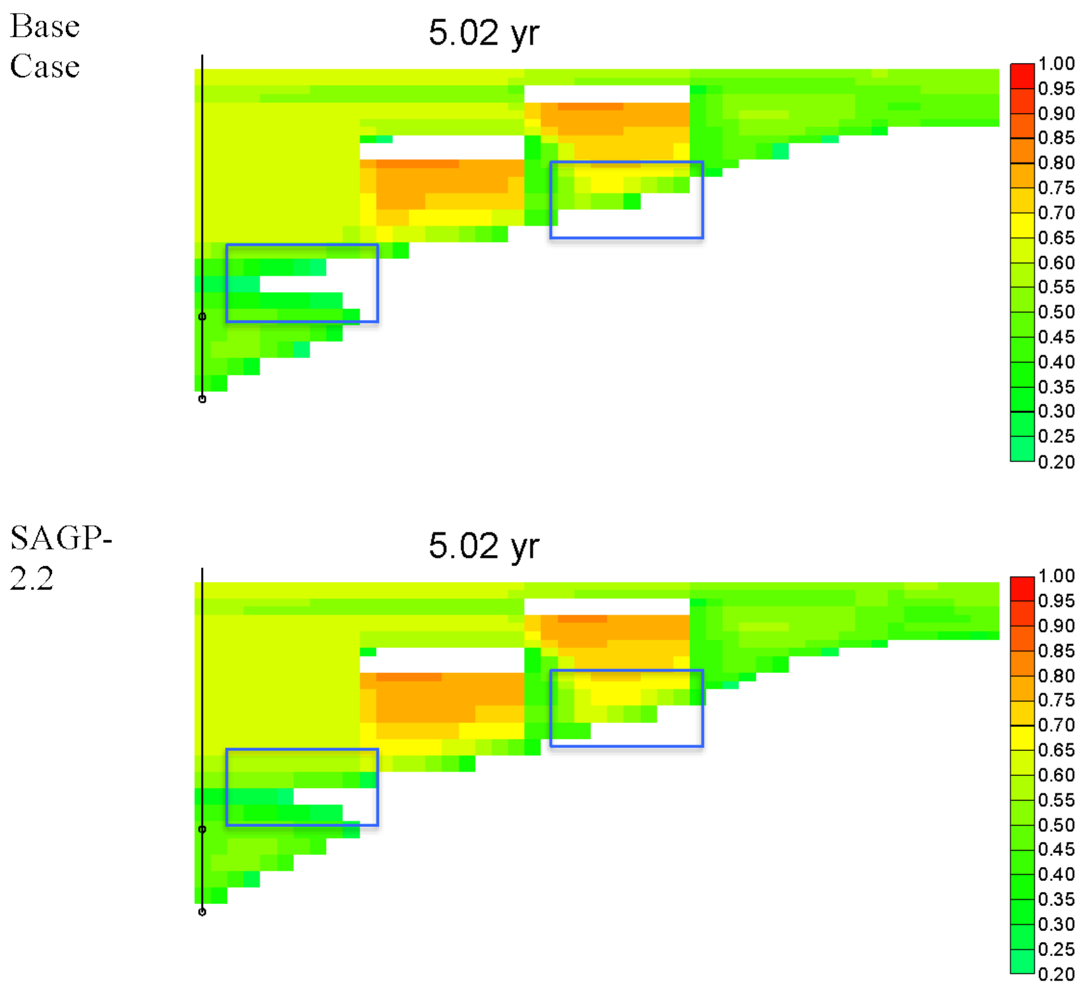

Figure 4.4: Gas saturation distributions after 5 years of operation for the base and SAGP-2.2 cases. The blank areas have gas saturation lower than 0.2. The boxes superposed on the distributions highlight differences between the two of them.

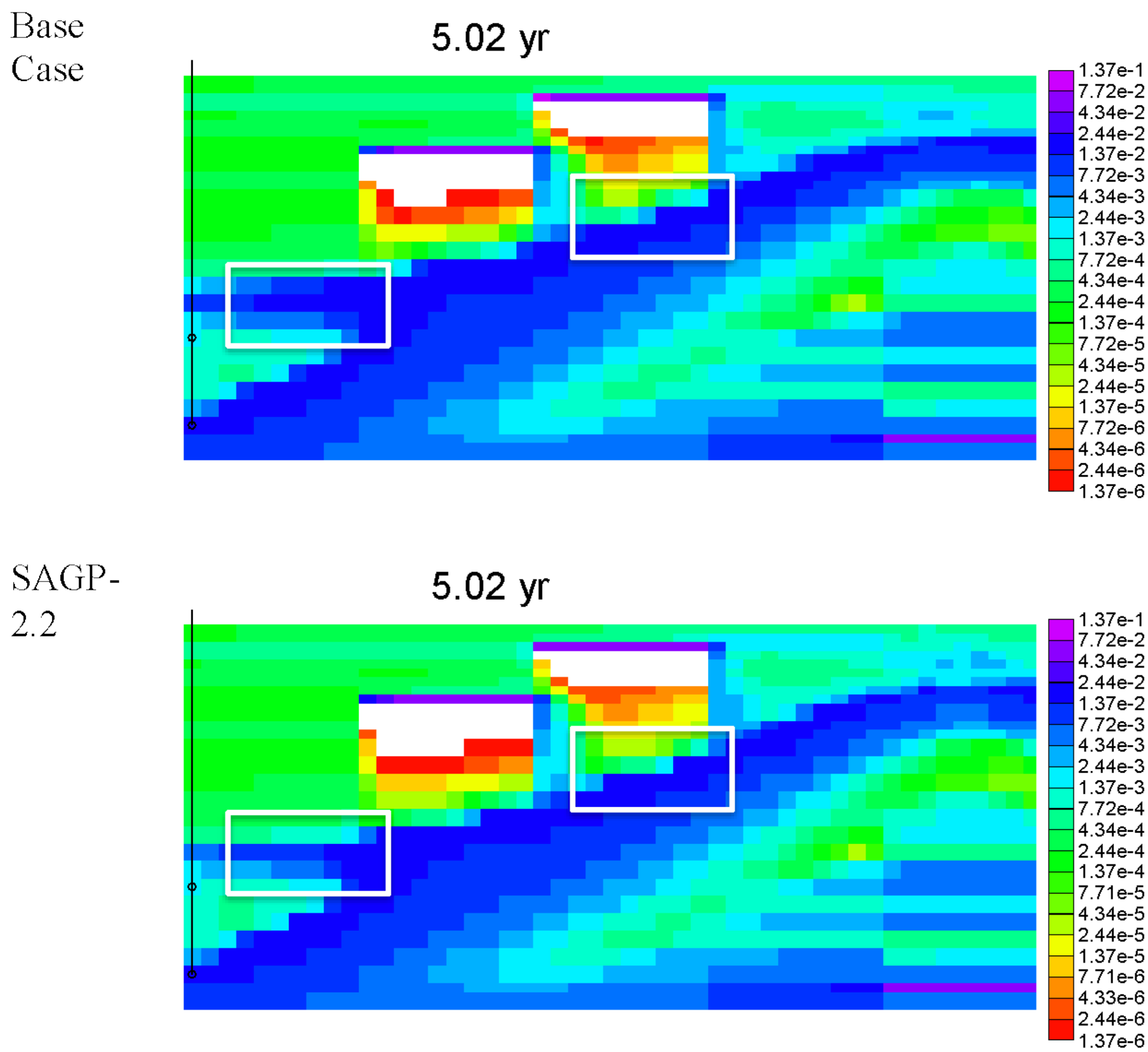

Figure 4.5: Water relative permeability distributions after 5 years of operation for the base and SAGP-2.2 cases. The blank areas have water relative permeability lower than 1.37×10^{-6}. The boxes superposed on the distributions highlight differences between the two of them.

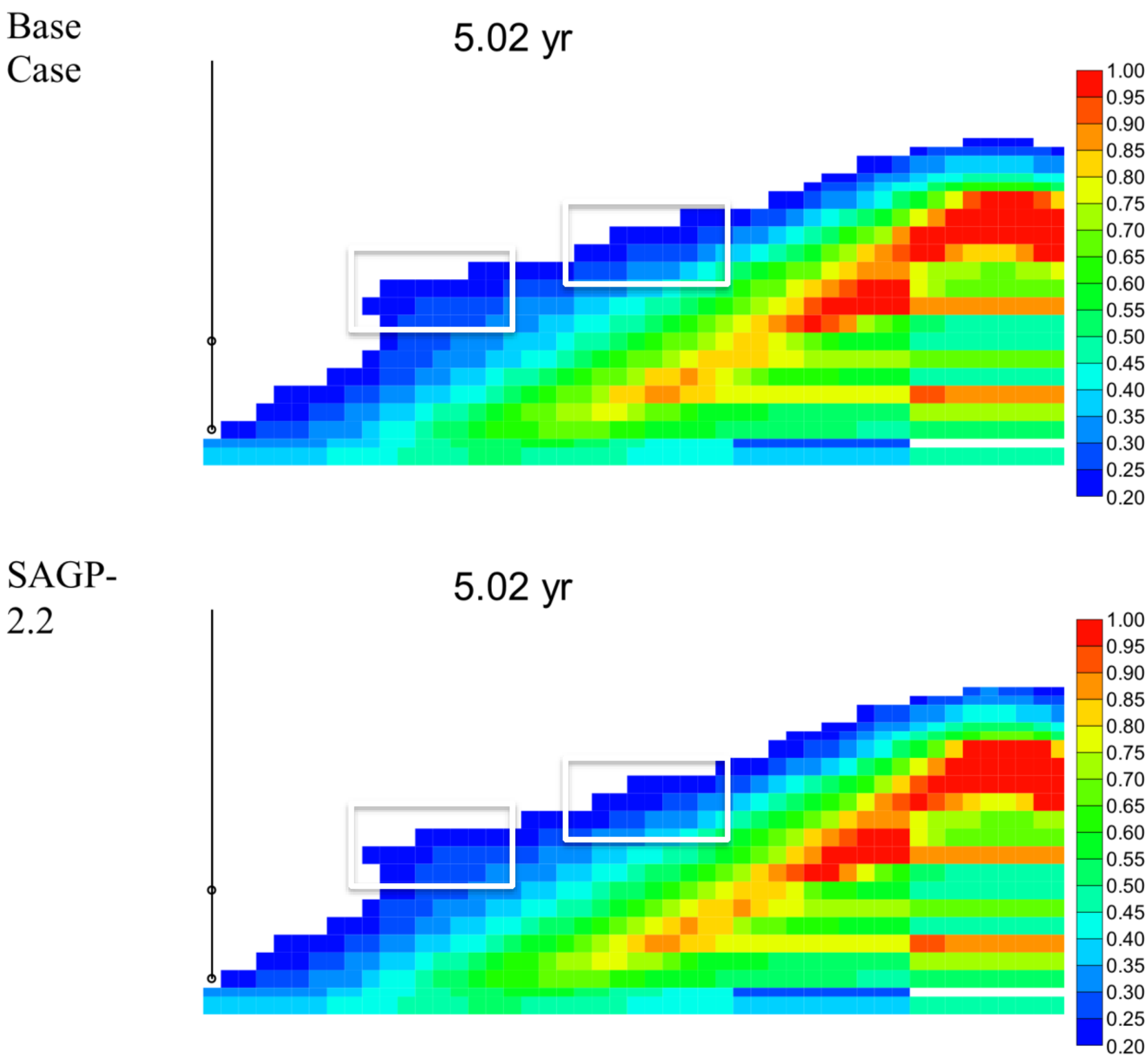

Figure 4.6: Oil relative permeability distributions after 5 years of operation for the base and SAGP-2.2 cases. The blank areas have oil relative permeability less than 0.2. The boxes superposed on the distributions highlight differences between the two of them.

4.4.2 SLUG Cases

In the SLUG cases, the NCG injection period was done in the 3 and 6 month periods prior to the pre-heat stage for cases SLUG-3 and SLUG-6, respectively. This means that the start date for SAGD operation is on the same date. Figure 4.7 compares the cumulative produced oil volume for the base and SLUG cases. The results demonstrate that the slug of NCG injected prior to SAGD mode does not increase the oil volume produced after 10 years of operation. There appears to be a small effect that is visible from Years 4 to 7 of the operation. Rate profiles for the individual well pairs are shown in the Appendix.

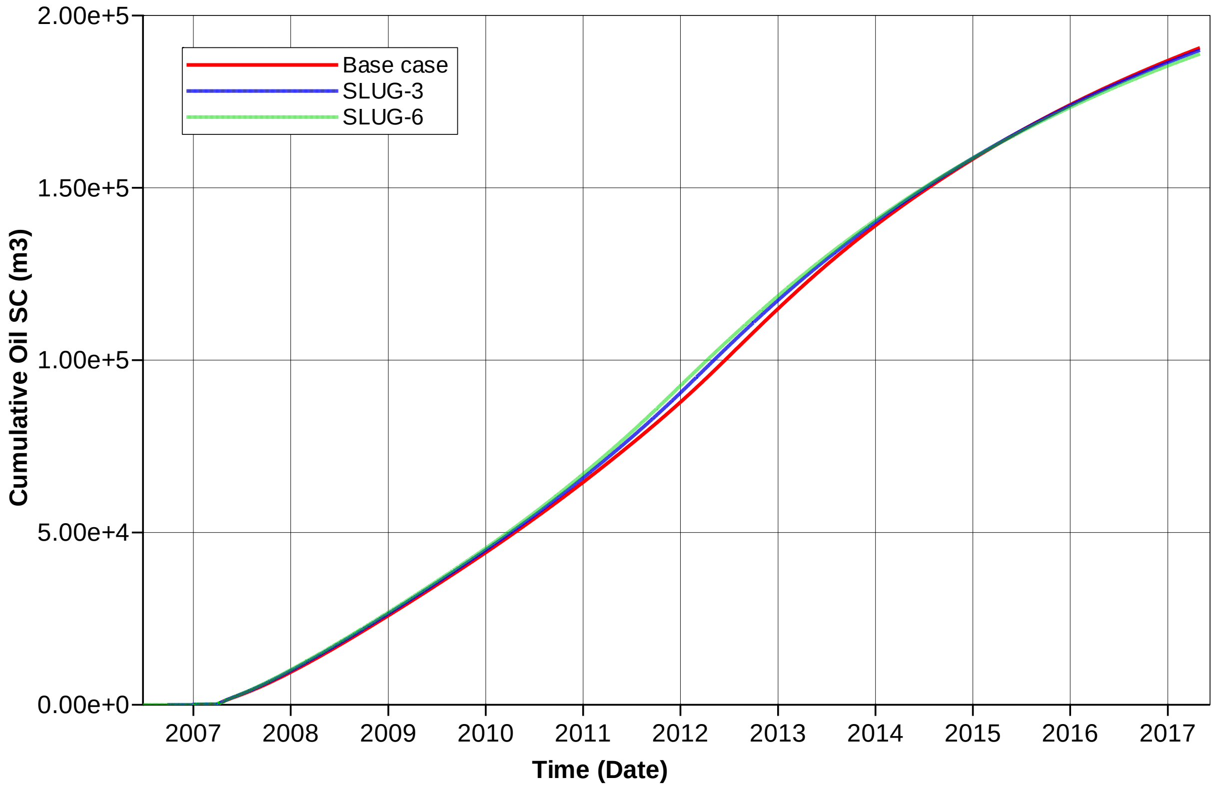

Figure 4.7: Cumulative oil volume produced from SLUG cases.

Figure 4.8 displays the cumulative steam injected and produced water for the base and SLUG cases. The results indicate that the differences between the profiles are minimal although the profiles diverge after about Year 5. Figure 4.9 shows plots of the cSOR profiles for the base and SLUG cases which reveal no significant differences between the cases. In summary, it does not appear that a slug of NCG improves or harms the injection, production, and cSOR profiles of the recovery process.

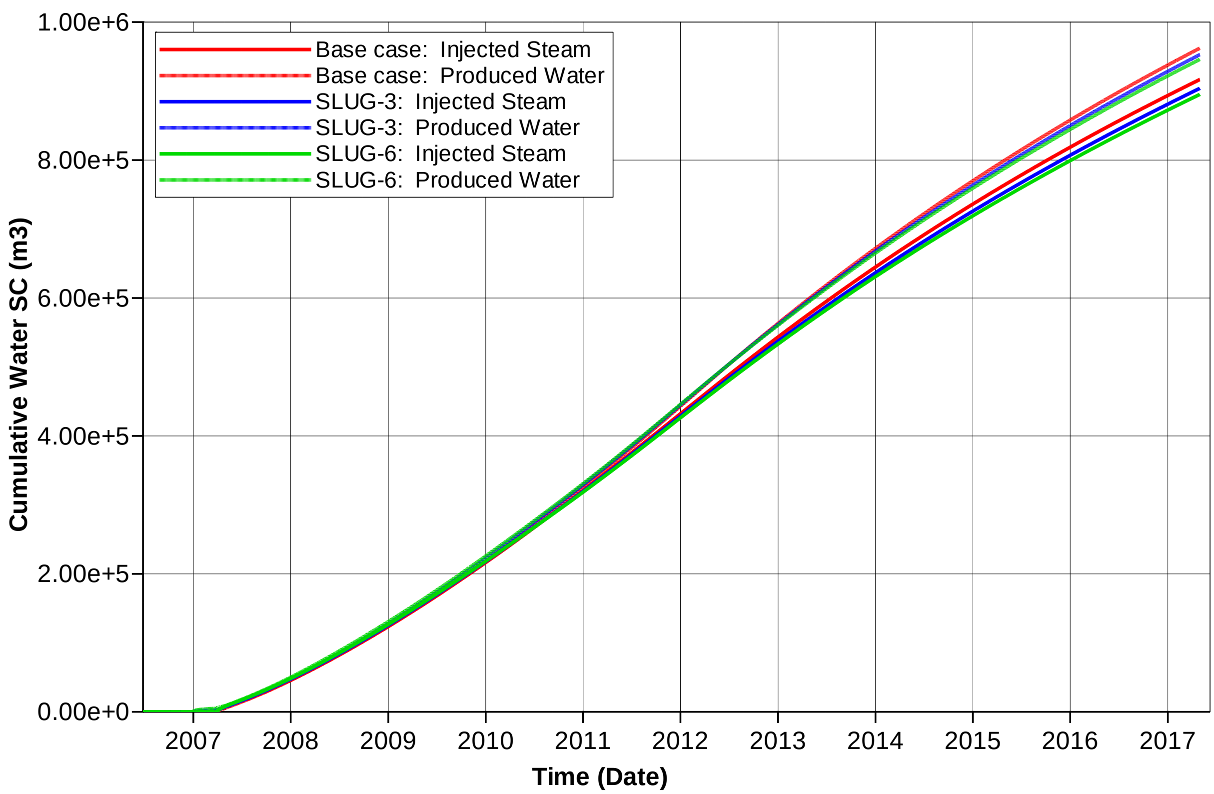

Figure 4.8: Cumulative steam (expressed as cold water equivalent) injected and water produced of the SLUG cases.

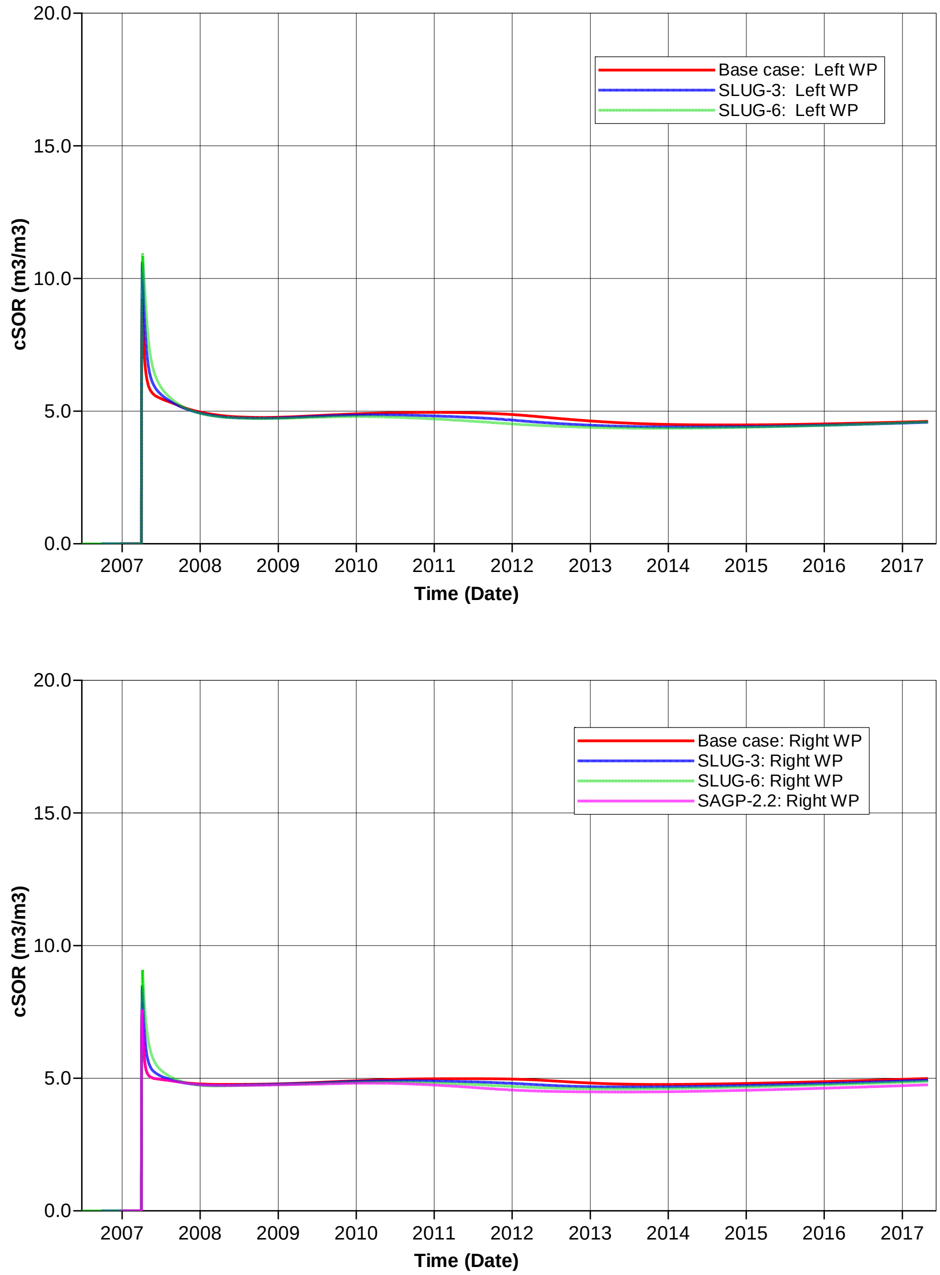

Figure 4.9: cSOR profiles for SLUG cases.

The results from the simulations described above reveal that NCG co-injection, over the range evaluated, does not appear to improve the performance of the recovery process. This is consistent with other published work (Heron et al. 2008; Alturki et al. 2011). The evidence from the simulations suggest that the presence of the gas in the reservoir reduces the relative permeabilities of the liquid phases. For water, this could be beneficial since this will reduce the mobility of water in the reservoir which could lead to less formation water interactions with the steam chamber which could lead to reduced heat losses. However, the reduction of the oil relative permeability coupled with the potential reduction of heat transfer since the gas acts as an insulator means that the overall oil mobility is reduced below that of the case without NCG co-injection.

4.5 Conclusions

The conclusions are as follows:

1. The co-injection of NCG does not improve the performance of an oil sands with relatively high water saturation.
2. The presence of additional gas saturation in the reservoir appears to harm the mobility of the oil which leads to reduced oil production rates in the higher gas co-injection rate case.
3. The NCG co-injection reduces the steam injection rate in order to maintain a constant injection pressure, which in turn reduces the produced water rate as well.
4. The additional gas saturation in the reservoir increases the challenges of mobility of the liquid phases.

Chapter Five: **Conclusions and Recommendations**

5.1 Conclusions

The following conclusions are made from the results of the research documented in this thesis:

1. The higher the initial oil saturation of the oil sands reservoir, the higher is the SAGD steam-to-oil ratio.
2. The performance becomes more uniform between SAGD well pairs as the initial water saturation increases in a heterogeneous oil sands reservoir.
3. Higher initial water saturation may lead to higher injectivity of the formation which permits faster access to oil which can result in enhanced oil production rates. However, if the initial water saturation is sufficiently high, the oil production rate drops due to lower content of oil in the reservoir.
4. Steam chamber grows faster with higher water saturation, resulting in early hydraulic communication of the chamber.
5. The performance of SAGD recovery process does not improve with NCG co-injection for water-rich oil sands reservoirs.
6. The co-injection of gas helps with reducing the steam volume injected but it appears to also harm the production rate of oil. Most likely, larger amounts of NCG co-injection may reduce the steam requirement further but with lower volume of produced oil, it

remains unclear if it will be beneficial with respect to the economics which are most tied to the cSOR and the oil rate.

5.2 Recommendations

The following recommendations are made:

1. The fraction of gas in the injection stream should be increased to see if large amounts of gas can improve the steam-to-oil ratio and to assess the impact on the oil production rate. Potentially, the oil rate can be improved by adding solvent (or another additive such as surfactant) to the injected mixture of steam and gas.
2. If a surfactant is added to the injected steam, the performance of steam foam within the reservoir should be evaluated. However, there is a need to conduct fundamental experiments to determine the kinetics of foam generation, the properties of steam foam (e.g. density and viscosity), and how steam foam flows and evolves within a porous medium.

References

AED (Alberta Economic Development). Oil Sands Industry Update. Available at Alberta Dept. of Energy Website: http://www.energy.gov.ab.ca. 2013.

Alturki, A., Gates, I.D. and Maini, B. On SAGD in Oil Sands reservoirs with No Caprock and Top water zone, Society of Petroleum Engineers, SPE-137234-PA, 2011.

Attanasi, E., and Meyer, R. (2007). Natural Bitumen and Extra-Heavy Oil. Retrieved March 13, 2012, from World Energy Council, http:// energy.cr.usgs.gov/oilgas/aadoilgas.pdf, 2012.

Beattie, C.I., Boberg, T.S., and McNab, G.S. Reservoir Simulation of Cyclic Steam Stimulation in the Cold Lake Oil Sands. SPE Reservoir Engineering, 6(2):200-206, 1991.

Bharatha,S. Chan, M.Y. Dissolved Gas Effects in SAGD, Paper 176, 6th Canadian international Petroleum Conference., Calgary, Canada, June 2005.

Bois A., Tec C. Mainguy M., 2013. Importance of Thermal Consolidation of Shale during SAGD Process. Paper SPE 150420 presented at the SPE Heavy Oil Conference and Exhibition. Kuwait City, Kuwait. 12-14 December 2011

Butler, R.M. Thermal Recovery of Oil and Bitumen. GravDrain Inc. ISBN 0-9682563-0-9, 1997.

Cenovus's Pelican Lake SAGD Pilot Approval # 11469B, AER Annual Performance Presentation, April 2, 2014.

Zhao, L. Law, D.H.S., Nasr, T.N., Coates, R., Golbeck, H., Beaulieu G., Heck, G. SAGD Wind-Down: Lab test and Simulation. Journal of Canadian Petroleum Technology, 44(1), 2005.

Computer Modelling Group (CMG). STARS™ User Manual, Version 2013.12, 2013.

Curtis, C., Kopper, R., Decoster, E., Huggins, C., Knauer, L. Oil Field Review. Retrieved November 18, 2011, from Schlumberger, http://www.slb.com, 2002.

Das, S. Improving the performance of SAGD. Paper SPE 97921 presented at the International Thermal Operations and Heavy Oil Symposium, Calgary, Canada, Nov, 2005.

Doan, L.T., Baird, H., Doan, Q.T., and Farouq Ali, S.M. An Investigation of the Steam-Assisted Gravity-Drainage Process in the Presence of a Water Leg. SPE Paper 56545, 1999.

Edmunds, N.R. Investigation of SAGD Steam Trap Control in Two and Three Dimensions. SPE 50413, 1998.

Edmunds, N. and Chhina, H. Economic Optimum Operating Pressure for SAGD Projects in Alberta. Journal of Canadian Petroleum Technology, 40(12):13-17, 2001.

Fairbridge, J.K., Cey, E., and Gates, I.D. Impact of Intraformational Water Zones on SAGD Performance. Journal of Petroleum Science and Engineering, 82-83:187-197, 2012.

Gates, I.D. and Chakrabarty, N. Optimization of Steam-Assisted Gravity Drainage (SAGD) in Ideal McMurray Reservoir. Journal of Canadian Petroleum Technology, 45(9):54-62, 2006.

Gates, I.D., Kenny, J., Hernandez-Hdez, I.L., and Bunio, G.L. Steam Injection Strategy and Energetics of Steam-Assisted Gravity Drainage. SPE Reservoir Evaluation and Engineering. 10(1):19-34, 2007.

Gates, I.D., Adams, J.J., Larter, S.R. The impact of oil viscosity heterogeneity on the production characteristics of tar sand and heavy oil reservoirs. Part II: Intelligent, geotailored recovery processes in compositionally graded reservoirs. Journal of Canadian Petroleum Technology, 47(9):40-49, 2008

Gates, I.D. and Leskiw, C. Impact of Steam Trap Control on Performance of Steam-Assisted Gravity Drainage. Journal of Petroleum Science and Engineering, 75(1-2):215-222, 2010.

Gates, I.D., and Wang, J. Evolution of in situ oil sands recovery technology: What's happened and what's new? Paper 150686 presented at the SPE Heavy Oil Conference and Exhibition held in Kuwait City, Kuwait, 12-14 December, 2011.

Gates, I.D. Basic Reservoir Engineering. ISBN: 978-1-4652-3684-5, September 2013.

Good, W. K., Razk, C. and Felty, B.D. "Possible Effects of Gas Caps on SAGD Performance." ADOE/AEUB Report, 1997.

Heron, C., Thimm, H., Sullivan, L., and Atkinson, I. NCG Behavior in SAGD – A Numerical Simulation Analysis. Paper SPE/PS/CHOA 117647 presented at the 2008 SPE/PS/CHOA International Thermal Operations and Heavy Oil Symposium, 2008.

Imperial Oil's Cold Lake SA-SAGD Experimental Pilot Approval # 10689, ERCB Annual Performance Review, November 28, 2012.

Ito, Y., and Suzuki, S. Numerical Simulation of the SAGD Process in the Hangingstone Oil Sands Reservoir. J. Cdn. Pet. Tech. 38(9), 27-35, 1999.

Ito, Y., Ichikawa, M., Hirtata, T. The Effect of Gas Injection on Oil Recovery During SAGD Projects. Journal of Canadian Petroleum Technology, 40(1), January 2001.

Oskouei, S.J.P., Maini,B., Moore, R.G., Mehta, S.A. Effect of Mobile Water Saturation on Thermal Efficiency of Steam Assisted Gravity Drainage Process. SPE Paper 138846 presented at the 2010 SPE Latin American and Caribbean Petroleum Engineering Conference, Lima, Peru, December 2010.

Kisman, K.E., and Yeung, K.C. Numerical Study of the SAGD process in the Burnt Lake Oil Sands Lease. SPE Paper 30276, 1995.

Law, D. H., Nasr, T. N., and Good, W. K. Field-Scale Numerical Simulation of SAGD Process With Top-Water Thief Zone. Journal of Canadian Petroleum Technology, Volume 42, No. 8, August 2003a.

Law, D.H.S., Nasr, T.N., and Good, W.K. Lab-Scale Numerical Simulation of SAGD Process in the Presence of Top Thief Zones: A Mechanistic Study. J. Can. Pet. Tech. 42(3):29-35, 2003b.

Law, D.H.S., Nasr, T.N., and Good, W.K. Field-Scale Numerical Simulation of SAGD Process with Top-Water Thief Zone. J. Can. Pet. Tech. 42(8):32-38, 2003c.

Leaute, R.P., and Carey, B.S. Liquid addition to steam for enhancing recovery (LASER) of bitumen with CSS: Results from the first pilot cycle. Paper 2005-161 presented at the 56th Canadian International Petroleum Conference. Calgary, Alberta, Canada, June 7-9, 2005.

Mehrotra, A.K., and Svrcek, W.Y. Viscosity of compressed Athabasca bitumen. Can. J. Chem. Eng. 64:844, 1986.

Nasr, T., and Isaacs, E. Process for enhancing hydrocarbon mobility using a steam additive. U.S. Patent 6230814, 2001.

Nasr, T.N., Korpany, G., SAGD Application in Gas Cap and Top water Oil Reservoirs. Paper presented at the petroleum Society's Canadian International Petroleum Conference, Calgary, Alberta, Canada , June 4-6, 2000.

Nasr, T., and Ayodele, O. (2005). Thermal techniques for the Recovery of Heavy Oil and Bitumen. Kuala Lumpur, Society of Petroleum Engineers, 2005.

Nasr, T.N., Law, D.H.S., Beaulieu, G., Golbeck, H., Korpany, G., Good, W.K. SAGD Application in Gas Cap and Top Water Oil Reservoirs. J. Can. Pet. Tech. 42(1):32-38, 2003.

Ong, T.S., and Butler, R.M. “Wellbore Flow resistance in Steam-Assisted Gravity Drainage”, Journal of Canadian Petroleum Technology. Volume. 29, No. 6, November-December, 1990.

Petroleum Technology Alliance Canada (PTAC). An Exploratory Study prepared by Petroleum Technology Alliance Canada (PTAC), March 31, 2007.

Shin, H. and Polikar, M. Fast-SAGD application in the Alberta Oil Sands Areaa, Journal of Canadian Petroleum Technology 45(9), 46-53, 2006.

Stalder, J.L. Cross SAGD (XSAGD) – An Accelerated Bitumen Recovery Alternative, SPE Reservior Evaluation and Engineering 10 (1), 12-18, SPE-97647-PA, 2007.

Strobl, R. S., Muwais, W. K., Wightman, D. M., Cotterill, D. K., and Yuan, L-P. Geological Modeling of McMurray Formation Reservoirs Based on Outcrop and Subsurface Analogues, in Pemberton, S. G. and James, D. P., eds. Petroleum Geology of the Cretaceous Mannville Group, Western Canada: Can. Soc. Petroleum Geologists, **18**: 292-311, 1997a.

Strobl, R. S., Muwais, W. K., Wightman, D. M., Cotterill, D. K., and Yuan, L-P. Application of Outcrop Analogues and Detailed Reservoir Characterization to the AOSTRA Underground Test Facility, McMurray Formation, Northern Alberta, in Pemberton, S. G. and James, D. P., eds. Petroleum Geology of the Cretaceous Mannville Group, Western Canada: Can. Soc. Petroleum Geologists. **18**: 375-391, 1997b.

Suncor 2013, Annual Performance Report submitted to the Alberta Energy Regulator.

Vinsome, P.K.W. and Westerveld, J.D. A Simple Method for Predicting Cap and Base Rock Heat Losses in Thermal Reservoir Simulators. Journal of Canadian Petroleum Technology. 19(3):87-90, 1980.

Wei, W. Steam Conformance Control: Reservoir Versus Wells. M.Sc. Thesis, University of Calgary, 2011.

Yang, G. and Butler, R. M., Effects of Reservoir Heterogeneities on Heavy Oil Recovery by Steam Assisted Gravity Drainage. Journal of Canadian Petroleum Technology, 31(8): 37-48, 1992.

Zhang, W., Youn, S. and Doan, Q. Understanding Reservoir Architectures and Steam Chamber Growth at Christina Lake, Alberta, by using 4D Seismic and Crosswell Seismic Imaging: SPE/PS-CIM/CHOA Internal Thermal Operations and Heavy Oil Symposium, Calgary, Alberta, Canada, SPE- 97808, 2005.

Appendix

Well Profiles for NCG-additive cases.

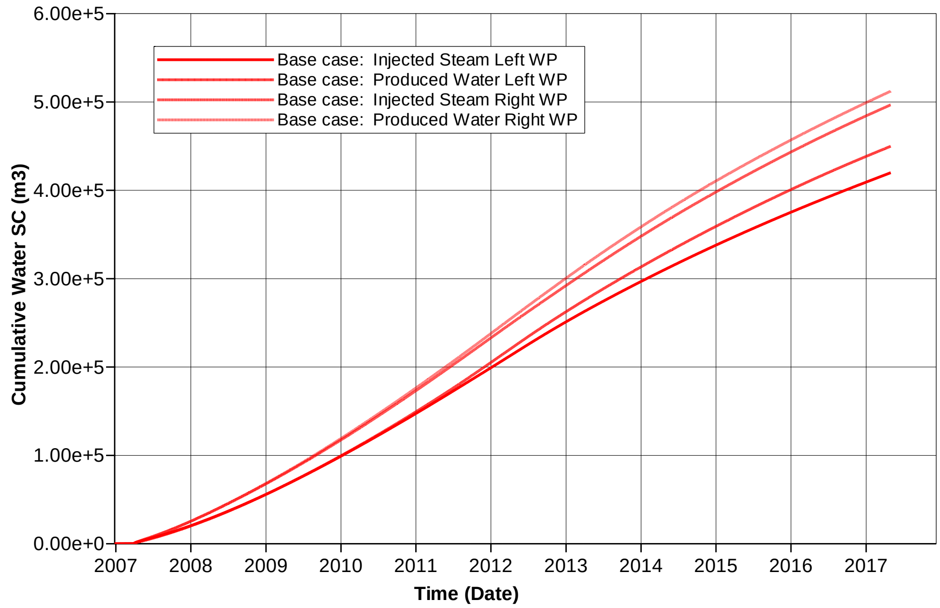

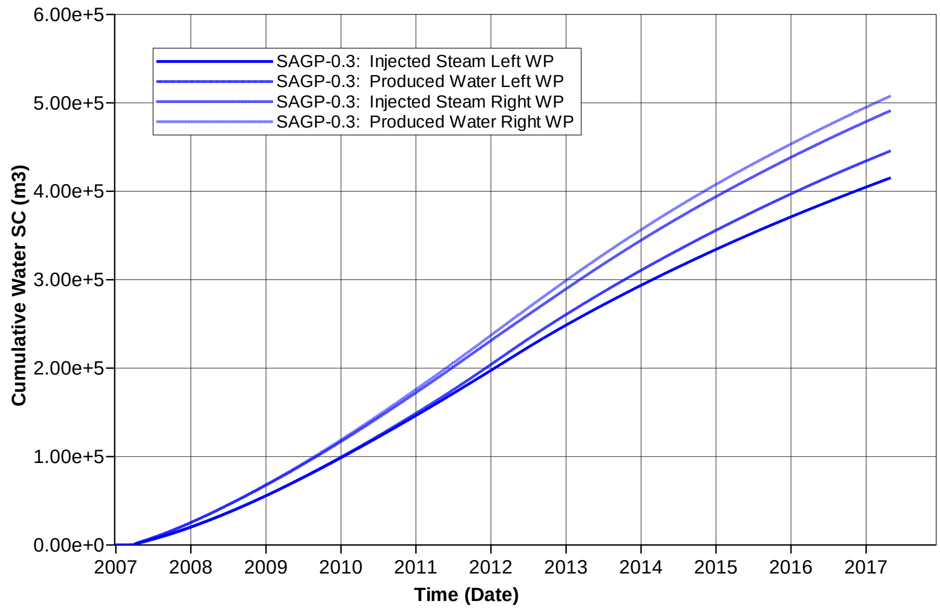

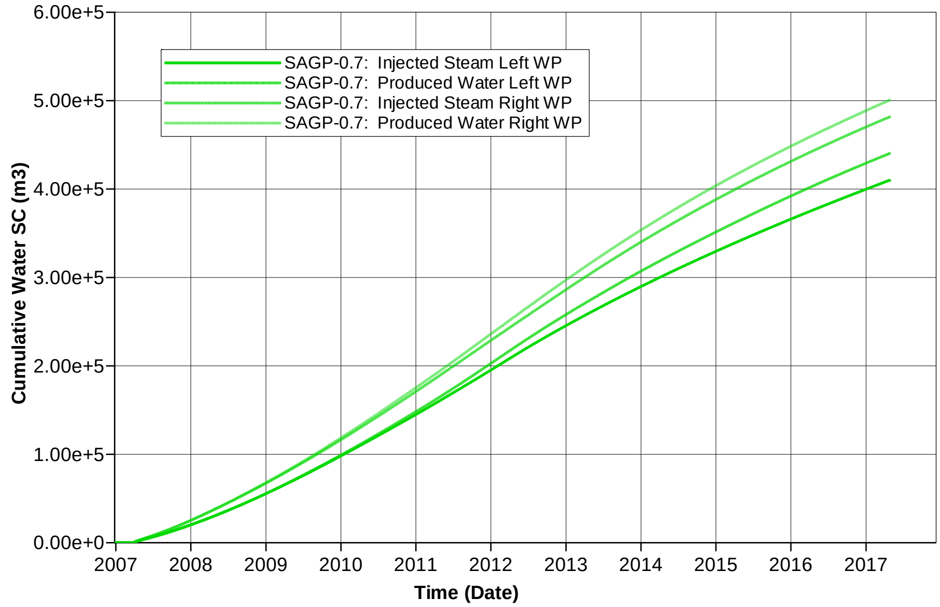

SAGP-0.7: Injected Steam Left WP
SAGP-0.7: Produced Water Left WP
SAGP-0.7: Injected Steam Right WP
SAGP-0.7: Produced Water Right WP
Cumulative Water SC (m3)
Time (Date)

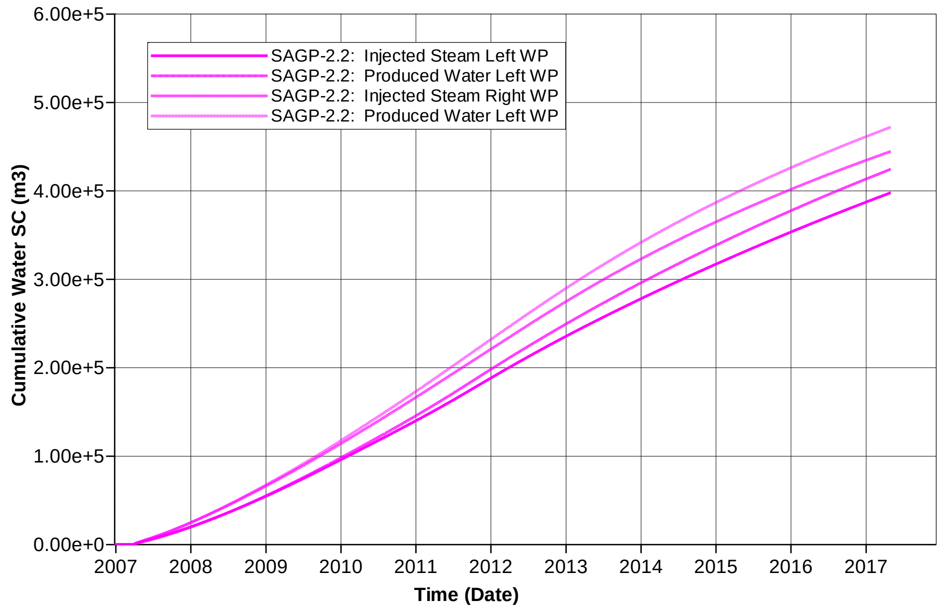

SAGP-2.2: Injected Steam Left WP
SAGP-2.2: Produced Water Left WP
SAGP-2.2: Injected Steam Right WP
SAGP-2.2: Produced Water Left WP
Cumulative Water SC (m3)
Time (Date)

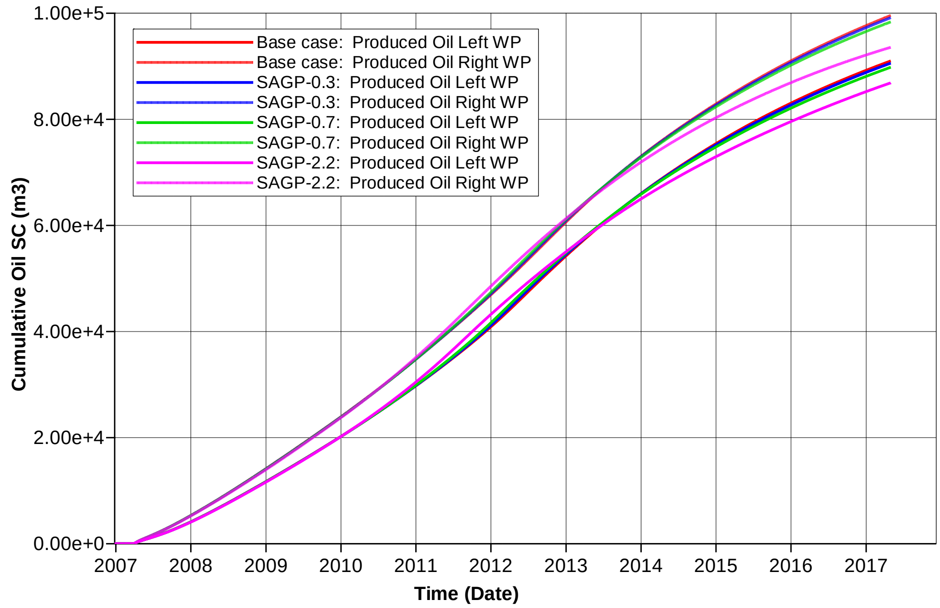
Base case: Produced Oil Left WP
Base case: Produced Oil Right WP
SAGP-0.3: Produced Oil Left WP
SAGP-0.3: Produced Oil Right WP
SAGP-0.7: Produced Oil Left WP
SAGP-0.7: Produced Oil Right WP
SAGP-2.2: Produced Oil Left WP
SAGP-2.2: Produced Oil Right WP
Cumulative Oil SC (m3)
1.00e+5
8.00e+4
6.00e+4
4.00e+4
2.00e+4
0.00e+0
2007
2008
2009
2010
2011
2012
2013
2014
2015
2016
2017
Time (Date)

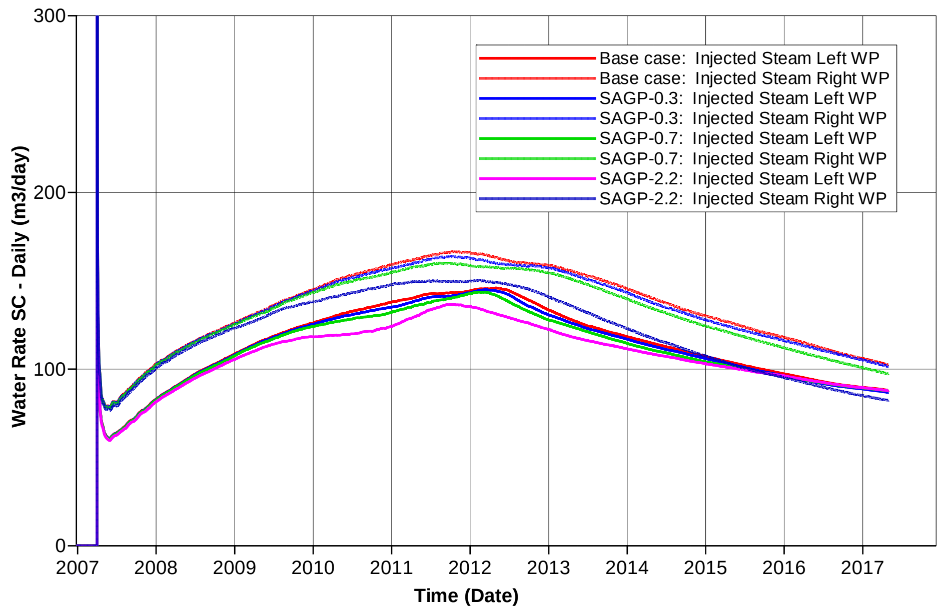
Base case: Injected Steam Left WP
Base case: Injected Steam Right WP
SAGP-0.3: Injected Steam Left WP
SAGP-0.3: Injected Steam Right WP
SAGP-0.7: Injected Steam Left WP
SAGP-0.7: Injected Steam Right WP
SAGP-2.2: Injected Steam Left WP
SAGP-2.2: Injected Steam Right WP
Water Rate SC - Daily (m3/day)
300
200
100
0
2007
2008
2009
2010
2011
2012
2013
2014
2015
2016
2017
Time (Date)

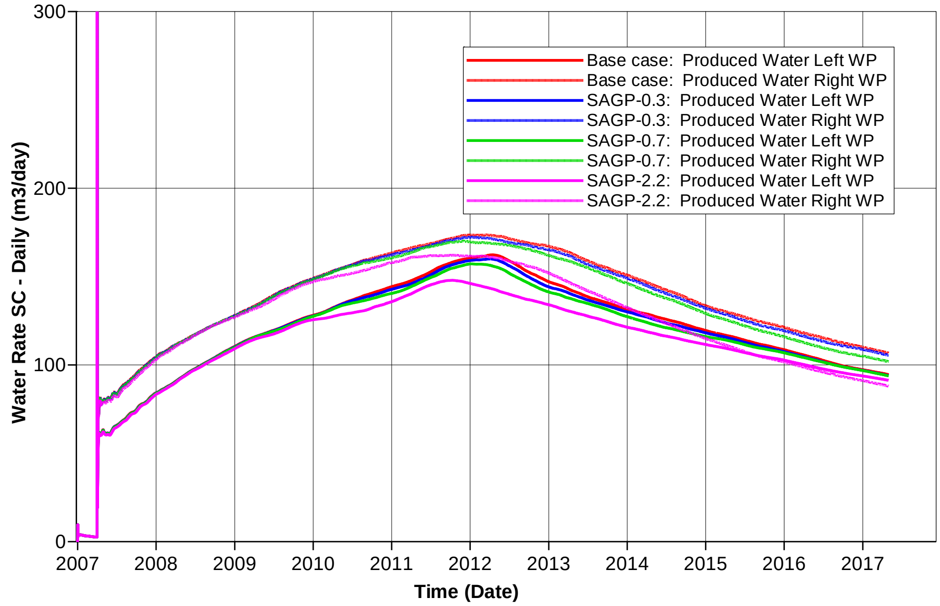

CL Model

PRD1_PRD SAGDBIG-3d-SW0.35R.irf

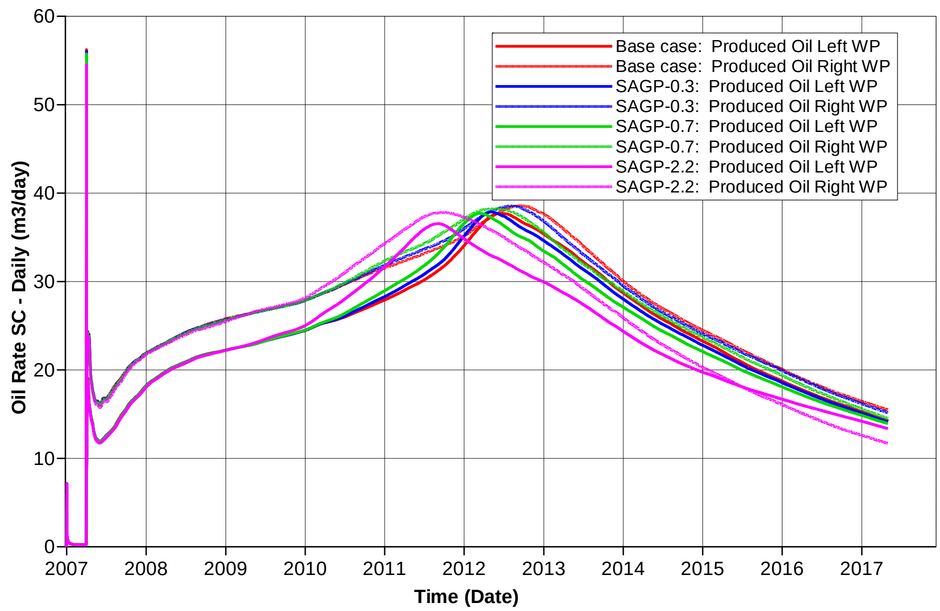

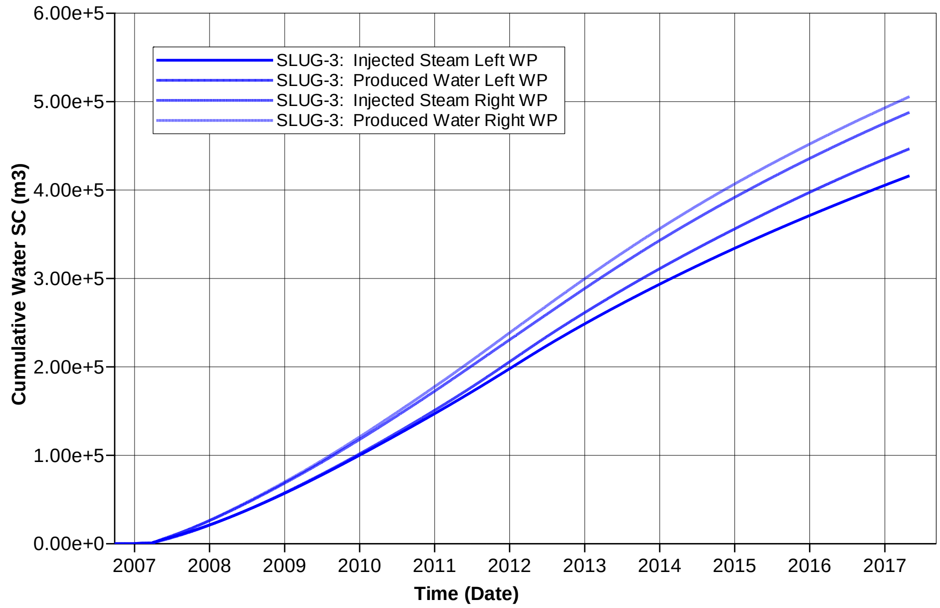

SLUG-3: Injected Steam Left WP
SLUG-3: Produced Water Left WP
SLUG-3: Injected Steam Right WP
SLUG-3: Produced Water Right WP
Cumulative Water SC (m3)
Time (Date)
0.00e+0
1.00e+5
2.00e+5
3.00e+5
4.00e+5
5.00e+5
6.00e+5
2007
2008
2009
2010
2011
2012
2013
2014
2015
2016
2017

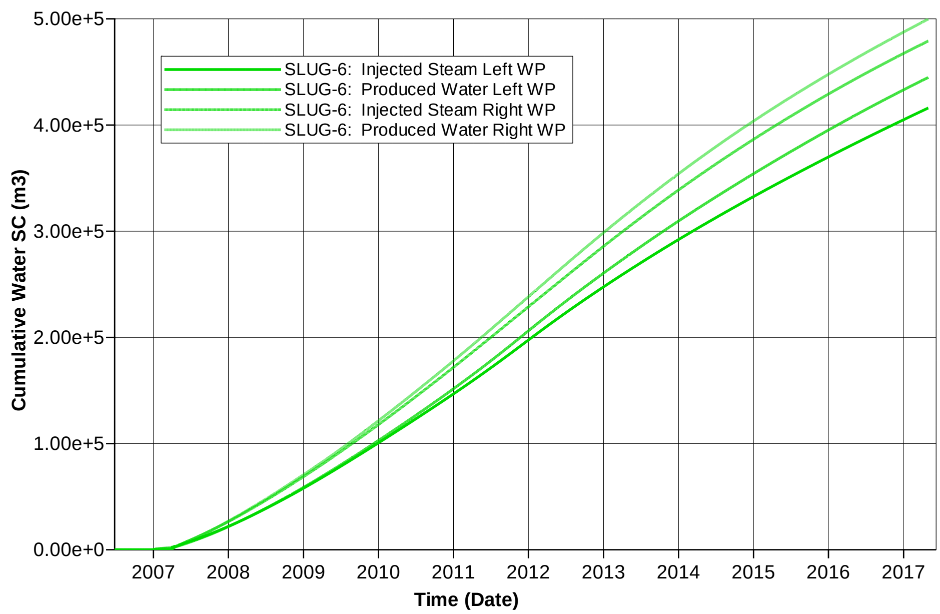

SLUG-6: Injected Steam Left WP
SLUG-6: Produced Water Left WP
SLUG-6: Injected Steam Right WP
SLUG-6: Produced Water Right WP
Cumulative Water SC (m3)
Time (Date)
0.00e+0
1.00e+5
2.00e+5
3.00e+5
4.00e+5
5.00e+5
2007
2008
2009
2010
2011
2012
2013
2014
2015
2016
2017

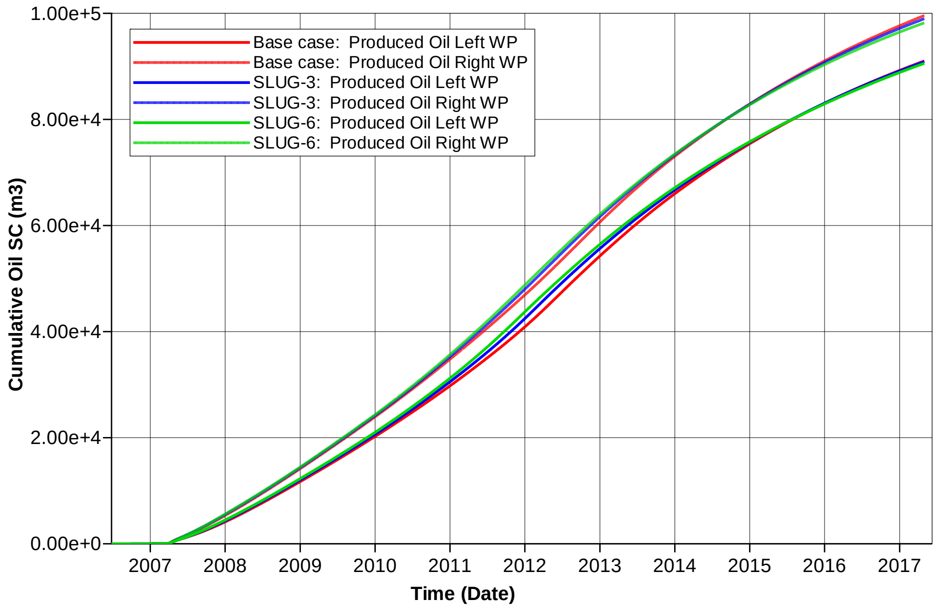

Cumulative Oil SC (m3)
1.00e+5
8.00e+4
6.00e+4
4.00e+4
2.00e+4
0.00e+0
2007
2008
2009
2010
2011
2012
2013
2014
2015
2016
2017
Time (Date)
Base case: Produced Oil Left WP
Base case: Produced Oil Right WP
SLUG-3: Produced Oil Left WP
SLUG-3: Produced Oil Right WP
SLUG-6: Produced Oil Left WP
SLUG-6: Produced Oil Right WP

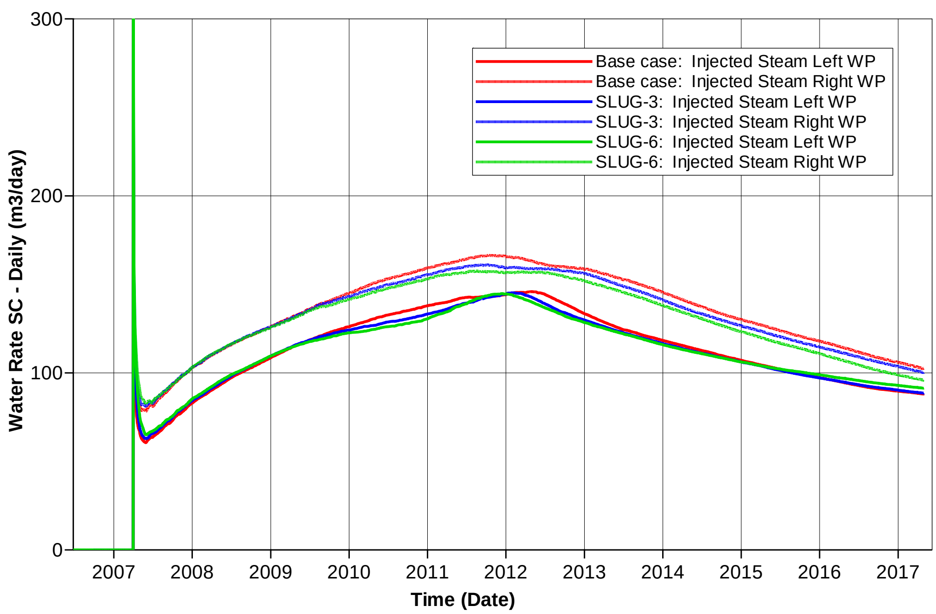

Water Rate SC - Daily (m3/day)
300
200
100
0
2007
2008
2009
2010
2011
2012
2013
2014
2015
2016
2017
Time (Date)
Base case: Injected Steam Left WP
Base case: Injected Steam Right WP
SLUG-3: Injected Steam Left WP
SLUG-3: Injected Steam Right WP
SLUG-6: Injected Steam Left WP
SLUG-6: Injected Steam Right WP

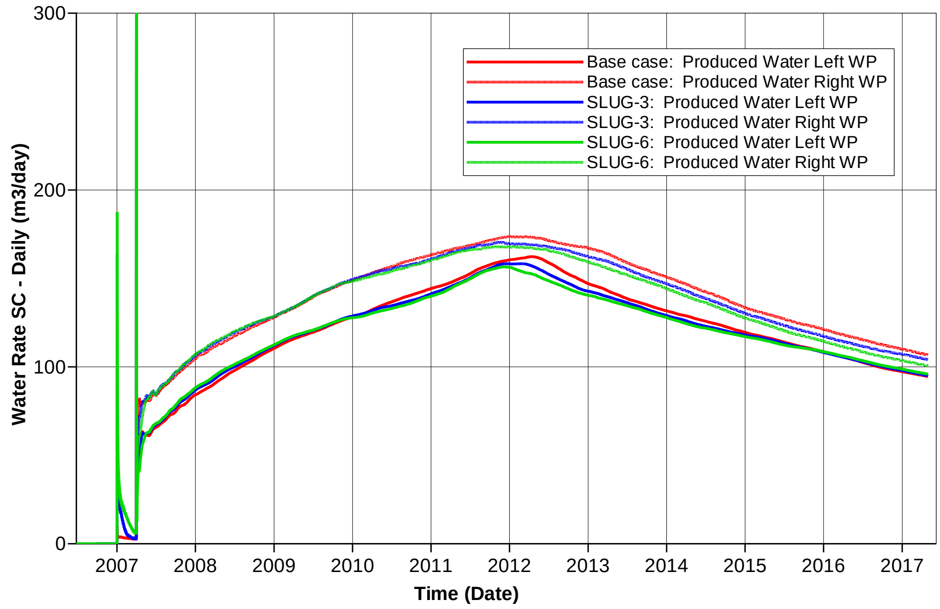

Base case: Produced Water Left WP
Base case: Produced Water Right WP
SLUG-3: Produced Water Left WP
SLUG-3: Produced Water Right WP
SLUG-6: Produced Water Left WP
SLUG-6: Produced Water Right WP
Water Rate SC - Daily (m3/day)
Time (Date)
0
100
200
300
2007
2008
2009
2010
2011
2012
2013
2014
2015
2016
2017

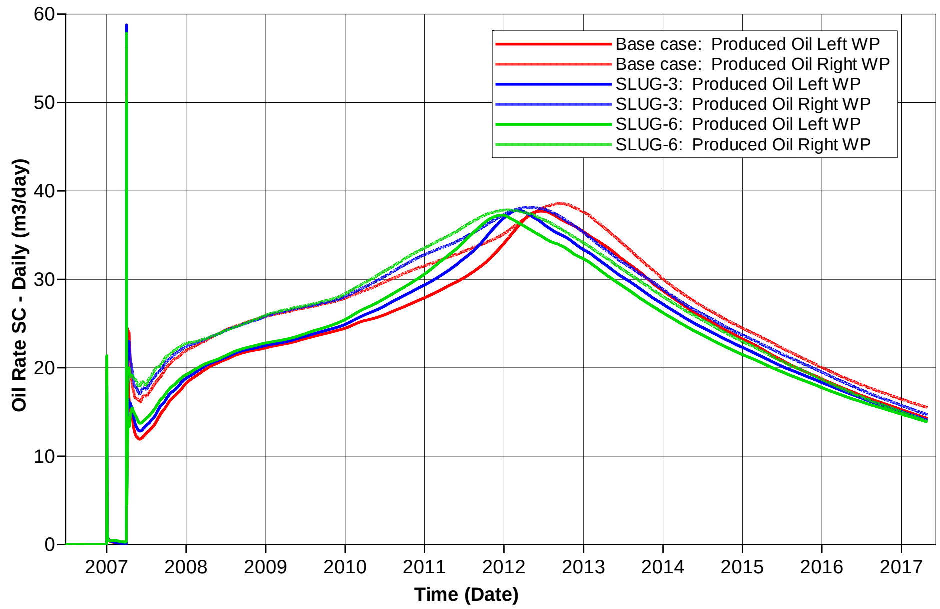

Base case: Produced Oil Left WP
Base case: Produced Oil Right WP
SLUG-3: Produced Oil Left WP
SLUG-3: Produced Oil Right WP
SLUG-6: Produced Oil Left WP
SLUG-6: Produced Oil Right WP
Oil Rate SC - Daily (m3/day)
Time (Date)
0
10
20
30
40
50
60
2007
2008
2009
2010
2011
2012
2013
2014
2015
2016
2017